Title
Investigating the cell type-specific potentials for axon regeneration in zebrafish

Author
Adula, Kadidia Pemba

Publication Date
2021

Peer reviewed|Thesis/dissertation

UNIVERSITY OF CALIFORNIA

Los Angeles

Investigating the cell type-specific potentials for axon regeneration in zebrafish

A dissertation submitted in partial satisfaction of the

Requirements for the degree of Doctor of Philosophy

in Neuroscience

by

Kadidia Pemba Adula

2021

ABSTRACT OF THE DISSERTATION

Investigating the cell type-specific potentials for axon regeneration in zebrafish

by

Kadidia Pemba Adula

Doctor of Philosophy in Neuroscience

University of California, Los Angeles, 2021

Professor Alvaro Sagasti, Chair

Synapses link neuronal populations into circuits, which in turn regulate behavior. Axon damage is a hallmark of traumatic injuries and neurodegenerative diseases such as Alzheimer's. Its ravages upon individuals and societies alike are well known, yet effective treatment of the consequences remains a challenge to modern medicine.

Axon regeneration in humans is quite poor due to the limited regenerative capacities of the peripheral nervous system (PNS) and the inhibitory conditions of the central nervous system (CNS). While axon regeneration is regulated by a fine-tuned balance between intrinsic and extrinsic factors, the contribution of intrinsic factors to this process is not fully understood. The MAP3Ks DLK and LZK are two such intrinsic factors. These axon damage sensors are activated in response to injury and direct diverse, context-specific outcomes to injury. Accounting for the environment around the cell, magnitude of the injury, cell type specificity, and subcellular localization of key actors offers insight into these disparate resolutions. This work designs an experimental approach to investigate the context-specific capacities for axon regeneration and finds that DLK and LZK have cell type- and injury type-specific responses to axon damage.

In chapter 1, I describe a new protocol for precise axon injury in single cells using zebrafish. Unlike in mammals, the zebrafish PNS and CNS are permissive to axon regeneration, making them a perfect environment to study the contribution of intrinsic factors. I take advantage of zebrafish genetic tractability and optic clarity to mosaically label neuronal cell types. I then use a precise laser to cut individual axons with minimal damage to the surrounding tissue. Using live imaging, I capture the post-axotomy processes of Wallerian degeneration and the axonal dynamics of regenerating axons.

In chapter 2, I describe a new zebrafish model to address the variability in DLK and LZK outcomes following axon injury. DLK and LZK CRISPR mutants, as well as DLK LZK double mutants, are

adult viable and fertile. Using the protocol described in chapter 1, I found that DLK and LZK are redundantly required for axon regeneration in motor neurons, but not in touch-sensing neurons. However, DLK and LZK regulate collateral sprouting in non-injured axons of touch-sensing neurons, at both the individual neuron and population levels.

In chapter 3, I describe an effort to create lines labeling DLK- and LZK- expressing neurons. In different organisms, RNA studies indicate that DLK and LZK translation is mostly neuronal; however, these studies lack cell-type specificity. Using CRISPR/Cas9 technology, I attempted to insert the signal amplifying GAL4 gene upstream of DLK and LZK start sites. These enhancer traps were characterized using confocal microscopy, and several techniques were used to validate the lines. Although validation revealed incorrect insertion of GAL4, identifying the cell types in which these proteins are expressed under basal and pathological conditions would be a powerful tool in elucidating their multifaceted activation.

This dissertation of Kadidia Pemba Adula is approved.

Stephen Lawrence Zipursky

Samantha Joanna Butler

Ming Guo

Alvaro Sagasti, Committee Chair

University of California, Los Angeles

2021

Dedication

To my all my siblings (all sixteen of them!), for whom I strive to be a role model.

To my mentors, for making visible an unseen world of possibilities.

TABLE OF CONTENTS

LIST OF FIGURES AND TABLES

ACKNOWLEDGEMENTS

I thank Annette Opler, Louise Handline, and Terry Krulwich for recognizing and cultivating my unique scientific perspective, which led to my pursuit of graduate training. I also thank Samantha Butler, Ming Guo, Lawrence Zipursky, and in particular Alvaro Sagasti, the members of my committee, for embarking with me on this scientific voyage of discovery. I am grateful to Alvaro for his mentorship, feedback, and open-mindedness as I navigated my way to scientific independence. The members of the lab, both past and present, contributed to my success with their comradery, intellectual stimulation and the fostering of a positive learning environment. Finally, I appreciate Matthew Shorey's and Melissa Rolls' collaboration on parts of my graduate research.

VITA

EDUCATION

2014 - Present	**University of California, Los Angeles:** PhD candidate	GPA 3.375
2012 - 2014	**Icahn School of Medicine at Mount Sinai**: PREP Scholar	GPA 3.00
2006 - 2011	Brooklyn College, CUNY: Biology BS	GPA 3.48
2004	Bronx Community College, CUNY	GPA 3.85

RESEARCH EXPERIENCE

2014 - Present **University of California, Los Angeles**, PhD student in Dr. Alvaro Sagasti's lab
Thesis project: The role of the MAP3Ks DLK and LZK in peripheral axon regeneration

2011 - 2014 **Icahn School of Medicine at Mount Sinai,** PREP Scholar in Dr. Patrizia Casaccia's lab
Project 1: The effect of cerebrospinal fluid on axonal damage in MS: investigating mitochondrial dynamics in neuronal cultures exposed to CSF from MS patients. *Project 2:* Regulation of HDAC1 export and function in neurodegeneration: generating HDAC1 mutants and establish HDAC1 sub-cellular localization, enzymatic activity and the response of mutated cells to damaging stimuli.

2010 - 2011 **Brooklyn College, CUNY,** undergraduate researcher in Dr. Amy Ikui's lab
Project: A novel function of MCK1p, a yeast homologue of GSK-3 kinase, in the control of DNA replication: characterizing cell cycle regulation abnormalities using *Saccharomyces cerevisiae* as a model organism.

2010 **Brown University,** summer research student in Dr. Andrea Simmons' lab
Summer project
Study of lateral line neuron interactions with hair cells using an amphibian model: documenting the lateral line nerve's response to damage and recovery of Bullfrog larval hair cells.

2008 - 2009 **Brooklyn College, CUNY**, undergraduate researcher in Dr. Juergen Polle's lab
Project
Algae to Jet Fuels: determining optimal conditions for identifying algae candidate strains for biofuel production.

2004 - 2005 **Brooklyn College and City College, CUNY**, **Storm Peak Laboratory Desert Research Institute guest researcher** to Dr. Neal Phillip and Dr. E. Hindman
Project
Chemical composition of cloud water and snow at Storm Peak Lab, Steamboat Springs: determining the amount of sulfur dioxide, nitrogen gases
and aerosol particles in the environment.

SELECTED PRESENTATIONS

2021 **International Zebrafish Conference**:
"The MAP3Ks DLK and LZK direct diverse responses to axon damage in zebrafish peripheral neurons", poster

2019 **Society For Neuroscience** conference, Chicago, Illinois:
"DLK and LZK direct diverse responses to axon damage in larval zebrafish", poster

2019 **MCDB Research Conference Program**-UCLA, Santa Barbara, California:
"DLK and LZK direct diverse responses to axon damage in larval zebrafish", poster

2018 **MCDB Research Conference Program**-UCLA, Lake Arrowhead, California:
"DLK/LZK are axon injury sensors that direct diverse responses to damage", oral

2018 **International Zebrafish Conference,** Madison, Winsconsin:

"Regulation of axon regeneration in somatosensory neurons by the MAP3Ks DLK and LZK", poster

2016 **MCDB Research Conference Program**-UCLA, Lake Arrowhead, California: "DLK and LZK intrinsic regulation of axon regeneration in zebrafish", poster

2015 **MCDB Research Conference Program**-UCLA, Lake Arrowhead, California: "What is the role of DLK in the regeneration of peripheral axon arbors?", poster

SELECTED FUNDING AND AWARDS

2021-2023 **NSF** Scholar Program Associate

2018 - 2021 **NRSA** F31NS106742-02: "Intrinsic pathways regulating sensory axon regeneration in zebrafish larvae"

2017 **NIH diversity supplement** for R01AR064582

2016 **NIH** and **HHMI** scholarship funds to attend the Marine Biological Laboratory's neurobiology course

2014, 2016 **Cota-Robles Fellowship**

2014 - 2016 **UCLA** Dean Scholar award

2014 **Bridge to the Doctorate,** research scholarship

PUBLICATIONS

2021, submitted **Kadidia Pemba Adula**, Matthew Shorey, Vasudha Chauhan, Khaled Nassman, Shu-Fan Chen, Melissa M Rolls, Alvaro Sagasti "The MAP3Ks DLK and LZK direct diverse responses to axon damage in zebrafish peripheral neurons"

2021, under review **Kadidia P Adula,** Alvaro Sagasti "Live imaging of axonal dynamics after laser axotomy of peripheral neurons in zebrafish" chapter in *Methods in Molecular Biology*'s volume on Axon Regeneration. Nature Springer series

2020 Kusick GF, Chin M, Raychaudhuri S, Lippmann K, **Adula KP**, Huiber EJ, Vu T, Davis MW, Jorgensen EM, Watanabe S. Synaptic vesicles transiently dock to refill release sites. Nat Neurosci. 2020 Nov 1,23(11):1329-1338

2017 Yunjiao Zhu, Oscar G. Vidaurre, **Kadidia P Adula**, Nebojsa Kezunovic, Maureen Wentling, George W. Huntley and Patrizia Casaccia "Subcellular Distribution of HDAC1 in Neurotoxic Conditions Is Dependent on Serine Phosphorylation" Journal of Neuroscience 2 August 2017, 37 (31) 7547-7559

2014 Oscar G. Vidaurre, Jeffery D. Haines, Ilana Katz Sand, **Kadidia P. Adula,** Jimmy L. Huynh, Corey A. McGraw, Fan Zhang, Merina Varghese, Elias Sotirchos, Pavan Bhargava, Vera Venkata, Ratnam Bandaru, Giulio Pasinetti, Weijia Zhang, Matilde Inglese, Peter A. Calabresi, Gang Wu, Aaron E. Miller, Norman J. Haughey, Fred D. Lublin, and Patrizia Casaccia
"Cerebrospinal fluid ceramides from multiple sclerosis patients impair Neuronal bioenergetics", BRAIN (2014) Volume: 137, Issue: 8, Publisher: Oxford University Press, Pages: 2271-2286

Introduction:

A brief introduction to neurons and axon injury:

A healthy, functional nervous system is not only essential for consciousness, but also key to experiencing life to the fullest. Stroke, traumatic injury, or disease leads to axon damage by disrupting neuronal circuits; these changes can result in disability. Neuronal dysfunction takes a heavy toll on both individuals and society ranging from lost wages and medical bills. Some patients lose the ability to perform daily tasks on their own, which in turn affects their independence and feelings of self-worth. Others may experience cognitive dysfunction, thereby losing the identity woven by a lifetime of memories and experiences. Others still can no longer distinguish between sensory inputs from distinct sources or of varying amplitudes; this loss in acuity may result in numbness or pain, presenting a challenge to patient safety. To identify potential pharmaceutical targets and provide relief to patients, the study of pathways regulating nerve damage and repair is paramount.

The nervous system is mainly composed of neurons and support cells known as glia. Neurons are electrical cells. A classic neuron is organized in three parts: dendrites, a cell body and an axon. Dendrites sense stimuli and transform it into electrical impulses. These impulses are then sent to the cell body, the control room of all cellular activity and the repository of its genetic material. From the cell body, the electrical signals gather into the axon. It is in the axon that these electrical signals are converted into chemical signals and released at synapses-- the sites of communication between neurons. Neurons form complex networks of connected synapses to disseminate information. This organization is the basis of neuronal circuits. Several organisms are used to study nervous system development, model disease progression, and injury. Invertebrates such as the *C.elegans* roundworm have a simple nervous system composed of basic neurons and support cells. The nervous system of vertebrates, which include fish, rodents, and humans, also contains neurons and support cells but, additionally, it is divided into a central

nervous system (CNS) and a peripheral nervous system (PNS). The CNS consists of the brain and the spinal cord, both of which are surrounded by bone; the peripheral nervous system is not. The PNS and CNS communicate extensively to collect, convert, and interpret environmental stimuli before coordinating an appropriate response.

Axon injury disrupts neuron to neuron communication. This break must be repaired to restore circuit transmission. Many types of tissues, such as the skin, rely on stem cells to restore their damaged components. Unlike skin cells, most neurons cannot be easily replaced. With the exception of the subventricular zone of the lateral ventricles and the dentate gyrus of the hippocampus, the neurons of our youth remain with us to old age. Therefore, neuronal maintenance and repair must occur individually and at the cellular level.

Following an injury, an axon is separated into a distal stump and a proximal stump. The distal stump is an axonal piece separated from the rest of the neuron at the time of injury; it eventually fragments and degenerates in a process known as Wallerian degeneration (Coleman and Freeman 2010). Axon debris is then cleared, an important step for successful axon regeneration. The proximal stump is the part of the axon that is still attached to the cell body and is the site of axon regeneration. Successful axon regeneration occurs in several steps: sensing the damage, transmitting the injury signal to the cell body, activating pro-regenerative genes, axon guidance towards appropriate targets, and finally, circuit reintegration.

Extrinsic and intrinsic factors contribute to axon regeneration:

Extrinsic and intrinsic factors regulate axon regeneration but their specific contributions are not well understood. Intrinsic factors are elements inside the neuron itself that have an effect on the cell's response to axon damage, whereas extrinsic factors are elements outside of the injured neuron that influence the cell's response. In the mature mammalian CNS, the balance between permissive and inhibitory extrinsic cues is shifted towards inhibition following axon injury. Glial

cells produce some of these extrinsic factors, which include myelin-associated glycoprotein (MAG), oligodendrocyte myelin protein (OMgP), and chondroitin sulfate proteoglycans (CSPGs). However, the mammalian PNS allows for some limited axon regrowth. A rodent study showed that following injury to a CNS nerve connecting the medulla to the spinal cord, the severed CNS nerve was able to regrow 30 millimeters into a bridge formed by the grafting of the PNS nerve segment (David and Aguayo 1981). By contrast, both CNS and PNS environments in zebrafish *Danio rerio* are permissive to axon regeneration. In fish, retinal ganglion cells are able to regenerate following optic nerve crush. However, in mammals the optic nerve does not regenerate. Goldfish axons from retinal explants are repelled by mammalian oligodendrocytes when cultured together (Bastmeyer et al. 1991). The reverse is also true, as rat retinal explants can extend growth cones and elongate on top of fish oligodendrocyte-like cells (Bastmeyer, Bähr, and Stuermer 1993). To get a complete picture of the axon regeneration process, the contribution of signals coming from both the injured neuron itself and signals in the surrounding milieu must be accounted for.

Understanding the contribution of intrinsic factors in relation to extrinsic factors gives us a more complete view of the processes involved in axon injury and repair. Some well-studied intrinsic factors include cyclic-AMP (cAMP), phosphatase and tensin homolog (PTEN), and dual leucine zipper-bearing kinase (DLK). This introduction will focus on DLK, an example that demonstrates how activation of an intrinsic factor can lead to different, or even opposite effects, depending on the environment around the cell. If we are to effectively treat axon damage, we must account for diversity in neuronal cell types. A central piece in this puzzle will be uncovering the tight regulatory mechanisms used by neurons to enable specific effects of DLK activation in different conditions.

DLK is a well conserved intrinsic factor frequently implicated axon injury responses. DLK is also known as mitogen-activated kinase kinase kinase 12 (MAP3K12), MAPK-upstream kinase

(MUK), and zipper protein kinase (ZPK). DLK's function as an axon injury sensor was first identified in a *C. elegans* genetic screen, in which mutant motor neurons failed to form growth cones after axotomy. DLK is a MAP3K family member which belongs to the Mixed Lineage Kinase (MLKs) subfamily (Holzman, Merritt, and Fan 1994). MAP3Ks regulate a myriad of cellular events, including growth, differentiation, and proliferation to stress responses. MAP3Ks can be activated downstream of G protein-coupled receptors (GPCRs), receptor tyrosine kinases (RTKs) or by intracellular signals. The signaling cascade initiated by this family of proteins starts with the activation of a MAP3K, which then phosphorylates and activates a MAP2K, which in turn phosphorylates and activates a MAPK. All MAP3Ks converge on one of three classes of MAPKs: extracellular regulated kinases (ERK1/2, ERK3, ERK4, ERK5, ERK6/P38γ, ERK7, ERK8), P38 mitogen-activated protein kinase (P38α, P38β, P38γ/ERK6, P38δ), or Jun NH_2 terminal kinases (JNK1, JNK2, JNK3) (Dhanasekaran et al. 2007). MAP3Ks can phosphorylate target proteins at serine/threonine residues. Like all MAP3Ks, MLKs are serine/threonine kinases. MLKs can also phosphorylate their targets at tyrosine residues (Gallo and Johnson 2002). Invertebrates have one DLK related gene while vertebrates have two: DLK and leucine zipper kinase (LZK) (Sakuma et al. 1997). Among MLKs, DLK and LZK are distinguished by having two leucine zipper domains instead of one. Upon activation, DLK and LZK form homodimers (Mata et al. 1996; Sakuma et al. 1997). Although DLK and LZK are not believed to form heterodimers with each other via their leucine zippers, they can bind to each other via their N-terminal domains (Pozniak et al. 2013; Deepak Nihalani, Merritt, and Holzman 2000). DLK and LZK have been consistently associated with neuronal development and responses to axon injury.

DLK and LZK protein structure, activation, and regulation:

DLK's kinase domain, especially its activation loop, is very well conserved across species. Roundworm DLK-1 can be activated via cytoskeletal disruption or calcium binding to its C-terminus calcium domain (Ghosh-Roy et al. 2010; Yan and Jin 2012). DLK-1 activation

phosphorylates MKK4, which in turn phosphorylates P38. In the *Drosophila* fly DLK, also known as Wallenda, does not have a calcium domain and is thought to be activated by cytoskeletal damage (Chisholm 2013). Wallenda phosphorylates MMK7, which in turn phosphorylates JNK. Although DLK has been more extensively studied than LZK, there exists the possibility that these two proteins could perform redundant, complementary, or completely different functions. Human DLK and LZK share 87% sequence similarity in their kinase domain (Sakuma et al. 1997). Vertebrate LZK has a calcium domain in its C-terminus, making it physiologically closer to invertebrate DLK-1 than vertebrate DLK. While vertebrate DLK and LZK can activate both MKK4 and MKK7 *in vitro*, in *vivo* they preferentially activate one *or* the other (Xu et al. 2001; Haeusgen, Herdegen, and Waetzig 2011; T. Itoh et al. 2014; Yang et al. 2015; Yunbo Li et al. 2021). Both MKK4 and MKK7 can activate JNK but MKK4 alone can activate P38. Scaffold proteins such as JNK-interacting proteins use palmitoylation to bring together a particular MAP3K, MAP2, and JNK into a signaling module, thereby determining the specificity of the cascade (Dickson et al. 2010; Holland et al. 2016).

DLK activation and signaling is well characterized in roundworms. *C. elegans* have two DLK-1 isoforms: DLK-1L (long isoform) and DLK1S (short isoform). DLK-1L heterodimerizes with DLK-1S in its inactive form. Upon activation DLK1-L disengages from DLK-1S to homodimerize with itself (Ghosh-Roy et al. 2010; Yan and Jin 2012). Activated DLK is then assembled into a complex by the JIP3 scaffolding protein with MKK4 and P38; this complex is retrogradely transported to the cell body where it activates pro-regenerative genes via CCAAT/enhancer-binding protein-1 (CEBP-1) and promotes the upregulation of cytoskeletal dynamics (Yan et al. 2009).

DLK and LZK RNA levels in neurons are not detected in most RNAseq experiments, implying that these MAP3Ks are tightly regulated (Jin and Zheng 2019). Various strategies are used by cells to regulate DLK and LZK activation. For example, JIP-1 association with DLK prevents DLK

dimerization (D. Nihalani 2001). Vertebrates do not have a short isoform of DLK, but they have a MAP3K12 binding-inhibitory protein-1 (MBIP). MBIP has been reported to keep DLK in its inactive state, but its function has not been studied in neurons (Fukuyama et al. 2000). The E3 ligases such as Regulator of Presynaptic Morphology 1 (RPM-1) also negatively regulate DLK (Nakata et al. 2005; Collins et al. 2006). While DLK signaling in invertebrates is well-understood, vertebrate DLK and LZK module formations, potential crosstalk, and regulation are still being unveiled.

DLK and LZK functions in neuronal development and homeostasis:

DLK and LZK are expressed in several human tissues. DLK mRNA was found in the brain of human fetuses and both the brain and kidneys in adults (Reddy and Pleasure 1994). LZK mRNA was found in the brain, pancreas, liver, placenta of adult humans (Sakuma et al. 1997). Because human experimentation to elucidate DLK and LZK function is not possible, studies in model organisms have been used to understand the functions of these kinases. This section summarizes what is known about DLK and LZK developmental functions.

Studies over the past two decades show that DLK, unlike LZK, is essential for various aspects of the developing nervous system in embryonic and postnatal mice. DLK mRNA is found in the CNS, spinal ganglia, the skin, intestine, pancreas and kidney of mouse embryos (Holzman, Merritt, and Fan 1994; Nadeau, Grondin, and Blouin 1997). DLK protein is broadly expressed in the brain, the spinal cord, dorsal root ganglia (DRG), trigeminal ganglia, parasympathetic neurons, and in the liver. In neuronal cells, DLK protein localizes preferentially to axons (Hirai et al. 2005). In cultured cortical cells, DLK is often associated with vesicles travelling along microtubules and the Golgi apparatus (Hirai et al. 2002). Knockout embryos display cellular migration and axonal abnormalities in the brain. DLK was shown to enable radial migration of differentiating neurons in the telencephalon by regulating cytoskeletal dynamics (Hirai et al. 2002). It is also essential for granule cell differentiation and migration in the postnatal

cerebellum (Suenaga et al. 2006). Moreover, DLK regulates the formation of axonal tracts by pyramidal neurons in the cerebellum. Mutant neonates have an excessive number of motor neurons, indicating a disruption of developmental programmed cell death (Sengupta Ghosh et al. 2011; T. Itoh et al. 2014). These data indicate that DLK is essential for organogenesis in several tissues and for cell differentiation of developing mice. It is no surprise therefore that DLK loss of function mutants die perinatally (Hirai et al. 2006). Less is known about the distribution of LZK expression in mouse embryos. However, LZK mutants have no apparent developmental abnormalities and survive to adulthood (Welsbie et al. 2017).

DLK and LZK are also expressed in the fully formed nervous system of adult mice, but their absence is not deleterious. DLK mRNA is present in the brain, gastro-intestinal tract, and testis (Holzman, Merritt, and Fan 1994; Blouin et al. 1996). In the brain, DLK and LZK proteins are present at synapses (Pozniak et al. 2013). This expression pattern implies homeostatic functions in healthy animals. For example, DLK was shown to regulate insulin-like growth factor-1 (IGF-1) signaling in the cerebellum (Goodwani et al. 2020). Therefore, it is startling that the loss of function of DLK and LZK in adult mice using inducible knockouts, protein inhibitory drugs, or down-regulation with RNAi does not appear to alter neuronal morphology (Pozniak et al. 2013; Goodwani et al. 2020; Yunbo Li et al. 2021). It is equally unexpected that over-expression of DLK and LZK *in vivo* led to self-activation and to neuronal death (Yunbo Li et al. 2021). These findings point to the tight spatio-temporal regulation of DLK and LZK activity by mammalian neurons *in vivo*.

Additional information about subcellular localization has come from studies in rats. In situ hybridization comparing DLK mRNA expression in rats and mice found similar patterns in both organisms. Subcellular fractionation of the adult rat cortex found that DLK protein is enriched in the synaptic membrane of neurons, but not in the myelin nor the synaptic vesicle fractions. Only unphosphorylated, inactive DLK is membrane-bound, whereas a lower amount of DLK protein,

both phosphorylated and unphosphorylated, is present in the cytosol of neuronal synapses (Mata et al. 1996).

In invertebrates, such as flies and roundworms, DLK loss-of-function mutants do not show a developmental phenotype. While DLK overexpression leads to aberrant synaptic structures, it does not cause cell death (Nakata et al. 2005; Collins et al. 2006). An interesting study in roundworms showed that DLK-1 regulation by two different E3 ligases, MEC-15 and RPM-1, led to opposite effects on axon growth and synaptic development in the same neuronal cell type (Liao et al. 2004; Bounoutas et al. 2009; Zheng et al. 2020). Controlling DLK-1 levels may help sequester it in specific subcellular compartments and avoid inappropriate associations.

DLK and LZK redundant functions in pathological conditions:

DLK and LZK have been repeatedly implicated in neuronal stress responses across organisms and life stages. Neuronal stress conditions, including axon damage and exposure to neurotoxins, lead to diverse and sometimes contradictory outcomes (Tedeschi and Bradke 2013; Jin and Zheng 2019; Asghari Adib, Smithson, and Collins 2018). Depending on the context, DLK and LZK activation following neuronal insult results in the regeneration of the proximal stump, degeneration of the distal stump, failure of axon regeneration, and cell death. Ample evidence suggests that DLK and LZK promote axon regeneration. DLK's function as an axon damage sensor was first discovered in a roundworm screen. In juvenile roundworm DLK-1 mutants, severed motor neurons fail to form growth cones (Hammarlund et al. 2009). Later that year, another study showed that DLK-1 is required for axon regeneration in the touch-sensing neurons of adult roundworms (Yan et al. 2009). In fly larvae, following segmental nerve crush, which includes motor and sensory neurons, DLK mutant axons fail to regenerate (Xiong and Collins 2012). Moreover, overexpression of DLK and LZK in cultures of cerebellar granule neurons isolated from postnatal mice promotes axon elongation after axotomy, and LZK additionally increases axon branching (M. Chen et al. 2016). However, a different study found

that LZK overexpression inhibits axon regeneration in postnatal mice cerebellar granule neurons cultured in the presence of myelin (Dickson et al. 2010).

DLK has been reported to be dispensable for growth cone formation but essential for the axon elongation step in primary cultures of cortical rat neurons, primary DRG neuronal cultures of juvenile mice, and following sciatic nerve transection (Eto et al. 2010; A. Itoh et al. 2009). DLK was also required for axon elongation in regenerating motor neurons, and following sciatic nerve crush in mice (Shin et al. 2012). It is possible that redundancy among MAP3Ks has evolved for some stages of regeneration.

Along with axon regeneration and axon elongation, DLK also regulates the execution of Wallerian degeneration. DLK deficiency significantly delays the degradation of distal axons in several contexts: in the olfactory neurons of adult flies, DRG cultures from mutant mice embryos post-axotomy or following exposure to a chemotoxic drug, and sciatic nerve of adult mice after transection (Miller et al. 2009; Summers, Milbrandt, and DiAntonio 2018; Summers et al. 2020). However, a study in fly larvae showed that a pre-conditioning lesion within the same nerve enables a DLK-mediated protective effect on distal axon integrity after the second nerve lesion (Xiong and Collins 2012).

Finally, DLK and LZK can also trigger cell death in adult mouse models of CNS injury. DLK is required for somal degeneration in retinal ganglion cells (RGC) but not for axonal degeneration following optic nerve crush (Fernandes et al. 2014). DLK inhibition increases survival of dopaminergic neurons in an *in vivo* model of Parkinson's disease, and of hippocampal neurons under *in vivo* excitotoxic conditions (X. Chen et al. 2008; Pozniak et al. 2013). Together, these results demonstrate the variety of DLK and LZK responses to neuronal insult.

How do DLK/LZK promote divergent outcomes to axon injury?

As MAP3K family members, DLK and LZK functions are expected to be context-specific. Various experimental paradigms have been used to investigate DLK and LZK activation under pathological conditions. A few settings can be highlighted for contributing to the diversity in

neuronal responses: the environment around the cell, magnitude of the injury, cell type specificity, and subcellular localization.

The environment surrounding a damaged neuron affects the consequence of DLK and LZK activation. Most invertebrate studies and those conducted in the mammalian PNS point to these MAP3Ks promoting cellular survival and axon regeneration in permissive conditions. Under non-permissive conditions, such as those in the mammalian CNS, DLK and LZK activation results in cell death or the formation of retraction bulbs at the injury site. This hypothesis is bolstered by *in vitro* experiments using cultured mouse cerebellar neurons. In primary mouse cerebellar cultures, individually expressing DLK or LZK was sufficient to promote axon regeneration after axotomy (M. Chen et al. 2016); however, the addition of myelin to the *in vitro* culture resulted in a Nogo A- and LZK-dependent regrowth inhibition (Dickson et al. 2010). These data underline the importance of considering the environment around the cell when injury occurs *in vivo*.

Controlling the scale of the damage is also key to understanding the contribution of intrinsic factors such as DLK and LZK. Nerve crushes cause damage to the tissues surrounding axons, confounding extrinsic factor contribution with that of intrinsic factors. With single cell axotomy, precise lasers can be used to cause minimal damage. Moreover, crushes are themselves incomplete injuries that include cut, partially cut, and completely spared axons. This ambiguity makes it difficult to distinguish collateral sprouting from de novo regeneration: two growth mechanisms that may differentially engage MAP3Ks (Steward, Zheng, and Tessier-Lavigne 2003; Tuszynski and Steward 2012). From single cell resolution to large scale injury models, the outcomes of complete axon severing and complete nerve transections should be interpreted differently from partial axotomies and nerve crushes.

With the environment surrounding the cell and scale of the injury taken into account, it is also important to address cell type specificity. Nerve crushes are commonly used in axon regeneration studies. Nerves are composed of axons from different neuron subtypes, making it difficult to assess cell-type-specific responses to damage. LZK and DLK activate neuronal as

well as non-neuronal cells to respond in a cell-type-specific manner to axon injury. In motor neurons, DLK has been reported to be required for multiple steps of axon regeneration, including growth cone formation in roundworms and axon elongation in mice (Hammarlund et al. 2009; Shin et al. 2012). In astrocytes, LZK upregulation leads to their activation and mobilization to the site of spinal cord injury (M. Chen et al. 2018). The treatment of diseases that impact specific neurons, such Parkinson's, Huntington's, and amyotrophic lateral sclerosis (ALS), would greatly benefit from studies with cell-type specificity and single-cell resolution (Fu, Hardy, and Duff 2018).

Several studies indicate that DLK and LZK can direct compartment-specific responses such as regeneration or no regeneration of the axonal compartment, and degeneration of the distal axon. Even in a seemingly global response, such as cell death, these MAP3Ks can form distinct signaling complexes in the same neuron (Fernandes et al. 2014; Watkins et al. 2013). For example, following optic nerve crush, DLK signaling is required for death of the RGCs' soma but not for axon degeneration (Fernandes et al. 2014). It is possible that LZK is capable of compensating for DLK function in axon degeneration but not in somal degeneration. It is also likely that DLK forms distinct signaling complexes in different subcellular compartments. For axon degeneration, which does not require transcriptional activation, DLK is reported to associate with scaffold protein Sterile Alpha And TIR Motif Containing 1 (SARM-1) in the distal axon (Summers, Milbrandt, and DiAntonio 2018; Summers et al. 2020). For somal disintegration, which involves transcriptional activation, DLK is reported to associate with a JNK-interacting protein scaffold (Jin and Zheng 2019; Tedeschi and Bradke 2013). Moreover, the Wallerian degeneration slow mutation (WldS) mutation, which delays SARM-1 activation, prevents axonal degeneration but not somal death following optic nerve crush (Beirowski et al. 2008). Loss of BAX, a cell death activating protein downstream of JNK, prevents somal death but not axonal degeneration following optic nerve injury (Y. Li et al. 2000). These results

indicate that DLK and LZK form distinct signaling complexes in different subcellular compartments even within the same neuron.

Specificity lies in a precise signaling complexosome code:

Downstream of the specific environment, injury, cell type, and subcellular localization is the assembly of a signaling module. Different subcellular localizations have different protein compositions. The variety of outcomes seen in DLK and LZK activity reflect the variety of signaling partners with which they can be complexed locally resulting in distinct assembly signatures. Scaffolding proteins, E3 ligases, and protein chaperones determine the composition of locally available signaling partners.

It has been proposed that this specificity is a result of the formation of distinct signaling modules by specific scaffolds that assemble different downstream proteins (Elion 2001; Faux and Scott 1996; Qi and Elion 2005).Scaffolding proteins contain domains and sequence motifs with affinities to particular ligands. These affinities enable scaffolds to form specific signaling modules whose amplitude and duration they control. JNKs are the most commonly reported MAPKs participating in axon damage responses; therefore, investigating the different JNK-associated scaffolding proteins is key to deciphering DLK and LZK signal specificity. JNK scaffolds are known as JNK-interacting proteins (JIPs); each JIP has preferences for particular members of the MAP3K cascade (Whitmarsh 2006). JIPs include JIP1, JIP2, JIP3/JSAP1, JIP4/JPL, and POSH. JIPs were reported to have region-specific distribution in the brain of adult mice. While high levels of JIP3 and POSH were detected in the forebrain, the cerebellum has high levels of JIP1 (Goodwani et al. 2020). JIPs are also reported to form homo- and hetero-oligomers (Whitmarsh 2006) . Oligomerization may enable signal amplification, or offer additional specificity.

Along with JIPs, the presence or absence of particular E3 ligases could help explain the subcellular specificity of DLK and LZK action. E3 ligases mark protein targets for degradation, thereby providing local control of protein content (Pinto, Tomé, and Almeida 2021). These

ligases display specific subcellular localization in neurons. Active Cdc20-containing APC and NeuroD2 are present in the cell body. While Nedd4, CHIP, and HUWE1 activity are found in the axon shaft during axon outgrowth, ZNRF-1 and FBXW7 activity localizes to the axon shaft during axon degeneration. Active RPM-1, RNF, MEC15-containing SCF, and Cdh1-containing APC were reported in the presynaptic terminal, along with inhibited forms of Siah1 and Sel10-containing SCF. A developmental study in roundworms showed that a MEC15 mutation results in DLK-dependent inhibition of axon growth, whereas RPM-1 mutation facilitates axon growth (Zheng et al. 2020). These data bolster the idea that interaction partner availability affects the formation of distinct signaling complexes.

Chaperones are another group of proteins that can influence the interaction partners available to DLK and LZK. Chaperones ensure the proper folding and stabilization of their client proteins. Over the last three decades, it has become clear that chaperones play pivotal roles in the resolutions of CNS and PNS insults (Ousman, Frederick, and Lim 2017; Meriin and Sherman 2005). DLK is a client protein of the Heat Shock Protein 90 family (HSP90), which has an additional role in facilitating signaling complex assembly and sub-cellular specificity (Taipale, Jarosz, and Lindquist 2010). Pharmaceutical inhibition of HSP90 prevents DLK-mediated induction of axon regeneration in DRG cultures of adult mice and DLK-mediated injury signaling following ventral nerve crush in fly larvae (Karney-Grobe et al. 2018). Ectopic expression of HSP70 and HSP26 in the fly mushroom body protects axons from Wallerian degeneration in an age-dependent model of axon degeneration; HSP70 and HSP26 confers axon protection from Wallerian degeneration in a manner similar to WldS (Rallis, Lu, and Ng 2013). These findings indicate that specific chaperones can either support DLK signaling, as in axon regeneration, or counteract it, as in axon degeneration.

Since the consequences of DLK and LZK activation are context-specific, a clear understanding of the kinases' action *in vivo* is a prerequisite to their use as drug targets. It is important to determine all potential DLK- and LZK-dependent outcomes following axon injury, and the

specific cell types in which each arises. For the same reason, inhibiting or upregulating these MAP3Ks cannot occur on a global scale. While DLK and LZK inhibition may prevent cell death in some instances, their activity is also important for axon degeneration of the distal stump and regeneration of the proximal stump. Cell-type-specific treatment of axon damage in humans is the next biomedical frontier.

Zebrafish as a model to study axon regeneration:

While most invertebrate studies suggest that DLK is required for axon regeneration after injury, the consequences of DLK and LZK activation in vertebrates are more diverse. Indeed, rodent studies are more relevant to human health but, unlike invertebrates, they lack specificity and precision at the single cell level. Among vertebrate model organisms, DLK and LZK function in zebrafish is the least understood. Prior to this study, no zebrafish model existed to study DLK and LZK function. To clarify the disparate effects of DLK and LZK activation following neuronal insult, I created a zebrafish model.

This thesis recognizes that variability of outcomes observed in studies of neuronal injury poses a challenge to treatment. Here, I identify four experimental settings that need to be accounted for when evaluating and comparing study outcomes. Chapter 1 offers an experimental protocol that enables assessment of axon regeneration in zebrafish with single cell resolution. In chapter 2, I use this protocol to determine the effects of DLK and LZK activation in different cell types and after different types of injuries. In chapter 3, I seek to capture the cell-autonomous expressions of these kinases with enhancer traps.

Chapter 1:

Live imaging of axonal dynamics after laser axotomy of peripheral neurons in zebrafish

Kadidia P. Adula, Alvaro Sagasti

Affiliation: Department of Molecular, Cell and Developmental Biology, University of California, Los Angeles

Running head: Severing axons and imaging regeneration in live zebrafish

Abstract

Axon severing results in diverse outcomes, including successful regeneration and reestablishment of function, failure to regenerate, or neuronal cell death. Experimentally injuring an axon makes it possible to study degeneration of the distal stump that was detached from the cell body and document the successive steps of regeneration. Precise injury reduces damage to the environment surrounding an axon, and thereby the involvement of extrinsic processes, such as scarring or inflammation, enabling researchers to isolate the role that intrinsic factors play in regeneration. Several methods have been used to sever axons, each with advantages and disadvantages. This chapter describes using a laser on a 2-photon microscope to cut individual axons of touch-sensing neurons in zebrafish larvae, and live confocal imaging to monitor its regeneration, a method that provides exceptional resolution.

Keywords Axotomy, Transient transgenesis, Somatosensory, Regeneration, Axon, Zebrafish, Live imaging

1. Introduction

Outcomes of axon injury are variable. A severed axon may regenerate to reinnervate its correct target, fail to regenerate altogether, regenerate but grow in the wrong direction, or die. Successful axon regeneration is dictated by both intrinsic and extrinsic factors that integrate a balance of positive and negative cues *(1–4)*. Intrinsic factors refer to the state of signaling pathways in the injured neuron itself, while extrinsic factors are signals from nearby cells and the extracellular matrix. For example, in the mammalian central nervous system glial and immune cells release a myriad of both positive and negative factors *(5)*. These extrinsic cues make it difficult to experimentally disambiguate the contribution of intrinsic growth pathways from those of external factors in the axon regeneration process. Methods that use scissors or forceps to create injuries, including spinal cord, sciatic nerve, and optic nerve crushes, as well

as traumatic brain injury models, damage multiple axons and surrounding tissues, and are thus more likely to trigger extrinsic cells to participate in the axon injury response.

Determining an individual neuron's contribution to the repair process is essential for understanding the heterogeneous outcomes of repair responses. MicroPoint UV pulsed lasers and femtosecond lasers mounted on 2-photon microscopes can be used to target individual axons, but the latter offers more control and thus more precisely limits damage to the target *(6–15)* . Zebrafish (*Danio rerio*) is an excellent model organism in which to ask these questions because both its central and peripheral nervous systems are permissive to axon regrowth *(1, 16)*. Moreover, transient transgenesis can be used to label and image individual neurons in living animals. Zebrafish larvae have been used to elucidate mechanisms of Wallerian degeneration, axon regeneration, engulfment of axonal debris, and to characterize physiological changes during these processes *(17–21)*. This chapter describes precise axotomies in zebrafish using a laser mounted on a 2-photon microscope. Although this protocol focuses specifically on severing the peripheral axons of larval sensory neurons, called Rohon-Beard (RB) neurons *(22, 23)*, with different transgenes this approach can be easily adapted to study other types of zebrafish peripheral neurons, including motor and lateral line neurons.

2. Materials

2.1 Somatosensory neuron labeling

1. Zebrafish: 3–18-month-old type male and female fish (e.g., ZFIN: ZDB-GENO-960809-7)**.** Fish are kept in a 14/10 dark/light cycle. Embryos are raised in a 28.5℃ incubator until 5dpf.
2. 20ng/uL of tg(isl1[ss]: Gal4-VP16, UAS:DsRed) or Tg(isl1[ss]:Gal4-VP16,UAS:GFP) *(24)*
3. Pulled borosilicate glass needles (with a filament): 10cm in length, inner diameter (0.78mm), outer diameter (1.0mm).

4. Injection mold (2% agarose, molecular biology grade): add 0.8g of agarose, 50 mL of 1X E3 embryo buffer in a 500 mL Erlenmeyer flask. Obstruct the opening of the flask with a crumpled paper towel. Microwave the flask for 2 minutes, stopping every 20 seconds to swirl the flask (*see* **Note 1**), or until the agarose is fully dissolved. Cool until warm to the touch. Pour the agarose gel into a 10cm plate. Place a plastic micro-injection mold with straight ridges on top of the gel and press gently (*see* **Note 2**). Wait for the gel to solidify. Remove the plastic mold and store the 2% agarose gel at 4C.

2.2 Fish embryo cultivation

1. 60X E3 embryo buffer (1L): Dissolve 17.2g NaCl, 0.76g KCl, 2.9g $CaCl_2 \cdot 2H_2O$, 4.9g $MgSO_4 \cdot 7H_2O$ in deionized (ddH2O) water *(25)*, use 0.1 M NaOH to bring to pH 7.2. Autoclave.

2. 1X E3 embryo buffer: In a 20 L carboy, mix 333 mL of 60X E3 embryo buffer with 19.667 L of ddH2O, and twelve drops of 0.05 wt. % methylene blue aqueous solution. Store at room temperature (*see* **Note 3**).

2.3 Preventing pigment development

1. 50X PTU solution: Dissolve 0.3g of 1-phenyl 2-thiourea (PTU) in 200 mL of 1X E3 embryo buffer in a chemical hood. Heat the solution to 60℃ on a hot plate with a magnetic stirrer until dissolved. Divide the 50X stock solution (10mM) into 10 mL aliquots and store at -20℃.
2. E3P (E3 buffer with 0.2 mM PTU): Thaw 20 mL 50X PTU aliquot, mix with 980 mL of 1X E3 embryo buffer. Heat the 1L diluted solution to 60℃. Cool down to room temperature before use (*see* **Note 4**).

2.4 Anaesthetizing fish

1. Tricaine methanesulfonate (MS-222 or 3-amino benzoic acid ethyl ester): 400mg of tricaine in 97.9 mL of ddH2O, 2.1 mL of 1M Tris solution (pH 9.0), 0.1 M NaOH, pH to 7.0. Make 50 mL aliquots and store at -20℃. Keep an aliquot at 4℃ when in use.

2.5 Mounting embryos for imaging

1. 5mm-thick Delrin rings (*see* **Note 5**): Oval ring (inner diameter 12mm x 23mm, outer diameter 19mm X 30mm); circular ring (inner diameter 12mm, outer diameter 16mm) (Fig. 2)

2. Microscope cover glass: 24 X 60mm

3. Pre-cleaned and single frosted end glass slides: 75 X 25 X 1mm

4. Dow Corning high vacuum grease

5. A curved probe: Insert a black enameled insect pin into a microdissecting needle holder. Manually curve the insect pin tip.

6. For 1% agarose (molecular biology grade): Add 0.5g of low melting agarose, 50 mL of 1 X E3 embryo buffer in a 500 mL Erlenmeyer flask. Obstruct the opening of the flask with a crumpled paper towel. Microwave the flask for 2 minutes, stopping every 20 seconds to swirl the flask (*see* **Note 1**), or until the agarose is fully dissolved. Cool until warm to the touch and aliquot 1 mL of melted agarose into 1.5 mL tubes. Store the tubes in a 42℃-heat block with a cover to maintain temperature uniformity.

3. Methods

These instructions use Zeiss 800 series microscopes for laser axotomy and imaging, but this procedure can be adapted to any confocal microscope, imaging software, or standard operating parameters.

3.1 Injections

1. Set up zebrafish crossing tanks with adult male and female zebrafish in the evening. Separate males and females with a divider.

2. The next morning, remove the divider to allow the fish to breed. After ~20 minutes collect freshly fertilized eggs using a tea strainer and wash into a petri dish.

3. Bring the 2% agarose gel injection mold to room temperature. Gently load embryos into the mold (as described elsewhere in detail *(26)*). Fill the mold with 1 X E3 embryo buffer.

4. Load 20ng/uL of Tg(isl1[ss]: Gal4-VP16, UAS:DsRed) plasmid into a pulled glass needle (*see* **Note 6**).

5. Inject embryos at the 1- to 4-cell stage (Fig. 1) with 5nL of this plasmid (for details see *(26)*). Injecting plasmids into larvae at this stage results in transient expression. Since extrachromosomal plasmids are inherited unequally during cell division, this approach results in mosaic labeling of touch-sensing neurons (TSN) in the skin, making it possible to screen for animals with expression in isolated neurons (*see* **Note 7** and Fig. 1).

6. Maintain embryos in 1 X E3 embryo buffer and raise them in a 28.5C incubator.

3.2 Screening embryos

1. At 22-23 hours post-fertilization (hpf), exchange the medium for E3P (E3 + PTU). Pigment cells interfere with laser axotomy and make it difficult to image neuronal arbors; PTU inhibits pigmentation, enabling embryos to remain transparent (Fig. 2, upper right panel) (*see* **Note 8**).

2. A few hours before axotomy, manually dechorionate embryos using forceps (*see* **Note 9**).

3. To immobilize larvae, in a 10 cm dish with E3P, add ten drops of tricaine (~0.08%) with a 3 mL plastic pasteur pipette and monitor them under a microscope to confirm that they stop moving.

4. Screen through embryos to find animals with isolated labeled neurons, using a dissecting or compound fluorescence microscope (e.g., Zeiss, Axioskop 2 Fs Plus). For our experiments, we identified larvae with a single labeled neuron innervating the tail (*see* **Note 10** and Fig. 1).

5. Transfer screened larvae to a small petri dish. Label each dish, indicating whether the identified axon innervates the right or left side of the body. Animals must be mounted so that the side with the identified axon faces the coverslip, since laser illumination for severing and imaging does not penetrate through the animal.

6. Once screening is complete, replace media with E3P (without tricaine). Place the larvae in a 28.5℃ incubator until they reach the 48 hpf stage.

3.3 Mounting

1. Using a micropipette tip, collect and apply a thin layer of vacuum grease on one side of an oval mounting ring (*see* **Note 11**) and press the ring onto a clean cover glass (Fig. 2, top left panel).

2. When larvae are 48 hpf (Fig. 2, top right panel), anesthetize them with tricaine (10 drops, or ~0.08%). For larvae in a 10cm petri dish, 10 drops of tricaine is sufficient. If the larvae are in a 6cm petri dish, add fewer drops. Confirm that the animals have stopped moving.

3. Mix in one drop of tricaine into the 1% melted agarose tube. Use a glass pasteur pipette inserted into a pump pipettor (*see* **Note 12**) to pick up one anesthetized embryo with as little media as possible, and transfer it to a tube containing 1% low melting agarose. Use the pipette to transfer the larvae along with melted agarose onto the cover glass, inside the mounted ring (*see* **Note 13**). Rinse the inside of the glass pipette a few times with E3P + tricaine to remove residual agarose.

4. Arrange the animal in the molten agarose under a dissecting light microscope. Use a curved probe (Fig. 2, second right panel) to gently press the larva (the side with the labeled neuron), as close to the cover glass as possible (Fig. 2, third right panel and bottom panel). To target touch-sensing neurons in the tail, larvae should be mounted horizontally (on their sides) and the two eyes should be aligned when viewed from above. If the larva floats away from the cover slip, gently push it back down with the curved probe. The agarose should reach ~⅓ of the mounting ring in height. Wait ~15 minutes for the agarose to solidify (*see* **Note 14**).

5. Grease the other side of the mounted ring and fill the rest of the chamber with E3P + tricaine.

6. Press the microscope slide with the frosted end against the greased ring. Clean off any excess water around the mounted ring with a kimwipe (Fig. 2, third right panel and bottom panel).

3.4 Pre-axotomy imaging

1. Use a confocal microscope to collect images of the target neurons from living larvae (Fig. 3)**.** Imaging parameters for acquisition with a Zeiss LSM-800 (or LSM 880) upright microscope and

the Zen Blue 2.3 software are as follows: Under the “Acquisition Mode” tab, optimize imaging parameters, including: bits per pixel, image frame size, pixel dwell time, averaging, image size and pixel size. We usually use a 8 bits per pixel format, an image frame size of 512 X 512, a 1.52 usec pixel dwell time, a 1.86 sec scan time, an averaging number of 2, and a 1.25 um pixel size. Under the “Channels” tab, choose the appropriate laser wavelengths, gain, and pinhole diameter to image the neurons. For eGFP or dsRed, we use 488 nm and 561 nm laser lines, respectively, and a master gain of 650V. We set a pinhole diameter to an Airy unit of 1, which maximizes confocality.

2. Start the Zen Blue 2.3 software to visualize cells. If the system is being used for the first time that day, the stage and focus should be calibrated to avoid accidents (*see* **Note 15**). After hardware initialization is complete, a “Stage/Focus not calibrated” dialog window will appear. Select “Calibrate Now”. Calibration will take less than a minute. Maintain the stage at a 28.5C temperature with a heated stage or objectives.

3. Go to the “Acquisition” window and open your protocol. Go to the “Locate” window and under “Reflected Light” activate the “On” tab. Under “Favorites” select the “DsRed” configuration setting. Using the eyepiece, find the larva with the 10X objective (Plan-Neofluar, NA = 0.3) and center it in the field of view. Switch to a 20X (Plan-Apochromat, NA = 0.8) objective and focus on the axon.

4. Go to the “Acquisition” window. Open the DsRed fluorescent beam by checking and highlighting the “DsRed track” sub-tab in the “Channels” tab. Return to the protocol tab and press the “Live” tab to see the neuron on the screen. In the “Acquisition Mode” tab, you may adjust the zoom. Press the “Live” sub-tab in the protocol tab to image and center the axon (*see* **Note 16**).

5. Under the “Z-Stack” tab, optimize your “slice interval”; we usually set ours at 1 um. Use the manual focus knob, and the manual monitor to set the range of your z-stack by selecting a “Set First” slice position and a “Set Last” slice position. In the protocol tab, exit the “Live” mode.

Press the “Start Experiment” tab to acquire the pre-axotomy image (*see* **Note 17**). As the image acquires, a stack-by-stack 2D projection will be displayed on the monitor (*see* **Note 18**). Save the image as a “.czi” file.

3.5 Axotomies with a 2-photon microscope

1. For axotomies, we use a LSM-880 inverted confocal/2-photon microscope equipped with a laser (Chameleon, 690-1064 nm) for 2-photon imaging and Zen Black 2.1 SP3 software, but this procedure can be adapted to any equivalent microscope. To begin, turn the key on the 2-photon laser box from “Standby” to “On”. Let the power ramp up. Wait until the screen on the laser box displays the following messages: “Power: 3960 mV”, “813 nm” and “Status: Ok”.
2. Start the Zen Black 2.1 SP3 software to visualize the neuron. Go to the “Locate” window and under “Reflected Light” activate the “On” tab. Under “Configuration” select “DsRed”. Locate and center your sample through the objectives, starting with a 10X objective (Plan-Apochromat, NA = 0.45) to find the larva. Center the larva in the field of view before switching to a 20X objective (Plan-Apochromat, NA = 0.8) to focus on the axon.
3. Go to the “Acquisition” window. Activate the DsRed fluorescent laser by checking and highlighting the “DsRed track” sub-tab in the “Channels” tab. Return to the protocol tab and press the “Live” tab to see the neuron on the screen. In the “Acquisition Mode” tab, adjust the zoom to 1X zoom and center the peripheral axon in the field of view. Press the “Live” tab a second time to exit the “Live” mode and use the “Crop” tab to zoom into the area of the target axon. Zoom to a minimum of 100X. Ensure that DsRed fluorescence is below saturation by reducing the gain. Exit “Live” mode in the protocol tab. Imaging parameters for the axon severing protocol are as follows: Under the “Acquisition Mode” tab, optimize imaging parameters including: image frame size, pixel dwell time, scanning time, averaging, and pixel size. Use the imaging parameters described under Subheading 3.4. Under the “Channels” tab, choose the appropriate laser wavelengths, gain, pinhole diameter, and slice interval for your neurons.

4. Activate the 2-photon laser (813 nm) by checking and highlighting the “2-photon track” tab (*see* **Note 19**). Start with 5.0% laser power. In the protocol tab, press “Live” again for 1 second; a burst of fluorescence indicates damage to the axon. Exit “Live” mode. Turn off the 2-photon laser beam (813 nm) by unchecking and deselecting the “2-photon track” tab. Switch back to the “DsRed track” and return to 1X zoom to see if the axon is cut. It may take a few moments for the axon to be severed. Axon beading adjacent to the target site is a good indication that it will be severed. If the axon remains uncut, raise the 2-photon laser power in 0.5% increments and repeat, until cutting is successful (*see* **Note 20**).

5. At the end of the microscopy session, exit the program. A “Laser Off” window will appear. Turn off all the lasers and press “OK”.

6. Take a “post-axotomy” confocal image using the same settings as described for pre-axotomy under Subheading 3.4. Within a few hours post-axotomy, the detached branch will degenerate by Wallerian degeneration (Fig. 3, middle panel).

3.6 Larva recovery

1. Recover zebrafish larvae under a dissecting light microscope. Separate the cover slide from the mounting ring. The agarose might remain attached to the cover glass or detach to float in the E3P + tricaine-filled chamber formed by the mounting ring. In either case, use a glass pipette to remove media around the agarose. Remove the mounting ring.

2. Use a thin metal spatula or a razor blade to trim away the agarose surrounding the larva. Use 2 sets of forceps to carefully push away the remaining agarose from the larva. Pay particular attention not to puncture the yolk or damage the tail.

3. Once the larva is free, add a few drops of E3P. Use a glass pipette to transfer the larva from the glass slide to an individually labeled small petri dish. Fill the petri dish with E3P.

4. Allow 5-10 minutes for the larva to recover. When it responds to touch, put the petri dish back into the 28.5C incubator. After 24 hours, remount the larva and take a 24-hour post-axotomy image.

3.7 Post-regeneration imaging and time-lapse movies

1. Remount larvae to assess regeneration after the desired time-interval (*see* Subheading 3.3). We typically assess RB neuron regeneration 24 hours after axotomy. Image the neuron with the same confocal settings as described under Subheading 3.4.

2. In addition to taking static images of peripheral axons at specific time points, time-lapse movies of the regeneration process can be recorded. To record the first 12 hours post-injury, start the movie immediately after-axotomy (do not recover animals from the agarose). To record later phases of regeneration, recover the larva after axotomy (*see* Subheading 3.6), and remount it later (*see* **Note 21**). Set up imaging acquisition as described above, but add additional sections to the z-stack, both above and below the axon, to accommodate potential drift of the stage or neurons as the larva continues to grow. Using the “Time-series” option under the “Acquisition” tab, you can collect a single movie for up to 12 hours, without harming the animal. We typically collect movie frames at 5 minutes intervals for 144 cycles (12 hours). Using the “Tiles" option allows the recording of several movies within the same time period. To capture dynamics of an entire peripheral arbor, movies can be made using a 20X air or water objective. To focus on growth cone dynamics, use a 40-63X oil objective.

3.8 Peripheral axon arbor tracing

1. Most RB neurons have a single peripheral arbor (Fig. 4, left panel) which extends from the cell body and leaves the spinal cord to penetrate the skin, at which point it branches between epithelial cells, like the arbors of a tree *(22, 23)*. We compare arbor sizes pre-axotomy to arbor sizes immediately after axotomy and 24 hours post-axotomy. For tracing, use the Simple Neurite Tracer (SNT) plugin in FIJI *(27)* with the images in a z-stack format. SNT is part of FIJI’s Neuroanatomy suite (*see* **Note 22**).

3.9 Post-imaging processing

1. For presentation and analysis, use imageJ (FIJI) or other image processing software to produce maximum projections of the .czi files. We convert images to grayscale and invert them

before saving them as tiff images to maximize contrast. Multiple images of large neurons can be stitched together to create a complete representation.

4. Notes

1. Remove the crumpled paper towel and orient the flask away from you before swirling to release pressure. Reinsert the crumpled paper towel and return the flask to the microwave for the next 20-second heating cycle.

2. To make the agarose injection mold, a plastic mold is placed on the gel before it solidifies. For specific dimensions, see *(26)*. We use molds with straight ridges to make trenches into our 2% agarose injection molds. Trenches are used to align the embryos and secure the chorions in place for ease of injection. Plastic molds can imprint various shapes onto agarose gels, including spirals and linear trenches.

3. Ringer's solution optimized for zebrafish may also be used to grow zebrafish embryos *(29)*.

4. PTU crystals form during freezing and may not dissolve completely once thawed. Heating the solution to 60℃ will dissolve them. Let the solution cool to room temperature before use. If making several bottles of E3P, leave one out at room temperature for use, and store the rest at 4℃.

5. A white delrin acetal resin sheet, 5mm thick, was laser cut to fashion mounting rings. Alternatively, mounting rings can be 3D printed or cut from other materials. If you plan to treat mounted larvae with drugs during imaging, you may want to use rings made with sheets 2mm in thickness. These shorter rings will reduce the volume of the imaging chamber, and thus require less medium to fill the chamber. A 22mm X 22mm microscope cover glass may also be used.

6. Other transgenes can be used to label different neuron types *(e.g. 30, 31)*.

7. To achieve sparser labeling, and thus maximize the probability of labeling single neurons, inject the plasmid into the yolk between the 2- and 4-cell stages, rather than the 1-cell stage.

8. PTU specifically prevents the formation of the pigment melanin in zebrafish melanophores, which can obstruct neurons during imaging. Embryos should be switched to PTU-containing medium before the onset of melanogenesis in the skin. Alternatively, mutant embryos lacking pigment cells can be used *(32, 33)*.

9. To dechorionate embryos, use two forceps. Under the light microscope, being careful not to poke and injure the larva, pinch and hold the top of the chorion with the first forcep. Pinch the chorion with the second forcep, close to the first forcep, and gently pull the forceps apart to rip the chorion and free the wriggling larvae.

10. The cell body of a tail-innervating neuron may be anywhere in the caudal spinal cord, but its peripheral arbor typically arborizes at or posterior to the cloaca. Moreover, a tail-innervating neuron has an ascending central axon but no descending central axon.

11. A 10 mL syringe, with a Luer-Lok Tip, filled with vacuum grease can be used to facilitate the application of grease onto the sides of a mounting ring.

12. A pump pipettor offers more control than a bulb for transferring liquids with a glass pasteur pipette.

13. Several larvae can be simultaneously mounted within a ring; however, to keep track of individual larvae and facilitate rescue, mount a single larva in a circular ring and a maximum of two larvae in an oval ring.

14. If you are mounting larvae to record a time-lapse movie, wait more than 15 minutes for the agarose to solidify or until wrinkles can be seen over the surface of the agarose drop with the naked eye. This extra polymerization time ensures the solidity of the agarose, preventing the larva from drifting out of z-stack range.

15. To avoid crushing slides and potentially damaging objective lenses, the first user of the day should calibrate both the stage and the focus.

16. The “Stage” tab can be used to change the position of the neuron on the monitor with the mouse instead of using the manual knob. By clicking on the arrowheads of the “x-position” and

the “y-position”, the neuron can be moved to the left and right, or upwards and downwards respectively.

17. It can be useful, for presentation purposes, to collect separate images of the cell body and peripheral axon, since the spinal cord and the skin are at different focal depths. The images can then be collaged and stitched together using FIJI or Photoshop to create a complete representation of the neuron.

18. To see a preview of your image as a maximum projection before saving your image as a “.czi” file, go to the “Ortho tab”, select the “Ortho-Display” sub-tab, and select “Maximum Intensity Projection”.

19. At 813 nm, the 2-photon laser beam is out of the visible spectrum. Although the beam cannot be seen, the damage it inflicts can. Choose any wavelength to visualise the fluorescent debris resulting from the 2-photon laser damage; if severing is successful, a burst of light will appear across the screen.

20. It is essential to be patient at this step and switch back to the “DsRed track” to check for axonal damage after each 0.5% increase of the 2-photon laser (813 nm), whether or not there is a burst of fluorescence indicating the scattering of debris. Depending on how a larva is mounted, 5% to 8% of 2-photon laser power should be sufficient to cut an axon innervating the skin. As mounting between individual larvae varies slightly, starting at 5.0% for each larva is important. If more power is required to cut an axon, remount the larva. If remounting does not solve the issue, the 2-photon laser may need to be realigned.

21. In our experiments, we observed a slower axon regeneration rate for larvae that were in tricaine during 12-hour movies, in comparison with freely moving, unanesthetized larvae that were remounted after 12 hours. While tricaine does not block axon regeneration, the slowed growth rate could be related to its effect on a neuron’s electrical activity.

22. Note that a small number of RB neurons have more than one peripheral arbor; for example, a peripheral axon can branch in the spinal cord, creating a neuron with two separate peripheral

arbors innervating the skin. We measure total arbor length for such neurons by adding together the lengths of the two arbors. The point at which an axon exits the spinal cord is often detectable as a kink in the axon's trajectory. Lengths between branches of peripheral arbors can vary considerably, which can sometimes make a single arbor appear to be two separate arbors (Fig. 4, lower right panel).

Acknowledgements

KPA was supported by a Cota-Robles fellowship, Bridge to the Doctorate Fellowship, and NIH fellowship F31NS106742-02. This work was supported by NIH grant R01AR064582 (to AS).

Figure Legends

Fig. 1

Upper panels: zebrafish embryo at the 1-, 2-, and 4-cell stages. **Middle panel**: Cartoon of zebrafish larva with a single tail-innervating RB neuron depicted in red. RB cell bodies are located in the dorsal spinal cord. The peripheral axon, after exiting the spinal cord, arborizes upon reaching the skin. **Lower panel**: A tail-innervating RB neuron, with the cell body, the ascending central axon in the spinal cord, and the peripheral axon indicated. Arrowheads point to PTU-resistant pigment cells. The image was converted to grayscale and inverted. Scale bar, 100 μm.

Fig. 2

Left panel: Schematic of oval and circular rings with dimensions indicated. **Upper right panel**: Zebrafish larva at 48 hours post-fertilization. The larva was anesthetized with tricaine (E3P + tricaine). Middle right panel: Manually curved probe. **Lower right panel**: Two larvae mounted against a microscope cover slide. The larvae were sealed in an oval mounting ring, which was sandwiched between the microscope cover glass and a glass slide. The chamber was filled with

E3P with tricaine. **Bottom panel**: Labeled cartoon with a side-view of larvae mounted in an oval ring.

Fig. 3

At 48 hours post-fertilization, a touch-sensing neuron innervating the tail was imaged before axotomy. Using a laser mounted on a 2-photon microscope, its peripheral arbor was cut at the second branching point, and imaged again within the hour. The detached distal axon branch, outlined in red, underwent Wallerian degeneration a few hours after the injury. At 24 hours post-axotomy, the neuron was imaged again to assess regeneration. Regeneration from the injury site is shaded in green, and the spared branch is shaded in red. The ability to distinguish injury site regeneration from spared branches illustrates the clarity provided by labeling and injuring a single neuron. For display purposes, the image was converted to a maximum projection and inverted. Scale bar, 100 μm.

Fig. 4

Left panel: Cartoon depicting a RB neuron with a single peripheral arbor. The spinal cord is usually at a deeper focal plane than the peripheral arbor. **Upper right panel** : A RB neuron with two peripheral arbors. **Lower right panel**: A RB neuron with a single peripheral arbor with one significantly longer branch. The Simple Neurite Tracer plugin in FIJI was used to trace all images in a z-stack format.

Fig. 1

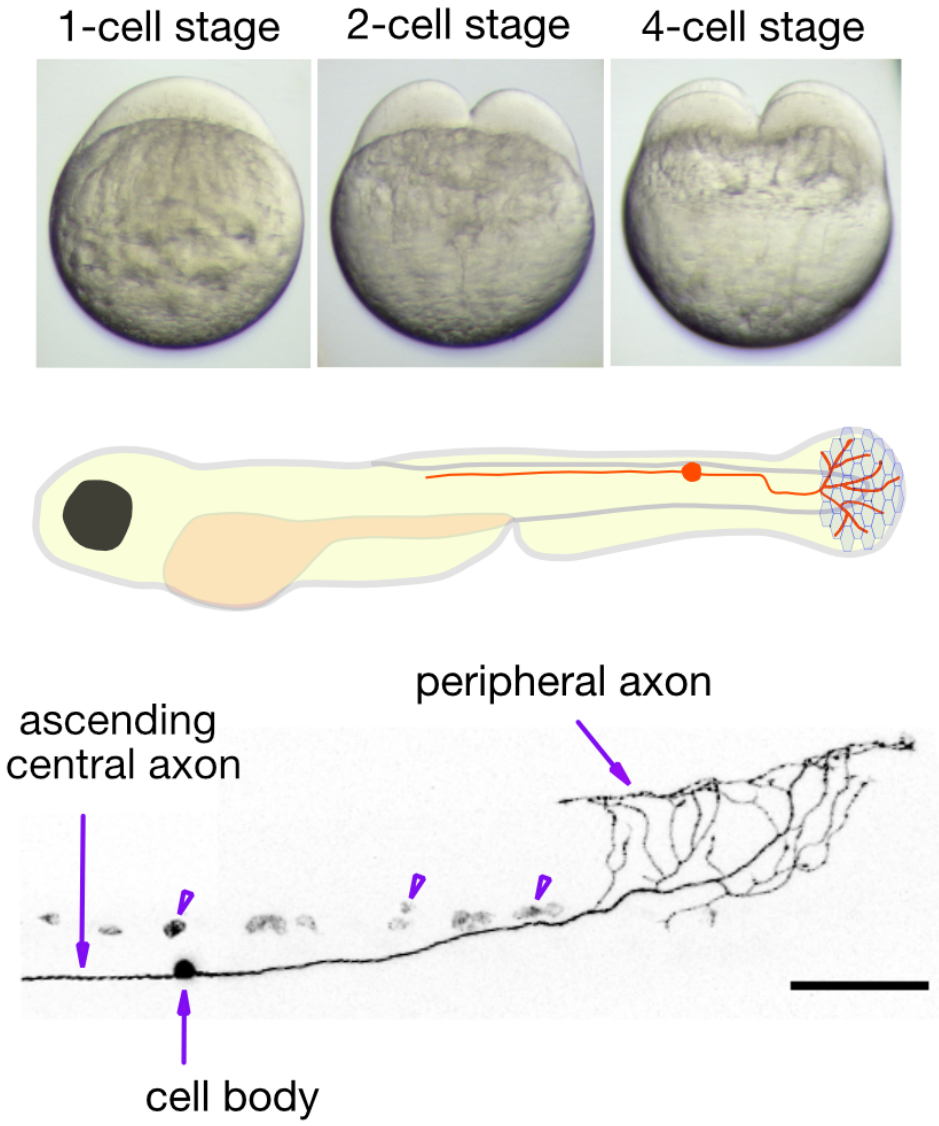
1-cell stage
2-cell stage
4-cell stage
peripheral axon
ascending
central axon
cell body

Fig. 2

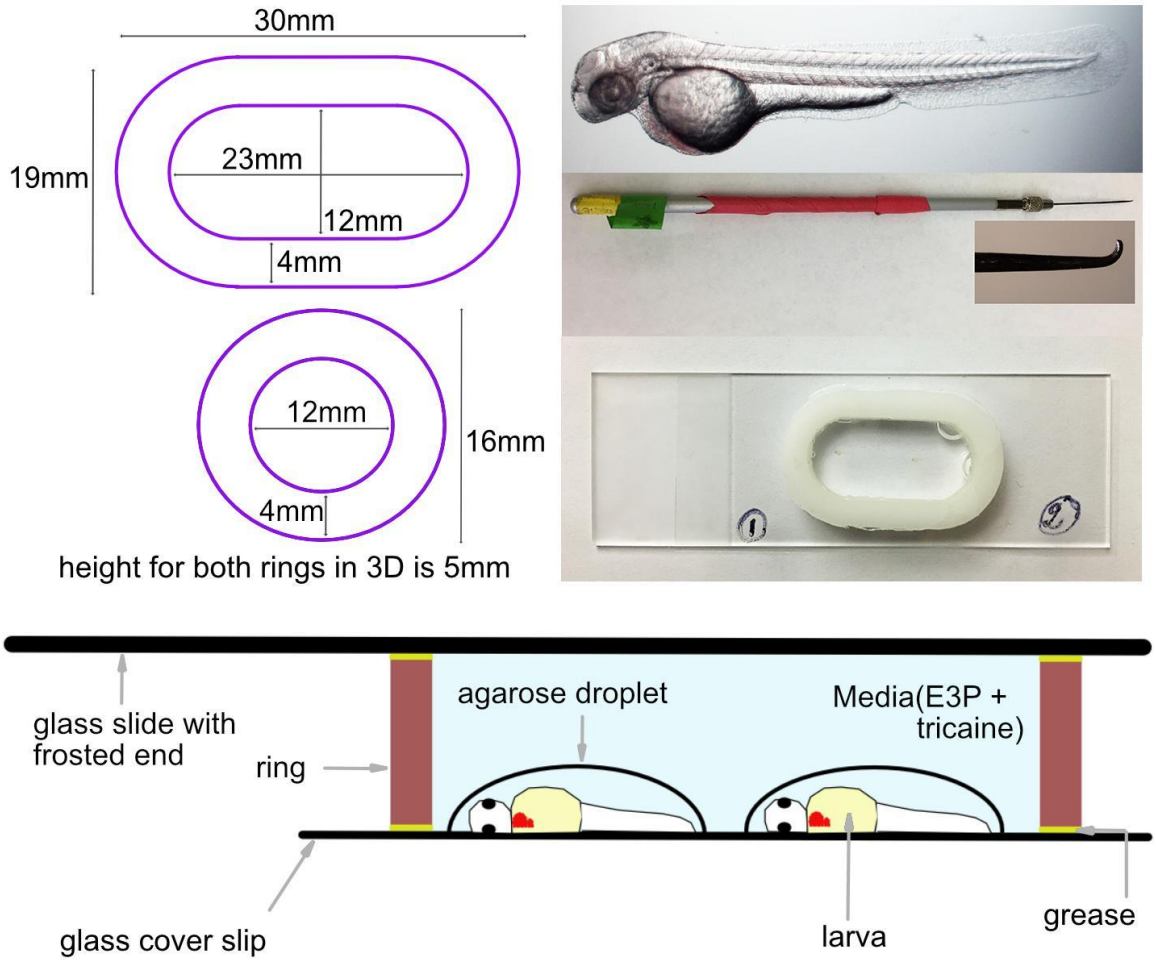
30mm
19mm
23mm
12mm
4mm
12mm
4mm
16mm
height for both rings in 3D is 5mm
glass slide with frosted end
ring
agarose droplet
Media(E3P + tricaine)
glass cover slip
larva
grease

Fig. 3

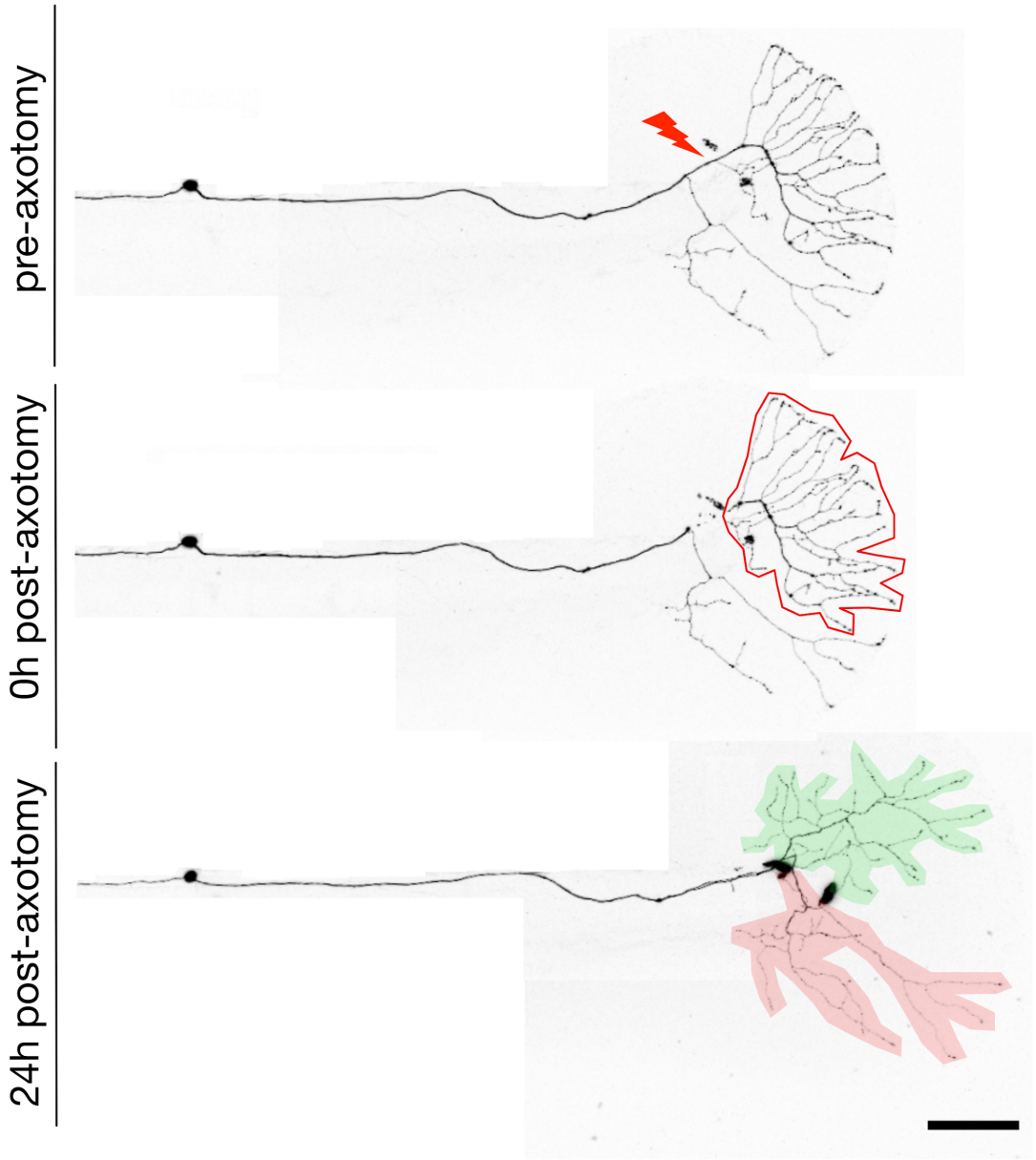

Fig. 4

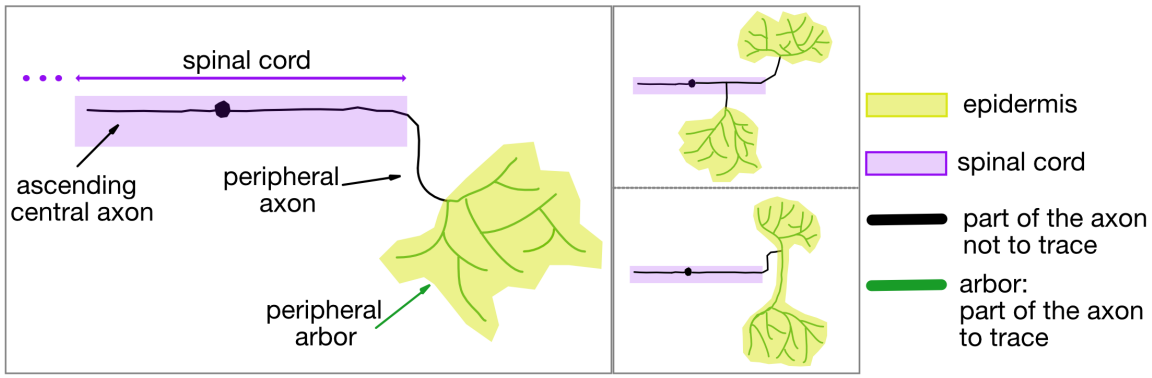
spinal cord
ascending
central axon
peripheral
axon
peripheral
arbor
epidermis
spinal cord
part of the axon
not to trace
arbor:
part of the axon
to trace

References

1. Rasmussen JP and Sagasti A (2016) Learning to swim, again: Axon regeneration in fish. Exp Neurol 287:318–330

2. Mahar M and Cavalli V (2018) Intrinsic mechanisms of neuronal axon regeneration. Nat Rev Neurosci 19:323–337

3. Huebner EA and Strittmatter SM (2009) Axon regeneration in the peripheral and central nervous systems. Results Probl Cell Differ 48:339–351

4. Uyeda A and Muramatsu R (2020) Molecular Mechanisms of Central Nervous System Axonal Regeneration and Remyelination: A Review. Int J Mol Sci 21:8116

5. Giger RJ, Hollis ER 2nd, and Tuszynski MH (2010) Guidance molecules in axon regeneration. Cold Spring Harb Perspect Biol 2:a001867

6. Stone MC, Albertson RM, Chen L, et al (2014) Dendrite injury triggers DLK-independent regeneration. Cell Rep 6:247–253

7. Wlaschin JJ, Gluski JM, Nguyen E, et al (2018) Dual leucine zipper kinase is required for mechanical allodynia and microgliosis after nerve injury. Elife 7:e33910

8. O'Brien GS, Rieger S, Martin SM, et al (2009) Two-photon axotomy and time-lapse confocal imaging in live zebrafish embryos. J Vis Exp 1129

9. Burgess HA and Granato M (2007) Sensorimotor gating in larval zebrafish. J Neurosci 27:4984–4994

10. Yanik MF, Cinar H, Cinar HN, et al (2004) Neurosurgery: functional regeneration after laser axotomy. Nature 432:822

11. Hammarlund M, Jorgensen EM, and Bastiani MJ (2007) Axons break in animals lacking beta-spectrin. J Cell Biol 176:269–275

12. Ylera B, Ertürk A, Hellal F, et al (2009) Chronically CNS-injured adult sensory neurons gain regenerative competence upon a lesion of their peripheral axon. Curr Biol 19:930–936

13. Jackson J, Canty AJ, Huang L, et al (2015) Laser-Mediated Microlesions in Mouse

Neocortex to Investigate Neuronal Degeneration and Regeneration. Curr Protoc Neurosci 73:2.24.1–2.24.17

14. Allegra Mascaro AL, Sacconi L, and Pavone FS (2010) Multi-photon nanosurgery in live brain. Front Neuroenergetics 2:21

15. Bormann P, Zumsteg VM, Roth LWA, et al (1998), Target contact regulates GAP-43 and alpha-tubulin mRNA levels in regenerating retinal ganglion cells. J Neurosci 52(4):405:-419

16. Bastmeyer M, Beckmann M, Schwab ME, et al (1991) Growth of regenerating goldfish axons is inhibited by rat oligodendrocytes and CNS myelin but not but not by goldfish optic nerve tract oligodendrocyte like cells and fish CNS myelin. J Neurosci 11:626–640

17. Vargas ME, Yamagishi Y, Tessier-Lavigne M, et al (2015) Live Imaging of Calcium Dynamics during Axon Degeneration Reveals Two Functionally Distinct Phases of Calcium Influx. J Neurosci 35:15026–15038

18. Rasmussen JP, Sack GS, Martin SM, et al (2015) Vertebrate epidermal cells are broad-specificity phagocytes that clear sensory axon debris. J Neurosci 35:559–570

19. Lewis GM and Kucenas S (2013) Motor nerve transection and time-lapse imaging of glial cell behaviors in live zebrafish. J Vis Exp. doi:10.3791/50621

20. Rosenberg AF, Wolman MA, Franzini-Armstrong C, et al (2012) In vivo nerve-macrophage interactions following peripheral nerve injury. J Neurosci 32:3898–3909

21. Rieger S and Sagasti A (2011) Hydrogen peroxide promotes injury-induced peripheral sensory axon regeneration in the zebrafish skin. PLoS Biol 9:e1000621

22. Palanca AMS, Lee S-L, Yee LE, et al (2013) New transgenic reporters identify somatosensory neuron subtypes in larval zebrafish. Dev Neurobiol 73:152–167

23. Katz HR, Menelaou E, and Hale ME (2021) Morphological and physiological properties of Rohon-Beard neurons along the zebrafish spinal cord. J Comp Neurol 529:1499–1515

24. Sagasti A, Guido MR, Raible DW, et al (2005) Repulsive interactions shape the morphologies and functional arrangement of zebrafish peripheral sensory arbors. Curr Biol

15:804–814

25. Cold Spring Harbor Laboratory Press (2021). 1559-6095. http://cshprotocols.cshlp.org. Accessed 13 May 2021

26. Rosen JN, Sweeney MF, and Mably JD (2009) Microinjection of zebrafish embryos to analyze gene function. J Vis Exp. doi: 10.3791/1115

27. Schindelin J, Arganda-Carreras I, Frise E, et al (2012) Fiji: an open-source platform for biological-image analysis. Nat Methods 9:676–682

29. The Zebrafish Information Network (1994-2021). https://zfin.atlassian.net. Accessed 13 May 2021

30. Stil A and Drapeau P (2016) Neuronal labeling patterns in the spinal cord of adult transgenic Zebrafish. Dev Neurobiol 76:642–660

31. Satou C, Kimura Y, Hirata H, et al (2013) Transgenic tools to characterize neuronal properties of discrete populations of zebrafish neurons. Development 140:3927–3931

32. Lister JA, Robertson CP, Lepage T, et al (1999) nacre encodes a zebrafish microphthalmia-related protein that regulates neural-crest-derived pigment cell fate. Development 126:3757–3767

33. D'Agati G, Beltre R, Sessa A, et al (2017) A defect in the mitochondrial protein Mpv17 underlies the transparent casper zebrafish. Dev Biol 430:11–17

Chapter 2:

Anatomy of zebrafish motor and Rohon-Beard touch-sensing neurons

To determine whether DLK and LZK outcomes following axon injury are cell-type-specific, I compare two neuronal cell types with distinct structures: motor neurons (MNs) and touch-sensing neurons. The following sections give a brief description of their anatomies.

Motor neurons innervate muscles and their signaling enables movement. The bodies of zebrafish larvae are arranged into repeating muscle segments. Muscle segments are further divided into dorsal and ventral myotomes and innervated by primary MNs (Issa et al. 2011). MNs express Homeobox Protein 9 (HB9), also known as Pancreas and Motor Neurons Homeobox Protein 1 (MNX1). There are 3 subtypes of primary MNs: rostral primary MN (RoP), middle primary MNs (MiP), and caudal primary MN (CaP). Rop MNs innervate dorsal muscles and grow in an upwards direction. MiP MNs innervate dorsal muscles in a downward direction but stop at the myoseptum or the separation between dorsal and ventral myotomes. Cap MNs innervate the ventral muscles. With their cell bodies positioned in the spinal cord, a bouquet containing each MN subtype exits the spinal cord at a common point; this arrangement is repeated in all muscle segments. The dendrites of larval MNs are small in comparison to the axon, and remain in the spinal cord.

There are three types of somatosensory neurons in zebrafish: Rohon-Beard (RB) and dorsal root ganglion (DRG) neurons, which innervate the body, and trigeminal (TG) neurons, which innervate the head (Wang, Julien, and Sagasti 2013; Katz, Menelaou, and Hale 2021). All vertebrate touch-sensing neurons are pseudounipolar. Instead of having dendrites and an axon, vertebrate somatosensory neurons have one axon that splits into two to innervate separate targets: a canonical central axon which remains in the spinal cord and a peripheral axon that senses touch stimuli in the skin. Microtubules are important structural elements in neurons and their organization distinguishes axons from dendrites. In axons, the growing ends of

microtubules are oriented towards the cell body, whereas in dendrites, the growing ends face away from the cell body or are a combination of microtubules facing away from and others towards the cell body (Burton and Paige 1981; Heidemann, Landers, and Hamborg 1981). RB neurons are transient touch-sensing neurons that innervate the body of zebrafish larvae. Most of this neuronal population is replaced by DRG as the zebrafish gets older.

There are several subtypes of RBs but their distinct categorization is not well understood. However, all RBs express the enhancer islet somatosensory 1 (isl1 [ss]). RB cell bodies are in the spinal cord; they extend a central axon connecting to downstream targets and a peripheral axon that exits the spinal cord to emerge in the skin. Once in the skin, the axon arborizes and tapers into free endings that sense mechanical, thermal, and chemical stimuli. Unlike RBs, the cell bodies of DRG and trigeminal neurons are organized into ganglia outside of the spinal cord. A DRG ganglion is found beneath the spinal cord; this arrangement is repeated in all segments of the body. From this position, each ganglion extends a central nerve to connections within the spinal cord. A peripheral nerve reaches into the skin, where it branches into free axonal endings. One TG ganglion is situated on each side of the head. All RBs express the enhancer islet somatosensory 1 (isl1[ss]). TG neurons can also be visualized using isl1[ss]. An enhancer from the P2RX3 gene drives expression in DRG neurons and also in a subset of RB neurons (Palanca et al. 2013).

Title:

The MAP3Ks DLK and LZK direct diverse responses to axon damage in zebrafish peripheral neurons

Authors:

Kadidia Pemba Adula[1], Mathew Shorey[2], Vasudha Chauhan[1], Khaled Nassman[1], Shu-Fan Chen[1], Melissa M Rolls[2], and Alvaro Sagasti[1,*]

Affiliations:

[1] Molecular, Cell and Developmental Biology Department and Molecular Biology Institute, University of California, Los Angeles, CA 90095

[2] Department of Biochemistry and Molecular Biology and the Huck Institutes of the Life Sciences, The Pennsylvania State University, University Park, PA 16802

* Corresponding author: sagasti@mcdb.ucla.edu

Abstract:

The MAP3Ks Dual Leucine Kinase (DLK) and Leucine Zipper Kinase (LZK) are essential mediators of axon damage responses, but their responses are varied, complex, and incompletely understood. To characterize their functions in axon injury, we generated zebrafish mutants of each gene, labeled motor neurons (MN) and touch-sensing neurons in live zebrafish, precisely cut their axons with a laser, and assessed the ability of mutant axons to regenerate. DLK and LZK were required redundantly and cell autonomously for axon regeneration in MNs, but not in larval Rohon-Beard (RB) or adult dorsal root ganglion (DRG) sensory neurons. Surprisingly, in *dlk lzk* double mutants, the spared branches of wounded RB axons grew excessively, suggesting that these kinases inhibit regenerative sprouting in damaged axons. Uninjured trigeminal sensory axons also grew excessively in mutants when neighboring neurons were ablated, indicating that these MAP3Ks are general inhibitors of sensory axon growth. These results demonstrate that zebrafish DLK and LZK promote diverse injury responses, depending on the neuronal cell identity and type of axonal injury.

Significance statement:

The MAP3Ks DLK and LZK are damage sensors that promote diverse outcomes to neuronal injury, including axon regeneration. Understanding their context-specific functions is a prerequisite to considering these kinases as therapeutic targets. To investigate DLK and LZK cell-type specific functions, we created zebrafish mutants in each gene. Using mosaic cell labeling and precise laser injury we found that both proteins were required for axon regeneration in motor neurons, but, unexpectedly, were not required for axon regeneration in Rohon-Beard or dorsal root ganglion (DRG) sensory neurons, and negatively regulated sprouting in the spared axons of touch-sensing neurons. These findings emphasize that animals have evolved distinct mechanisms to regulate injury site regeneration and collateral sprouting, and identify differential roles for DLK and LZK in these processes.

Introduction:

Axon damage caused by stroke, trauma, or disease disrupts the circuits required for sensation, movement and cognition. Unlike other tissues that rely on stem cells to recover from damage, most neurons cannot be replaced, so damaged cells must themselves be repaired to restore function. Successful axon regeneration requires damage sensing, the transmission of injury signals to the nucleus, activation of pro-regenerative genes, axon guidance, and circuit reintegration (Curcio and Bradke, 2018). Our understanding of the factors regulating each of these steps is incomplete.

Mitogen-activated protein kinase kinase kinases (MAP3Ks) regulate many cellular processes, including development, differentiation, and stress responses (Craig et al., 2008). Among MAP3Ks, Dual Leucine Kinase (DLK/MAP3K12), which belongs to the Mixed Lineage Kinase (MLK) MAP3K subfamily (Gallo and Johnson, 2002), has been implicated in neuronal development (Nakata et al., 2005; Hirai et al., 2006, 2011) and axon injury responses (Hammarlund et al., 2009; Miller et al., 2009; Xiong et al., 2010; Welsbie et al., 2017, 2019) in a variety of organisms. DLK is activated by axon injury and in turn activates downstream P38 or JNK signaling cascades to induce transcription of injury response genes (Tedeschi and Bradke, 2013; Jin and Zheng, 2019). In addition to DLK itself, vertebrates have another DLK-related gene that contributes to injury responses, Leucine Zipper Kinase (LZK/MAP3K13), which has a domain analogous to the calcium-sensing domain in the worm DLK protein (Yan and Jin, 2012).

In invertebrates, activation of DLK is a major signal initiating responses to axon injury and stress. Without DLK, regenerative axon growth is eliminated in motor and sensory neurons in both *C. elegans* (Hammarlund et al., 2009; Yan et al., 2009) and *Drosophila* (Xiong et al., 2010; Stone et al., 2014). In mammals, the outcomes of DLK and LZK activation in response to axon damage

are varied and context-dependent: DLK or LZK can promote neurite branching (Chen et al., 2016b), axon elongation (Shin et al., 2012), inhibition of axon regeneration (Dickson et al., 2010), axon degeneration of the distal stump (Miller et al., 2009; Summers et al., 2018), cell death (Ghosh et al., 2011; Watkins et al., 2013; Yin et al., 2017; Welsbie et al., 2019; Li et al., 2021), or microglial and astrocyte responses to injury (Chen et al., 2018; Wlaschin et al., 2018). In mice with a DLK gene-trap, downstream responses were reduced after sciatic nerve injury, and explant cultures of DRG grew shorter axons than controls (Itoh et al., 2009). Selectively eliminating DLK in neurons strongly reduced motor axon target reinnervation after sciatic nerve crush (Shin et al., 2012). Peripheral axons of DLK mutant DRG neurons, on the other hand, initiated regeneration normally, but by three days post-injury had regenerated less than controls (Shin et al., 2012).

Studying genetic regulators of axon regeneration is complicated by the complexity of in vivo experimental injuries. In nerve crush or severing models, nerve bundles contain axons of many different types of neurons, thus convoluting cell type-specific responses to injury. Moreover, axon branching and fasciculation within nerves can obscure the source of growth after incomplete injuries--without single cell resolution, it is difficult to distinguish axon growth from regenerating neurites, regenerative sprouting from unsevered branches of damaged cells, or collateral sprouting from undamaged neurons (Steward et al., 2003; Tuszynski and Steward, 2012), each of which has distinct functional implications.

To better understand the roles of *dlk* and *lzk* in axon damage responses, we created zebrafish mutants in both genes. Single-cell labeling allowed us to compare regeneration not only in different cell types, but also in central axons, peripheral axons, and specific branches of damaged axons. Our findings indicate that *dlk* and *lzk* are required redundantly for motor axon regeneration, but not for axon regeneration in RB or DRG neurons. Surprisingly, DLK inhibited sprouting of

larval peripheral sensory axons, emphasizing the context-dependent multifunctionality of these axon damage sensors.

Results:

dlk^{la231} and *lzk*^{la232} mutant zebrafish develop normal motor and sensory neurons

To study the functions of zebrafish DLK and LZK in axon regeneration, we identified the closest homologous genes to mammalian DLK and LZK in the zebrafish genome, which were located on opposite ends of chromosome 9, and generated a phylogenetic tree with the full amino acid sequences (Figure 1A). Human, mouse, and zebrafish DLK proteins share 93% sequence similarity in their kinase domain, and 95% similarity in their leucine zipper domains; human, mouse, and zebrafish LZK proteins share 97% sequence similarity in their kinase domain, 98% similarity in their leucine zipper domains, and an identical C-terminal hexapeptide involved in calcium regulation.

We created mutations in each gene using the CRISPR/Cas9 system. Using two guide RNAs (gRNAs), we made a 3289 base pair (bp) genomic deletion in zebrafish *dlk*, which removed 519 coding base pairs, including most of the kinase domain. Using the same approach to target LZK, we created an allele with two separate deletions in exon 1 (a 28 base pair deletion and a 30 base pair deletion), placing the gene out-of-frame, upstream of the kinase domain (Figure 1B). Unlike DLK mutant mice, which die perinatally (Hirai et al., 2006), *dlk*^{la231}, *lzk*^{la232}, and *dlk*^{la231} *lzk*^{la232}double mutant zebrafish survived to adulthood and appeared grossly normal, similar to mutants in invertebrate DLK homologs, although both mutants were slightly smaller on average than wildtype fish at three larval stages (48 hpf, 72 hpf, and 5 dpf), indicating a developmental delay (Figure 1C-E).

Zebrafish *dlk* mRNA is expressed broadly in the nervous system at early developmental stages (Thisse et al., 2004), prompting us to test if *dlk* is required for the initial development of peripheral neurons. To label motor neurons (MNs), one-cell stage embryos were co-injected with MN driver (HB9:GAL4) (Issa et al., 2011) and effector (UAS:GFP) transgenes, which drive expression of cytoplasmic GFP. Since transient transgenesis results in mosaic inheritance, we screened for animals expressing GFP in isolated MNs. To minimize morphological variability, we selected only those MNs that innervated ventral muscles (Figure 2A_B), enriching for the caudal primary (CaP) MNs (Westerfield et al., 1986). At 5 days post-fertilization (dpf) we imaged each MN and measured several morphological parameters, including axon branch tip number, and total axon length. Despite the fact that mutant animals are slightly smaller than controls, there were no significant differences in neuronal morphology between *dlk*^{la231}, *lzk*^{la232}, or *dlk*^{la231} *lzk*^{la232} double mutants and wt animals (Figure 2C-D). These observations indicate that *dlk* and *lzk* are not required for the morphological development of MNs.

To image larval RB touch-sensing neurons (Palanca et al., 2013; Katz et al., 2021), we injected animals with a reporter driving expression of a red fluorescent protein in these cells (Isl1[SS]:Gal4;UAS:DsRed) (Sagasti et al., 2005), and screened for animals expressing this reporter in isolated RB neurons, which allowed us to unambiguously visualize the morphology of the entire neuron and distinguish central from peripheral axons. To minimize variability, we selected only tail-innervating RB neurons for analysis, since they are flat and relatively easy to trace (Figure 3A-B). As with MNs, there were no significant morphological differences between the peripheral arbors of *dlk*^{la231}, *lzk*^{la232}, or *dlk*^{la231} *lzk*^{la232} double mutant and wt fish at 48 hours post-fertilization (hpf) (Figure 3C-E). At 72 hpf, *dlk*^{la231} and double mutant peripheral axon morphologies were also comparable to wildtype axons, but *lzk*^{la232} neurons were somewhat smaller than wildtype neurons on average, potentially reflecting their mild developmental delay.

Together these results indicate that, similar to homologs in invertebrate animals, DLK and LZK do not play major roles in initial neuronal development.

dlk and *lzk* are redundantly required for motor axon regeneration

Few studies have directly tested the relationship between these two closely related, potentially redundant MAP3K proteins in axon damage responses. To assess if *dlk* or *lzk* are required for motor axon regeneration in larval zebrafish, we severed axons of isolated MNs in wt, single mutant, and double mutant fish, and compared their ability to regenerate. Specifically, 5 dpf axons were severed 50 µm distal to the spinal cord exit point (Figure 4A), using a laser mounted on a 2-photon microscope (O'Brien et al., 2009b). To minimize potential contributions from extrinsic factors, only neurons in which laser axotomy caused no obvious damage or scars were used for regeneration experiments. Motor axons were assessed for regeneration 48 hours post-axotomy (hpa) (Figure 4A), as in previous studies (Rosenberg et al., 2012). Wallerian degeneration appeared to occur normally in these mutants. Motor axon regeneration was modestly reduced in dlk^{la231} mutants, compared to wt motor axons, but strongly impaired in dlk^{la231} lzk^{la232} double mutants (Figure 4B-C). These observations suggest that *dlk* and *lzk* are partially redundant (or genetically compensate for each other) for regeneration of larval motor axons.

Intriguingly, we observed that among dlk^{la231} lzk^{la232} double mutant MNs displaying severe regeneration deficits, ~28% (8 out of 29) grew extremely long neurites within the spinal cord, which are likely dendrites (Figure 4D), a phenotype not seen in individual dlk^{la231} or lzk^{la232} mutants. This observation indicates that dlk^{la231} lzk^{la232} double mutant axons do not lack growth potential, but are specifically impaired in axon regeneration.

To determine if *dlk* or *lzk* are required cell-autonomously for motor axon regeneration, we attempted to rescue their regeneration defects by expressing *dlk* and *lzk* cDNAs specifically in

these neurons. Since *dlk* and *lzk* were required redundantly for motor axon regeneration, we expressed each cDNA separately in *dlk*^{la231} *lzk*^{la232} double mutants. Strong overexpression of these cDNAs with the Gal4/UAS system was toxic to neurons, causing dysmorphic axons, spontaneous axon degeneration, and cell death (not shown). We therefore expressed lower levels by creating bicistronic transgenes directly under a MN-specific promoter (HB9:DLK-T2A-GFP and HB9:LZK-T2A-GFP), which were co-injected with transgenes that strongly drive RFP expression throughout the cytoplasm (HB9:Gal4 and UAS:DsRed). Only cells that clearly expressed the rescue transgene (i.e., GFP+ cells), and had overtly normal axons, were used for these experiments (Figure 4A). Expressing each cDNA improved axon regeneration to levels comparable to the corresponding single mutant (e.g., *dlk*^{la231} *lzk*^{la232} neurons with *dlk* cDNA were comparable to *lzk*^{la232} mutants, Figure 4B-C). However, the difference in regeneration between rescued neurons and double mutants did not reach significance, likely due to variability in the assay. Nonetheless, these results are most consistent with DLK and LZK proteins acting cell-autonomously to promote motor axon regeneration, similar to DLK's well documented role in axon regeneration in worms, flies, and mice.

dlk and *lzk* are not required for RB central or peripheral axon regeneration

RB neurons are bipolar or pseudo-unipolar, with a receptive peripheral axon that innervates the epidermis and a central axon that connects to downstream circuits in the spinal cord (Palanca et al., 2013; Katz et al., 2021). Unlike in mammals, fish can often regenerate axons in the central nervous system (Rasmussen and Sagasti, 2016). To visualize RB neurons, we used the *Islet1*(ss) enhancer, which drives expression in all touch-sensing neurons (Higashijima et al., 2000; Sagasti et al., 2005). To identify a time point for regeneration experiments, we characterized the structure of tail-innervating RB neuron arbors as development progressed, with the aim of finding a stage when RB neurons were morphologically stable, but still expressed the transgene strongly. These analyses led us to choose 48 hpf for axotomies, since approximately ⅔ of RB peripheral arbors

in the tail had attained a stable branching pattern (i.e., new branches were no longer added) at this time point, although they continued to grow bigger via scaling growth.

To test if *dlk* or *lzk* are required for the regeneration of zebrafish RB central axons, we transiently labeled isolated RB neurons in the tail, laser severed their ascending central axons 200 µm from the cell body, and measured the total length of regenerated axons at 24 hpa (Figure 5A-B). We were careful to use the minimal effective laser power for axotomy, since we observed that even moderate damage and scarring in the spinal cord impedes regeneration. Surprisingly, RB central axons in dlk^{la231}, lzk^{la232}, and dlk^{la231} lzk^{la232} double mutants regenerated similar to wt neurons (Figure 5B). In fact, some central axons regenerated more on average than wt axons, although this effect did not reach significance. These data indicate that, unlike zebrafish motor axons, or central axons of sensory neurons in invertebrates and mice, central axons of RB neurons in zebrafish larvae do not require *dlk* or *lzk* for regeneration.

To test if *dlk* or *lzk* are required for the regeneration of RB peripheral axons, we labeled isolated tail-innervating RB neurons, removed the entire peripheral arbor by severing it at the first peripheral branch point at 48 hpf, and measured regeneration at 24 hpa (Figure 6A). (When a neuron had two arbors separately innervating the skin, both were removed). Although a few axons in each genotype failed to regrow, most severed peripheral axons in single and double mutants regenerated comparable to wt, whether measured as total axon growth or as percent regeneration of the severed arbor (Figure 6B-C). Although all genotypes regenerated on average similar size arbors (Figure 6B), there were some differences in regeneration between different mutant genotypes when measured as percent regeneration of the original arbor (Figure 6C), reflecting that each group had different sized arbors to begin with. Thus, neither central nor peripheral RB axons require DLK or LZK for regeneration.

dlk and _lzk_ are not required for DRG neuron peripheral axon regeneration in adult zebrafish

The finding that DLK and LZK are not required for regeneration of RB axons was surprising, since MNs in the same genetic background failed to regenerate and DLK signaling has been implicated in regeneration of another sensory neuron type, DRG neurons in culture and adult mice (Itoh et al., 2009; Shin et al., 2012). We therefore considered the possibility that RB neurons, which are replaced by DRG neurons over the course of development (Reyes et al., 2004; Rasmussen et al., 2018), might use a repair strategy different from neurons that persist into adulthood. To determine if DRG neurons require DLK and LZK for regeneration, we imaged them in a line stably expressing mCherry in sensory neurons (P2rx3a:LexA,4xLexAop:mCherry^{la207}), in wildtype, *dlk*^{la231}, *lzk*^{la232}, and *dlk*^{la231} *lzk*^{la232} double mutant animals. Some genotypes were crossed to the *casper* mutant background, which lacks pigmentation (White et al., 2008) to facilitate imaging (see Methods for details of transgenic genotypes). We first examined regeneration of adult (8–11-month-old) DRG neurons by severing sensory nerves immediately above and under a scale (Figure 7), as these nerves were easily accessible for injury with a pulsed UV laser (Rasmussen et al., 2018). Adult fish were intubated during injury and subsequent imaging sessions (Shorey et al., 2021). By 24 hours after axotomy, neurites distal to the cut site had degenerated, and by 96 hpa, scales were again fully innervated, comparable to pre-axotomy conditions, in wt, *dlk*^{la231}, *lzk*^{la232}, and *dlk*^{la231} *lzk*^{la232} double mutants (n= 10 wt; n= 7 *dlk*^{la231}; n= 5 *lzk*^{la232}; n= 5 double mutants) (Figure 7).

A previous study showing reduced regeneration of DRG peripheral axons in DLK mutant neurons monitored regrowth after injury closer to the cell body (Shin et al., 2012), so we considered the possibility that surface damage of sensory axons might be so common that it does not require DLK/LZK signaling. We thus severed DRG nerves close to the ganglion, using 2-photon laser surgery in 4–5-week-old juvenile fish (Figure 8A). At this age, DRG sensory arbors on the scale surface have not yet achieved a fully mature morphology, but tail-innervating neurites were indistinguishable from those of adults. We specifically cut the peripheral nerve exiting the most

caudal tail-innervating DRG (potentially the equivalent of the sacral ganglion nerve) at approximately 100 microns from the ganglion, resulting in the complete loss of tail fin innervation along the dorsal-most fin rays (Figure 8B). Surprisingly, the nerve regenerated robustly in both wt and *dlk*^{la231} *lzk*^{la232} double mutants (n= 5 wt; n= 6 double mutants); by 96hpa regenerated axons had reached the end of the tail (Figure 8B). Thus, unlike motor axons, sensory axons of RB and DRG neurons do not require LZK and DLK for regeneration.

Spared branches of damaged RB peripheral axons sprout excessively in *dlk*^{la231} *lzk*^{la232} double mutants

Axon regeneration from severed neurites, regenerative sprouting from spared branches of damaged axons, and collateral sprouting from undamaged axons are distinct processes (Steward et al., 2003; Tuszynski and Steward, 2012). Our single RB neuron labeling technique provided an opportunity to ask if DLK or LZK play distinct roles in these processes. To compare the behavior of severed and spared branches of a damaged axon, we severed RB peripheral axons at the second branch point, sparing the first branch (Figure 9A-B). Surprisingly, partially axotomized peripheral axons in *dlk*^{la231} and *lzk*^{la232} mutants regenerated more than wt axons--in other words, mutant axons gained more total peripheral axon length than wt axons after axotomy (Figure 9C). By separately measuring growth in the spared and axotomized branches, we found that regenerative sprouting contributed virtually all of the excess growth, rather than growth from the injury site (Figure 9D-E). The *dlk*^{la231} mutant phenotype was stronger than the *lzk*^{la232} mutant phenotype, but excess growth was more pronounced in *dlk*^{la231} *lzk*^{la232} double mutants than in either single mutant. These results indicate that *dlk* and *lzk* inhibit peripheral axon growth specifically in spared branches of damaged axons. To test if this effect is compartment-specific, we measured the growth of peripheral axons after severing the central axon of the same neuron. Cutting central axons did not promote growth of spared peripheral axons preferentially in mutants, indicating that growth inhibition by DLK and LZK occurs locally, within a compartment (Figure 5C).

To test if DLK acts cell-autonomously to inhibit regenerative sprouting, we expressed *dlk* cDNA in *dlk*^{la231} mutants. Like with MNs, strong overexpression of *dlk* cDNA with the Gal4/UAS system was toxic to RB neurons, causing cell death by 24 hpf (not shown). As a result, we expressed lower levels of the cDNA (Crest3:DLK-T2A-GFP, co-injected with Isl1[SS]:Gal4 and UAS:DsRed) in RB neurons. Expression of the *dlk* cDNA modestly reduced axon sprouting, when measured as percent of the initial arbor size regenerated. This effect did not reach significance when compared to the *dlk*^{la231} mutants (Figure 9C-E), but the rescued single mutants were significantly different from *dlk*^{la231} *lzk*^{la232} double mutants. However, when measured as total axon length regenerated there was no apparent rescue with *dlk* cDNA. These ambiguous results may reflect the difficulty of achieving the appropriate level of cDNA expression for rescue, but could also suggest that these proteins do not act strictly cell-autonomously to limit regenerative sprouting of spared branches in RB neurons.

dlk and *lzk* are general inhibitors of collateral sprouting in RB neurons

Given our unexpected finding that spared branches of damaged RB neurons grew more in mutants than wt animals, we wondered if increased axon growth in *dlk*^{la231} and *lzk*^{la232} mutants was specific to injured axons, or if sensory axon growth was generally disinhibited in these mutants. Since axon growth during development is limited by repulsive tiling interactions (Sagasti et al., 2005; Grueber and Sagasti, 2010), increased growth potential in *dlk*^{la231} *lzk*^{la232} mutants could be masked by tiling. We therefore compared peripheral axon growth in mutants and wt animals in which we relieved axon tiling by ablating an entire trigeminal ganglion, since larval trigeminal sensory neurons are similar to larval RB neurons (Gau et al., 2013; Palanca et al., 2013). Ablating a trigeminal ganglion early in development (24 hpf) allows axons to grow into the denervated side of the head significantly more than in non-ablated control animals, since axon arbors are not limited by their contralateral counterparts (Sagasti et al., 2005). However, this

growth ability diminishes by 78 hpf (O'Brien et al., 2009a). To reduce variegation of the reporter (i.e., silencing in some cells), we selected homozygous transgenic embryos (Isl1[SS]:Gal4;UAS:DsRed) in which most, if not all, trigeminal cell bodies were labeled. Although axons from each ganglion do not stop abruptly at a sharp midline, they rarely reach the contralateral eye in wildtype animals. 24 hours after ganglion ablation, axons of the spared ganglion grew markedly further into the denervated side of the head in *dlk*^{la231} *lzk*^{la232} than in wt animals (Figure 10A). Measuring the total axon length that grew over the contralateral eye revealed that *dlk*^{la231} and *lzk*^{la232} inhibit collateral sprouting of RB touch-sensing neurons, even in uninjured neurons (Figure 10B).

Discussion:

This study establishes and characterizes zebrafish mutants in the *dlk* and *lzk* genes, complementing existing worm, fly, and mouse models to study the function of these critical neuronal injury regulators (Jin and Zheng, 2019). Zebrafish offers powerful advantages over other vertebrate models, including the ability to label single neurons of different types and precisely injure them with laser axotomy, thus making it possible to distinguish the responses of different neurite branches to injury. Using this approach, we found that *dlk* and *lzk* were required cell-autonomously, and partially redundantly, for MN regeneration in larval zebrafish. By contrast, *dlk* and *lzk* were not required for axon regeneration in larval RB touch-sensing neurons or adult DRG neurons. However, these kinases negatively regulated the sprouting of spared sensory neuron peripheral arbors, both within the injured neuron and in uninjured neighboring neurons. These findings reveal cell-type specific *dlk* and *lzk* functions and highlight the mechanistic differences between different kinds of regenerative growth, which can be promoted or inhibited by the same signaling molecules.

Invertebrates only have one DLK-related gene, but the existence of DLK's close relative LZK in vertebrates raises the possibility that these MAP3Ks act redundantly (Jin and Zheng, 2019). Despite their similarity, however, DLK lacks a key calcium-binding domain found in LZK and in invertebrate DLK homologs, suggesting that these kinases may be activated in different ways. Studies using optic nerve crush and traumatic brain injury (TBI) models found that inhibition of both *dlk* and *lzk* offered the strongest protection from cell death (Welsbie et al., 2019), indicating that they play overlapping roles in promoting injury-induced death. By contrast, other studies suggest distinct, cell-type-specific gene functions, including LZK's roles in activating astrocytes (Chen et al., 2018). We directly addressed the potential for redundancy between DLK and LZK in zebrafish axon regeneration by comparing each mutant to double mutants. In motor axons, dlk^{la231} mutants had a modest regeneration defect, but dlk^{la231} lzk^{la232} double mutants had a strong defect, suggesting partial redundancy. dlk^{la231} has an in-frame deletion of the kinase domain, so it is unlikely to trigger genetic compensation (Rossi et al., 2015; El-Brolosy et al., 2019; Ma et al., 2019). lzk^{la232} mutants, however, have a premature stop codon, which could trigger nonsense-mediated RNA decay and thus genetic compensation, perhaps explaining why lzk^{la232} mutants did not have a strong motor axon regeneration defect on their own. The fact that a few double mutant motor axons were able to regenerate may suggest compensatory contributions from other MAP3Ks in the MLK family or parallel pro-regenerative pathways. We saw a similar pattern for the suppression of RB neuron regenerative sprouting (sprouting was increased in dlk^{la231} animals, but it was more pronounced in dlk^{la231} lzk^{la232} double mutants), and only found motor dendrite overgrowth in double mutants. Together, these results suggest a partially redundant or compensatory relationship between these two kinases in axon regeneration.

DLK promotes axon regeneration in many different types of neurons and organisms, but in larval *Drosophila* sensory neurons it is dispensable for dendrite regeneration, even though it is required for axon regeneration in the same cells (Stone et al., 2014). This observation indicates that axon

and dendrite regeneration are mechanistically distinct, and indeed other factors differentially affect these processes (Nye et al., 2020). Vertebrate sensory neurons, while similar in many respects to *Drosophila* counterparts, have sensory axons rather than dendrites, as defined by physiological features and cytoskeletal organization (Shorey et al., 2021), so we initially hypothesized that DLK and LZK would be required for regeneration of both central and peripheral sensory axons. Surprisingly, however, central RB, peripheral RB, and peripheral DRG axons regenerated normally in *dlk*^{la231} *lzk*^{la232} mutants. These findings suggest that another, yet unknown pathway is used by fish somatosensory neurons to detect axon damage and activate the axon regeneration program.

When an entire nerve is damaged, it is difficult to deconvolute axon regeneration from a severed axon stump, regenerative sprouting from spared branches, and collateral sprouting from neighboring neurons (Steward et al., 2003; Tuszynski and Steward, 2012). The balance of these types of growth, however, has important functional consequences, particularly for sensory neurons. For example, RB sensory axons in larval zebrafish tile to innervate discrete, minimally overlapping territories in the skin that provide spatial information necessary for appropriate behavioral responses to touch (Sagasti et al., 2005). The balance between true regeneration and collateral sprouting thus determines the sensory map of the periphery. Our single cell labeling method allowed us to directly address this issue, revealing that DLK, potentially with some contribution from LZK, are required to limit sprouting from uninjured axon branches, even though it did not affect regeneration from severed axon branches. This finding emphasizes that forming a growth cone in a damaged axon branch, which has experienced cytoskeletal disruption, calcium influx, and local mitochondrial dysfunction, is a distinct process from reactivating growth in a dormant, uninjured axon branch. Since it is critical for sensory neurons to restore their spatial sensory map in the periphery, limiting sprouting may be as functionally important as promoting new growth from an injured branch. Indeed, excessive neuronal sprouting induced by pathological

conditions such as atopic dermatitis, or selective serotonin reuptake inhibitors (SSRI) treatment, is associated with oversensitivity and itch in the skin (Han and Dong, 2014; Tominaga and Takamori, 2014; Morita et al., 2015).

The cellular site in which DLK acts to limit sprouting remains unclear in our experiments, since expressing DLK cDNA only modestly reduced sprouting in *dlk*^{la231} RB neurons. Achieving rescue experimentally may be difficult, since overexpressing DLK was toxic to neurons, suggesting that precise regulation of DLK levels is required for an optimal injury response. These findings also allow the intriguing possibility that DLK may act non-cell-autonomously to limit sprouting. For example, DLK could function in the epidermal cells innervated by RB axons, since DLK regulates epidermal differentiation and integrity (Robitaille et al., 2005; Simard-Bisson et al., 2017), or in immune cells activated by the injury, since DLK and LZK regulate microglial and astrocyte responses to injury in the CNS (Chen et al., 2018; Wlaschin et al., 2018). Wherever DLK is functioning to limit sprouting, our findings reveal that regeneration from an injured growth cone and sprouting from uninjured axon branches are mechanistically distinct processes that differentially require DLK signaling.

Our discovery that zebrafish DLK and LZK are required to promote axon growth in one context (motor axon regeneration), and restrain it in others (growth of RB spared branches and trigeminal neurons) echoes the context-specific dual roles for DLK homologs in other neurons. For example, in addition to its differential effects on axon and dendrite regeneration in *Drosophila* sensory neurons (Stone et al., 2014), excess DLK promotes axon growth and inhibits dendrite growth in the same neurons (Wang et al., 2013). Moreover, although DLK is required for axon regeneration in *Drosophila* sensory neurons, it also promotes an opposing neuroprotective response that inhibits axon regeneration (Chen et al., 2016a). Thus, DLK has the potential to both activate and inhibit regeneration in these neurons, depending on the balance of its outputs. Similarly, in *C.*

elegans sensory neurites, excess DLK resulting from loss of a negative regulator can inhibit axon regeneration (Yan et al., 2009) or promote developmental overgrowth (Zheng et al., 2020), depending on which regulator was reduced.

Our study adds to a growing list of examples of distinct DLK functions in different cell types and conditions (Jin and Zheng, 2019). These diverse outcomes could be explained by the permissiveness versus non-permissiveness of the environment, expression levels of these signaling proteins, subcellular localization, the mode of activation, or even the duration of the signal, all of which could lead to the assembly of different signaling complexes that activate different responses (Goodwani et al., 2020). Understanding these diverse molecular processes, categorizing potential outcomes, and determining the neuronal cell types in which they occur in vivo, are prerequisites to considering *dlk* and *lzk* as targets in the treatment of axonal neuropathies and traumatic injuries.

Materials and methods:

Zebrafish

Zebrafish (*Danio rerio*) were raised on a 14h/10h light/dark cycle, and a water temperature of 28.5C. Embryos were incubated at 28.5C in E3 buffer (0.3g/L Instant Ocean salt, 0.1% methylene blue). For imaging purposes, pigment formation was blocked by treating embryos with phenylthiourea (1X PTU, 0.2mM) at 22-24 hpf. Embryos were then manually dechorionated using forceps. All mutant and transgenic lines were created using AB wildtype fish (ZFIN: ZDB-GENO-960809-7). Experimental procedures were approved by the Chancellor's Animal Research Care Committee at UCLA and the Pennsylvania State Institutional Animal Care and Use Committee.

CRISPR/Cas9 mutagenesis

Guide RNAs were engineered using the “Short oligo method to generate gRNAs”, as previously described (Talbot and Amacher, 2014). To mutagenize *dlk* and *lzk*, we created a DNA template for making gRNAs, containing the T7 RNA polymerase promoter, the gene targeting sequence, and the gRNA scaffold sequence. This template was amplified by PCR and its product was used to synthesize gRNAs using a T7 RNA polymerase kit. The gRNAs were then purified. Fish were injected with a mix containing 1uL of Cas9 mRNA (1500ng/ul), 1.5uL of gRNA1 (100ng/uL), and 1.5uL of gRNA2 (100ng/uL). Embryos at the 1-cell stage were injected with 5nL of the mix. At 48 hpf, PCR and restriction digests were used to test guide efficiency. To identify fish carrying mutations in their germline, injected embryos were raised to adulthood, crossed to wildtype fish, and their progeny were screened by PCR. at 48 hpf, mutant PCR products flanked by the common M13 primers, were sent for sequencing.

PCR genotyping

PCR was usually conducted with Taq polymerase for 40 amplification cycles. The denaturation cycle was 94℃ for 30s. Annealing was for 30s at 53℃ for *lzk* wildtype and *lzk*^{la232} bands, 59℃ for the *dlk* wildtype band, and 63℃ for *dlk*^{la231} band. Elongation was at 72℃; this step was 20s for *lzk* wildtype and *lzk*^{la232} bands, 1 minute for the *dlk* wildtype band, and 15s for the *dlk*^{la231} band.

Alternatively, PCR was occasionally conducted with Phusion polymerase for 40 amplification cycles. The denaturation cycle was 98℃ for 30s. Annealing was at 64℃ for *lzk* wildtype and *lzk*^{la232} bands, 71℃ for the *dlk* wildtype band, and 75℃ for *dlk*^{la231} band. Elongation at 72℃ for 11s for *lzk* wildtype and *lzk*^{la232} bands, for 30s for the *dlk* wildtype band, and 10s for *dlk*^{la231} band.

Transgene cloning

HB9(3X)-E1B-DLK-T2A-GFP

E1B-DLK-T2A was constructed by individually inserting E1B and DLK into the MCS region of a PME: MCS-T2A vector.

Step 1: E1B template

5’ TCTAGAGGGTATATAATGGATCCCATCGCGTCTCAGCCTCA 3’

5’ GAATTCGTGTGGAGGAGCTCAAAGTGAGGCTGAGACGCGATG 3’

An E1B template was created by PCR amplification of overlapping oligomers.

Step 2: att site-MCS-T2A-att site

5’ GGGGACAAGTTTGTACAAAAAAGCAGGCTACCGTCAGATCCGCTAG 3’

5’ GGGGACCACTTTGTACAAGAAAGCTGGGTATGGGCCAGGATTCTC 3’

MCS-T2A flanked by att sites was PCR amplified and inserted into a PME vector using a Gateway BP reaction (Kwan et al., 2007).

Step 3: EcorI-E1B-EcorI was inserted into the MCS region of PME: MCS-T2A vector using restriction digest and ligation resulting in aPME: MCS(E1B)-T2A vector.

5’ TAAGCAGAATTCTCTAGAGGGTATATAATGGATCCCA 3’

5’ TGCTTAGAATTCGAATTCGTGTGGAGGAGCT 3’

Step 4: SaLI-DLK(no stop codon)-SacII was inserted into the PME: MCS(E1B)-T2A vector using restriction digest and ligation resulting in a PME: MCS(E1B-DLK)-T2A vector.

5’ TAAGCAGTCGACATGGCTTGTGTCCATGAGCAG 3’

5’ TGCTTACCGCGGGTTTTGTGGACCCTGGCCC 3’

PME: MCS(E1B-DLK)-T2A, a P5E:HB9(3X), and P3E:GFP were incorporated into a Gateway destination vector via LR reaction resulting in HB9(3X)-E1B-DLK-T2A-GFP.

HB9(3X)-E1B-LZK-T2A-GFP

E1B-LZK-T2A was constructed using overlap PCR to assemble E1B-LZK-T2A framed by att sites:

Primer set 1: att site-E1B-part of *lzk,* use E1B sequence as a template

5’ GGGGACAAGTTTGTACAAAAAAGCAGGCTTCTCTAGAGGGTATATAATGGATCCC 3’

5’ TGGTGCTGTGCGTGTGCATGAATTCGTGTGGAGGAGC 3’

Primer set 2: part of E1B-*lzk* no stop codon-part of T2A, use *lzk* cDNA as template

5’ GCTCCTCCACACGAATTCATGCACACGCACAGCACCA 3’

5’ CCTCTGCCCTCTCCACTTCCCCAGGATGACGGAGCGCC 3’

Primer set 3: end of *lzk* no stop codon-T2A-att site, use T2A sequence as a template

5’ GGCGCTCCGTCATCCTGGGGAAGTGGAGAGGGCAGAGG 3’

5’ GGGGACCACTTTGTACAAGAAAGCTGGGTCTGGGCCAGGATTCTCCTCGA 3’

All three fragments were amplified independently. Fragment 1 was added to fragment 2 by overlapping PCR. The resulting fragment was added to fragment 3. The complete sequence was then inserted into Gateway’s PME donor plasmid via a BP reaction. The resulting PME: E1B-LZK-T2A, a P5E:HB9(3X), and P3E:GFP were incorporated into a Gateway destination vector via LR reaction resulting in HB9(3X)-E1B-LZK-T2A-GFP.

Crest3: DLK-T2A-GFP

DLK-T2A was constructed using overlap PCR to assemble DLK-T2A flanked by att sites for Gateway recombination:

Primer set 1: att site-*dlk* no stop-part of T2A, use *dlk* cDNA as template

5’ GGGGACAAGTTTGTACAAAAAAGCAGGCTTCATGGCTTGTGTCCATGAGCAG 3’

5’ CCTCTGCCCTCTCCACTTCCGTTTTGTGGACCCTGGCCC 3’

Primer set 2: end of *dlk* no stop-T2A-att site, use T2A sequence as template

5’ GGGCCAGGGTCCACAAAACGGAAGTGGAGAGGGCAGAGG 3’

5’ GGGGACCACTTTGTACAAGAAAGCTGGGTCTGGGCCAGGATTCTCCTCGA 3’

Both fragments were amplified independently. Fragment 1 was added to fragment 2 by overlapping PCR. The resulting PME: DLK (no stop codon)-T2A, a P5E: Crest3, and a P3E:GFP were incorporated into a Gateway destination vector via LR reaction resulting in Crest3: DLK-T2A-GFP.

Building the phylogenetic tree

Complete DLK and LZK protein sequences from several organisms were downloaded from the NCBI database. The sequences were aligned using the MUSCLE alignment algorithm on the

EMBL-EBI website. Phylogenetic analyses were performed with the RAxML software using a maximum likelihood method, the JTT substitution matrix, and empirical frequencies (Stamatakis, 2014). The RAxML software was accessed via the CIPRES Science Gateway (Miller et al., 2010). The Interactive Tree of Life website (Letunic and Bork, 2007) was used to visualize the evolutionary tree.

Larval body measurements

The body lengths of larvae of each genotype were measured at 48 hpf, 72 hpf and 5 dpf using a Zeiss Discovery V8 Stereomicroscope at a 2X magnification. Bodies were measured lengthwise from head to tail, and tail widths measured ventral to dorsal at the end of the spinal cord. Larvae from different clutches (n>8) and parents of different ages (3-24 months old) were mixed for this analysis.

Mounting larvae for live imaging

Larva were anesthetized with 0.2 mg/mL MS-222 in embryo media (0.08%) before mounting. Each larva was embedded in 1% agarose and placed on a cover slip. Upon solidification of the agarose (~15 minutes), a plastic ring was sealed onto the cover slip with vacuum grease. The resulting chamber was then filled with tricaine-containing embryo media and sealed with a glass slide using vacuum grease (O'Brien et al., 2009b).

Larval microscopy

Live confocal images were collected on an LSM 800 using a 20X air objective (Plan-APOCHROMAT, NA= 0.8). Images were acquired with Zen Blue software from Zeiss.

Laser axotomies were performed using a LSM 880 equipped with a 2-photon laser (Chameleon Ultra II, Coherent), as previously described (O'Brien et al., 2009b). Zen Black 2.1 SP3 software

was used to visualize axons and perform axotomies. Neurons were visualized with a 561nm or 488nm laser excitation, before switching to the Chameleon (813nm) laser for axon severing.

To cut axons of RB neurons in the tail, we initially used 5% laser power. If axons were not cut, the laser power was increased in 0.5% increments until cutting was successful. Since MNs are deeper in the animal, we first attempted axotomy with 6.5% laser power.

Adult experiments

Cutting DRG nerves in juvenile fish: 4-5 week-old fish of the genotype P2rx3a:LexA,4xLexOP:EB3-GFP (not shown in the figure), P2rx3a:LexA,4xLexAop:mCherry^{la207}, Roy^{a9}/Roy^{a9}, mifta^{w2}/mifta^{w2}, containing either wt or homozygous *dlk*^{la231} and *lzk*^{la232} were anesthetized in a VWR polystyrene petri dish, filled halfway with 0.16% tricaine in 0.6 g/L Instant Ocean salt solution, and immobilized by applying agarose to their midsection only, leaving both the head's respiratory apparatus, and tail free. Fish were then imaged on a Leica SP8 microscope equipped with an InSight X3 unit from Spectra-Physics. A 25X (NA= 1) water immersion objective with a working distance of 2.6mm was used to image the posterior spinal cord of the fish, and an ROI was chosen to restrict the cut site to the width of the nerve and positioned ~100 µm from the posterior-most DRG, along the posterior projecting nerve. The tunable laser was set to 900nm, and both the tunable and fixed wavelength 1045nm lasers were set to 100% on the slowest speed setting and scanned for ~1 second. The 2-photon overview showing the nerve stumps after cut was performed on the aforementioned SP8, all other images for this experiment were obtained with a Zeiss LSM 800 Axio Observer Z.1 with a 20X air objective (NA=0.8).

Cutting scale nerves: All fish were between 8 and 11 months old. The single *dlk*^{la231} and *lzk*^{la232} mutants were transgenic for P2rx3a:LexA,4xLexAop:mCherry^{la207}, and did not possess mutant roy or mifta alleles. Wildtype and double mutant fish were in a roy^{a9}/roy^{a9}, mifta^{w2}/mifta^{w2}

background and doubly transgenic for both P2rx3a:LexA,4xLexAop:EB3-GFP and P2rx3a:LexA,4xLexAop:mCherry^{la207}. All images shown were collected on a Zeiss LSM 800 Axio Observer Z.1. For wildtype, a 25X

a multi-immersion objective was used (NA= 0.8), and for the double mutants a 20X air objective (NA= 0.8) was used. Laser injury was performed using an Andor Micro-Point UV pulse laser.

Image analysis and statistics

Confocal images, saved as .czi files, were opened in ImageJ/Fiji and measured using the Simple Neurite Tracer (SNT) feature in z-stack format. One neuron was imaged per embryo. Axons of MNs were traced from the cell body to their endings in muscles. RB peripheral arbors were traced starting at the first branch point in the skin. If RB peripheral axons bifurcated in the spinal cord, creating two separate peripheral arbors, both arbors were traced. Three experimenters contributed to tracing. To test for tracing reproducibility between experimenters, a subset of RB central axons (n=76) and peripheral arbors (n=10) were separately traced by two experimenters. In both cases, tracings by the two experimenters were highly similar (r=0.93 for the central axons; r=0.99 for the peripheral arbors).

For figures, maximum projections were created in ImageJ/Fiji, converted to grayscale and inverted. To visualize entire RB neurons, images of different parts of each neuron were stitched together in Adobe Photoshop.

Dot plots, or box-and-whisker plots overlaid with dot plots were produced in R to visualize the data. In dot plots, the black bar indicates the mean. In box-and-whisker plots, the boxes indicate the interquartile range: the top of the box is the 75th percentile, the midline is the median, and the bottom of the box is the 25th percentile. Statistical analyses were performed in R. A generic quantile-quantile test was used to determine the normality of sample populations. Unless

otherwise specified, data distributions were non-parametric. Therefore, a Kruskal-Wallis, with a Bonferroni correction, was used to assess differences between experimental groups. A Wilcoxon paired test was used to identify groups with significant differences. * for a p-value < 0.05, ** for a p-value < 0.01, *** for a p-value < 0.005, and **** for a p-value < 0.001.

Table1: Accession numbers

DLK	Accession number	Common name
*Homo_sapiens*_DLK	NP_006292.3	Human
*Rattus_norvegicus*_DLK	NP_037187.1	Rat
*Mus_musculus*_DLK	NP_001345773.1	Mouse
*Gallus_gallus*_DLK	XP_025001292.1	Chicken
*Danio_rerio*_DLK	NP_996977.1	Zebrafish
Xenopus_laevis_DLK	NP_001094411.1	Frog
*Caenorhabditis_elegans*_DLK-1	sp|O01700.4	Worm
*Drosophila_megalogaster*_wallenda	NP_788541.1	Fruit fly
LZK		
*Homo_sapiens*_LZK	sp|O43283.1	Human
*Rattus_norvegicus*_LZK	NP_001014000.2	Rat
*Mus_musculus*_LZK	NP_766409.2	Mouse

*Gallus_gallus*_LZK	XP_025009526.1	Chicken
*Danio_rerio*_LZK	XP_017213349.1	Zebrafish
Xenopus_laevis_LZK	ABK15544.1	Frog

Table 2: Gene IDs, Cas9 gRNAs, genotyping primers

Gene	Ensembl#
dlk/Map3k12	ENSDARG00000103651
lzk/Map3k13	ENSDARG00000009493
CRISPR/Cas9 gRNAs, PAM site	
GTG GGT GGG CAG CGG CGC TC AGG	Deletion: gRNA for exon 2 to delete *dlk's* kinase domain, "-" strand
GCT GTG GGA GAT GCT GAC CG GGG	Deletion: gRNA for exon 5 to delete *dlk*'s kinase domain, "-" strand
CCC CGG AGG TGC TGT CCT GGA C	Deletion: gRNA 1 for exon 1 to make a small deletion in *lzk*, "+" strand
CCT CAA GCG CTC CTG CCT CCT GC	Deletion: gRNA 2 for exon 1 to make a small deletion in *lzk*, "+" strand
Genotyping primers	
5' GC CAA CCC TGT GGA GAC TAA	Forward primer for *dlk*'s mutant band

ACC 3’	(exon 2)
5’ CCA GCA CTG TCT GAG CAG GAT C 3’	Reverse primer for *dlk*’s mutant band (exon 5)
5’ AAG GGT TAC GGT TGG GGT TAG G 3’	Forward primer for *dlk*’s wildtype band (exon 4)
5’ GTT GCG CAG TGA TGT CTG TGA A 3’	Reverse primer for *dlk*’s wildtype band (exon 4)
5’ TCC TCG TGT TCC TCC AAC A 3’	Forward primer for *lzk* (exon 1)
5’ GCT GTA AGT GAT GGA GAG GCA T 3’	Reverse primer for *lzk* (exon 1)

Table 3: Plasmids used in injections, transgenic lines

Plasmids	**Source**
HB9(3X):GAL4	(Issa et al., 2011)
UAS:GFP	(Kwan et al., 2007)
UAS:DsRed	(Kwan et al., 2007)
Isl1[SS]:Gal4;UAS:DsRed	(Sagasti et al., 2005)
Isl1[SS]:Gal4;UAS:GFP	(Sagasti et al., 2005)
HB9(3X):E1B-DLK-T2A-GFP	This work

HB9(3X):E1B-LZK-T2A-GFP	This work
Crest3:DLK-T2A-GFP	This work
PME: MCS-T2A	This work
Transgenic lines	
Tg(Isl1[SS]:Gal4;UAS:DsRed)^{zf234}	(Sagasti et al., 2005)
Tg(p2rx3a:LexA;4xLexAop:mCherry)^{la207}	(Palanca et al., 2013)
Mutant lines	
dlk^{la231} mutant (519 coding bp deletion/3289 genomic bp deletion)	This work
lzk^{la232} mutant (58bp deletion)	This work

Table 4: Reagents, resources

Reagents	Source	
HiScribe T7 High Yield RNA Synthesis Kit	New England Biolabs	E2040S
RNeasy Mini Kit	Qiagen	74104
Alt-R S.p. Cas9 Nuclease 3NLS	IDT	1074182
PfuUltra II Fusion HotStart DNA	Agilent	600670

Polymerase		
Phusion High-Fidelity DNA Polymerase	New England Biolabs	M0520S
Taq DNA Polymerase with Standard *Taq* Buffer	New England Biolabs	M0273X
Zen 2.1(Blue edition)	Carl Zeiss Microscopy	http://www.zeiss.com
Fiji/ImageJ	(Schindelin et al., 2012)	https://fiji.sc/
R	R Foundation for Statistical Computing	https://www.r-project.org/

Acknowledgments:

We thank members of the Sagasti lab for comments on the manuscript, Son Giang and Yuan Dong for excellent fish care, and Adam Langenbacher for help with data presentation. KPA was supported by a UCLA Cota-Robles fellowship, a NSF Bridge to the Doctorate fellowship, and NIH F31 predoctoral fellowship NS106742. This study was supported by NIH grants R21NS090027 (MMR and AS) and R01AR064582 (AS).

Figure legends:

Figure 1. *dlk* and *lzk* zebrafish mutants.

A) Phylogenetic tree of DLK and LZK orthologs. B) Genotyping of *dlk*^{la231} and *lzk*^{la232} CRISPR/Cas9 mutants. Left, gene structure of zebrafish *dlk* and *lzk*, with gRNA sequences. Blue

indicates PAM sites. Right, DNA gel showing wt and mutant genotyping with primers indicated to the left (arrowheads). C) 48 hpf zebrafish larvae of the indicated phenotypes. D) Overlaid box and dot plots comparing animal lengths from the tip of the head to the end of the tail each genotype. E) Overlaid box and dot plots comparing tail width in each genotype. See Methods for details of statistical analyses.

Figure 2. Motor neurons develop normally in *dlk*^{la231} and *lzk*^{la232} mutants.

A) Cartoon of 5 dpf larva, showing the approximate location of the image below of a single labeled MN in a live animal. The cell body and dendrites are in the spinal cord; the axon exits the spinal cord to innervate the ventral muscles of one segment. B) Labeled MNs in each of the indicated genotypes. C) Dot plot showing lengths of MNs in each of the indicated genotypes. Bar indicates the mean. There was no significant difference between groups (because distributions were normal, groups were compared by ANOVA). D) Dot plot showing branch tip numbers of MNs in each of the indicated genotypes. Bar indicates the mean. There was no significant difference between groups. Scale bars: 100μm in A, 50μm in B.

Figure 3. Rohon-Beard neurons develop normally in *dlk*^{la231} and *lzk*^{la232} mutants.

A) Cartoon of 48 hpf larva, showing the approximate location of the image below of a single labeled RB neuron in a live animal. The cell body, central and peripheral axons are labeled. The cell body and central axon are in the spinal cord; the peripheral axon exits the spinal cord to arborize in the developing epidermis. B) Tail-innervating peripheral RB axon arbors of the indicated genotypes at 48 and 72 hpf. C-E) Quantification of RB peripheral axon arbor lengths (C), 2D arbor area (D), and branch tip number (E) at 48 hpf. See Methods for details of statistical analyses. Scale bars: 100μm.

Figure 4. Motor neuron regeneration is impaired in *dlk*^{la231} *lzk*^{la232} mutants.

A) Top: 5 dpf motor axons immediately after axotomy in the indicated genotypes. Lightning bolt indicates axotomy site. Magenta highlights the separated distal stump that will degenerate. Rightmost panels show neurons expressing rescue cDNAs; expression of rescue transgenes in cell bodies is shown below. Bottom: Same neurons 48 hours post-axotomy. Blue highlights regenerated axons. B-C) Dot plots showing total regenerated length in each genotype (B) and the percentage of the original axon length regenerated (C). Bar indicates the mean. D) Dendrite overgrowth phenotype following failure of axon regeneration in *dlk*^{la231} *lzk*^{la232} mutants. See Methods for details of statistical analyses.

FIgure 5. RB central axons regenerate in *dlk*^{la231} *lzk*^{la232} mutants.

A) Top: 48 hpf RB axon immediately after axotomy. Magenta highlights the separated distal stump that will degenerate. Bottom: Same neuron 24 hours post-axotomy. Blue highlights the regenerated axon. B) Overlaid box and dot plots showing central axon length regenerated in the indicated genotypes. C) Overlaid box and dot plots showing growth of peripheral arbors following central axotomy in the indicated genotypes. See Methods for details of statistical analyses. Scale bar: 100μm.

Figure 6. RB peripheral axon arbors regenerate in *dlk*^{la231} *lzk*^{la232} mutants.

A) Top panels: 48 hpf RB peripheral axon immediately after axotomy in the indicated genotypes. Magenta highlights the separated distal stump that will degenerate. Bottom panels: Same neurons 24 hours post-axotomy. Blue highlights the regenerated axon. B-C) Dot plots showing total regenerated length in each genotype (B) and the percentage of the original axon length regenerated (C). Bar indicates the mean. See Methods for details of statistical analyses. Scale bar: 100μm.

Figure 7. DRG axons innervating the adult scale regenerate in *dlk*^{la231} *lzk*^{la232} mutants.

Images of DRG neurons innervating the epidermis above scales in adult (8–11-month-old) zebrafish in indicated genotypes at 0 hours post-axotomy (top shows immediately after axotomy, bottom shows immediately before axotomy). Lightning bolts indicate axotomy sites of individual nerves growing into scales. Nerves innervating anterior scales (orange) are above the scale, whereas nerves innervating posterior scale (blue) are below the anterior scale. Legend refers to the image on the right. Most axons innervating these scales have degenerated by 24hpa (middle column), and reinnervated scales by 96hpa (right columns). Scales were re-innervated in all wt (n=10), *dlk*^{la231}(n=7), *lzk*^{la232}(n=5), and *dlk*^{la231} *lzk*^{la232} mutants (n=5). Scale bar: 200μm.

Figure 8. DRG axons innervating the juvenile tail regenerate in wildtype and *dlk*^{la231} *lzk*^{la232} mutants.

A) Top left: Cartoon of juvenile casper fish, showing tail-innervating DRGs in P2rx3a:LexA;4xLexAop:mCherry^{la207} transgenic fish. Lightning bolt indicates axotomy site. Blue indicates spinal cord. Legend refers to the image on the right. Top Right: 2-photon overview showing DRG cell body position, sensory nerve layout and an example of axotomy location in a 4–5-week-old zebrafish. Inset shows the axotomy site of the caudal-most DRG peripheral nerve. Green highlights separated arbors of the severed DRG nerve, which will degenerate after axotomy. B) Bottom left: Homozygous *dlk*^{la231} *lzk*^{la232} mutant experimental animal 24 hours post-axotomy showing that axons have grown past the axotomy site. Bottom right: Fin of the same animal 24 and 96 hours post-axotomy at different magnifications. At 24hpa, axons have grown into the fin, but have not yet reached the fin tip. By 96hpa, axons have reached the fin tip. Axons regenerated in all wt (n=5) and all *dlk*^{la231} *lzk*^{la232} mutants (n=6). Scale bars: 100μm.

Figure 9. Spared arbors of damaged RB neurons sprout excessively in *dlk*^{la231} *lzk*^{la232} mutants.

A) Cartoon of partial RB peripheral axotomy assay, which differentiates between regeneration from the cut site and regenerative sprouting from spared branches. B) Top: 48 hpf RB axons immediately after axotomy in the indicated genotypes. Lightning bolt indicates axotomy site. Magenta highlights the separated distal stump that will degenerate. Rightmost panel shows a neuron expressing rescue cDNA; expression of the rescue transgene in the cell body is shown below. Bottom: Same neurons 24 hours post-axotomy. Blue highlights regenerated axons; orange highlights the spared branch. C-E) Box and dot plots showing total new growth, including both from the axotomy site and spared branch (C), percent regeneration from just the injury site (D), and percent increase of the spared branch (E). See Methods for details of statistical analyses. Scale bar: 100μm.

Figure 10. Trigeminal axons grow excessively in *dlk*^{la231} *lzk*^{la232} mutants after ablation of the contralateral ganglion.

A) Images and cartoon of trigeminal axons in zebrafish heads at 78 hpf. Confocal images show two separate examples of wt (left) and *dlk*^{la231} *lzk*^{la232} mutant (right) fish. Insets magnify a region over the eye, with axons traced in orange. Bottom shows cartoon depictions of the result. B) Dot plot showing total axon length that grew over the contralateral eye. Bar indicates the mean. Scale bar: 500μm.

Figures

Figure 1

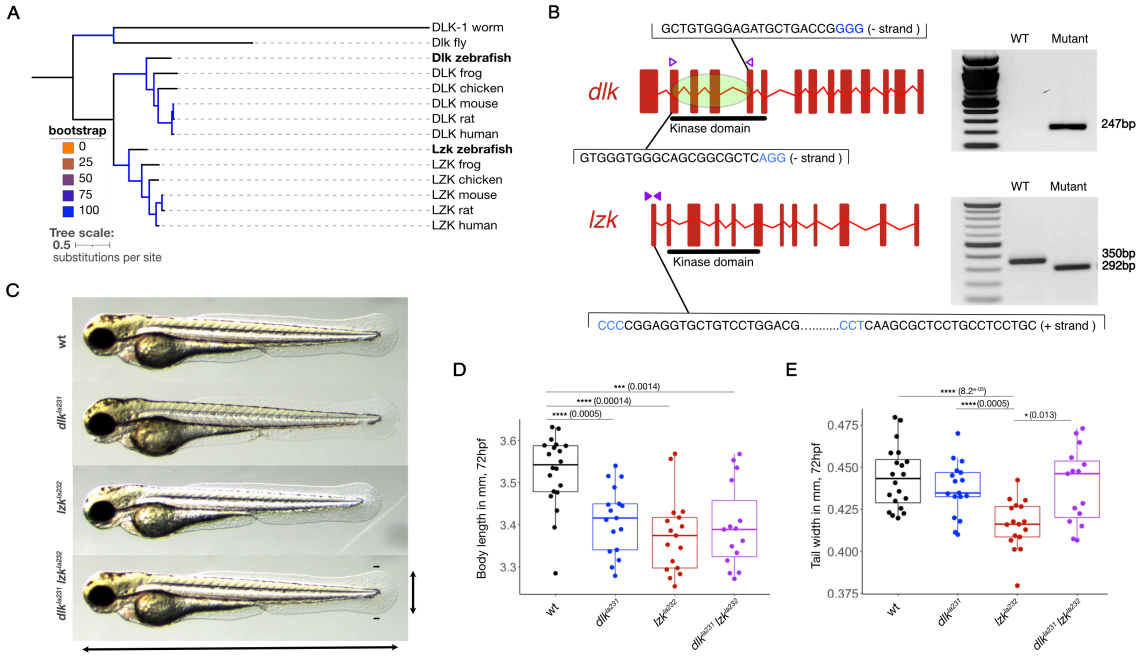

Figure 2

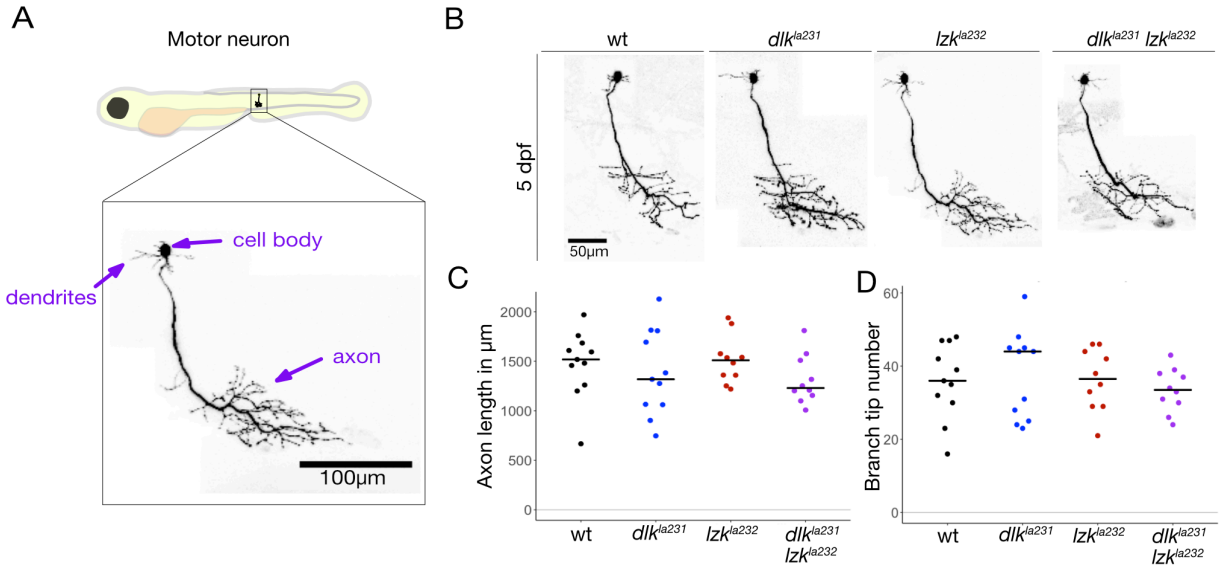
A
Motor neuron
cell body
dendrites
axon
100µm
B
wt
dlk^la231
lzk^la232
dlk^la231 lzk^la232
5 dpf
50µm
C
Axon length in µm
2000
1500
1000
500
0
wt
dlk^la231
lzk^la232
dlk^la231 lzk^la232
D
Branch tip number
60
40
20
0
wt
dlk^la231
lzk^la232
dlk^la231 lzk^la232

Figure 3

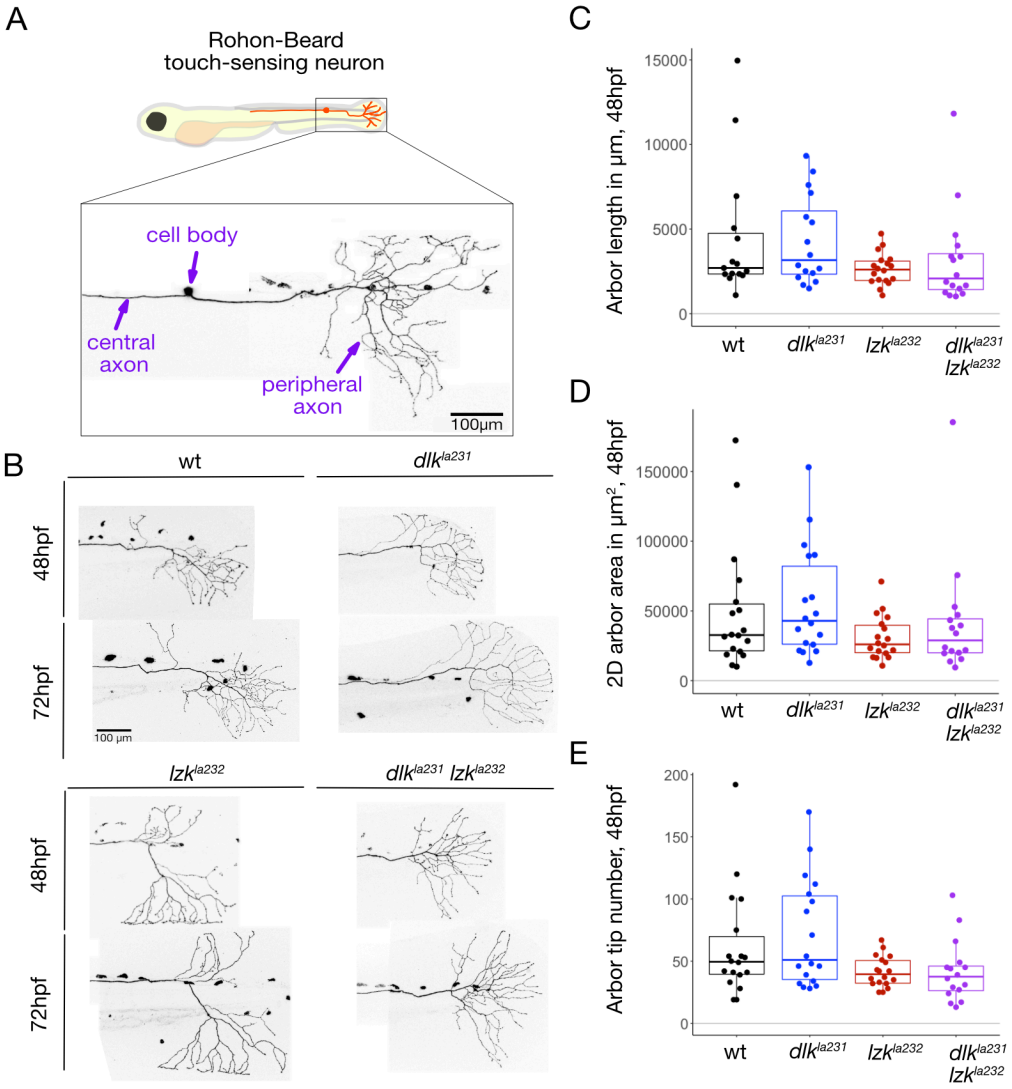
A
Rohon-Beard
touch-sensing neuron
cell body
central
axon
peripheral
axon
100µm
B
wt
dlk^la231
48hpf
72hpf
100 µm
lzk^la232
dlk^la231 lzk^la232
48hpf
72hpf
C
Arbor length in µm, 48hpf
15000
10000
5000
0
wt
dlk^la231
lzk^la232
dlk^la231
lzk^la232
D
2D arbor area in µm², 48hpf
150000
100000
50000
0
wt
dlk^la231
lzk^la232
dlk^la231
lzk^la232
E
Arbor tip number, 48hpf
200
150
100
50
0
wt
dlk^la231
lzk^la232
dlk^la231
lzk^la232

Figure 4

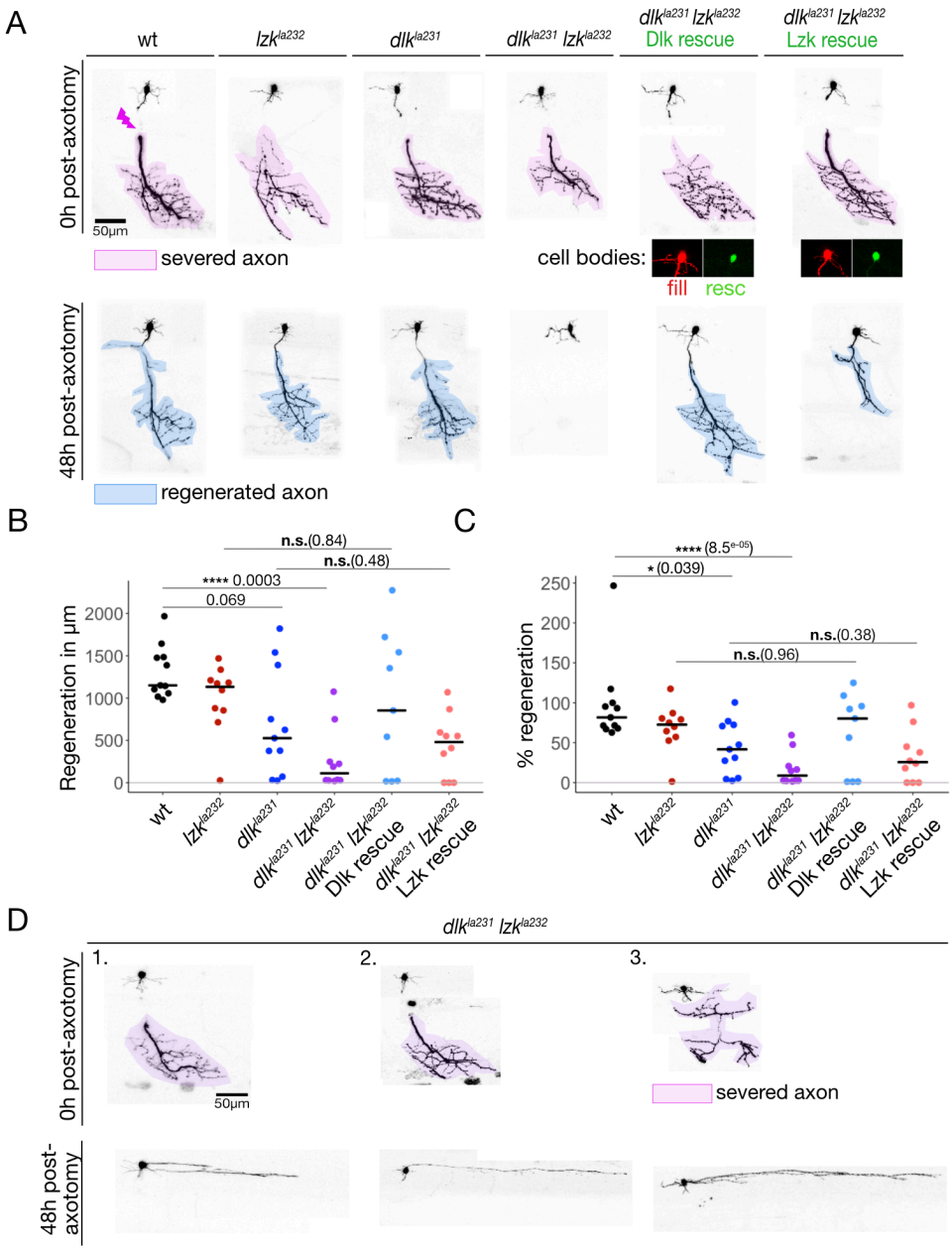
A
wt
lzk la232
dlk la231
dlk la231 lzk la232
dlk la231 lzk la232 Dlk rescue
dlk la231 lzk la232 Lzk rescue
0h post-axotomy
50µm
severed axon
cell bodies:
fill
resc
48h post-axotomy
regenerated axon
B
Regeneration in µm
n.s.(0.84)
n.s.(0.48)
**** 0.0003
0.069
C
% regeneration
**** (8.5e-05)
* (0.039)
n.s.(0.38)
n.s.(0.96)
D
dlk la231 lzk la232
1.
2.
3.
0h post-axotomy
50µm
severed axon
48h post-axotomy

Figure 5

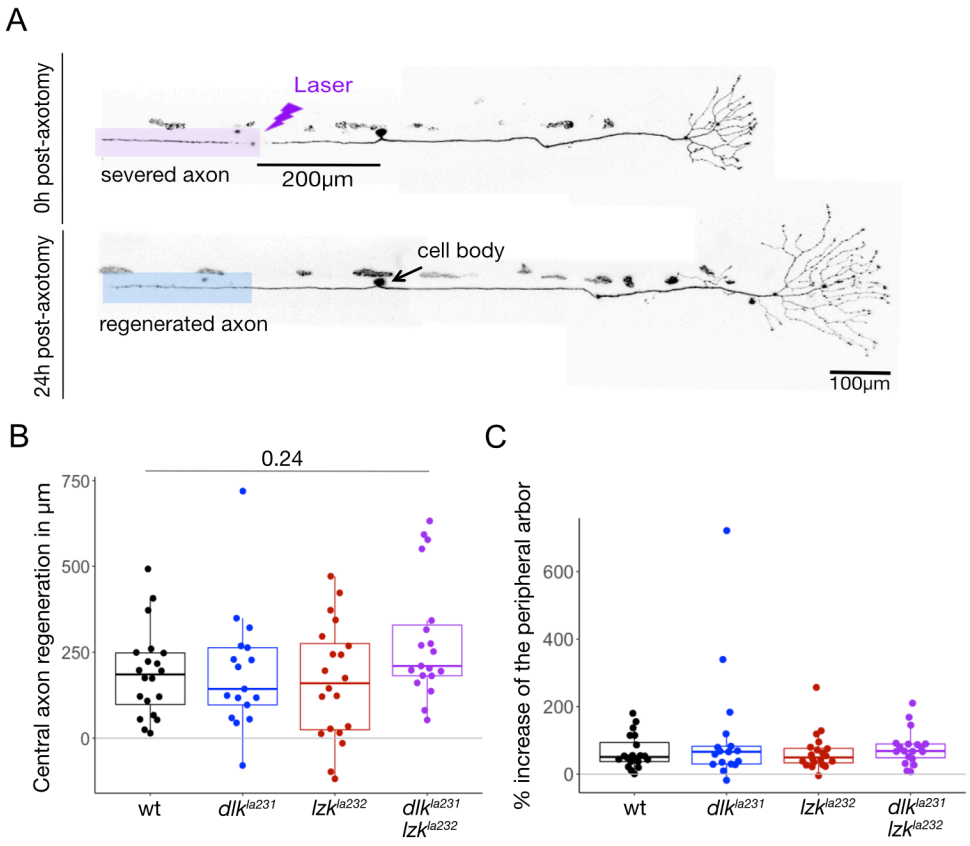
A
0h post-axotomy
Laser
severed axon
200µm
24h post-axotomy
cell body
regenerated axon
100µm
B
0.24
Central axon regeneration in µm
750
500
250
0
wt
dlk la231
lzk la232
dlk la231 lzk la232
C
% increase of the peripheral arbor
600
400
200
0
wt
dlk la231
lzk la232
dlk la231 lzk la232

Figure 6

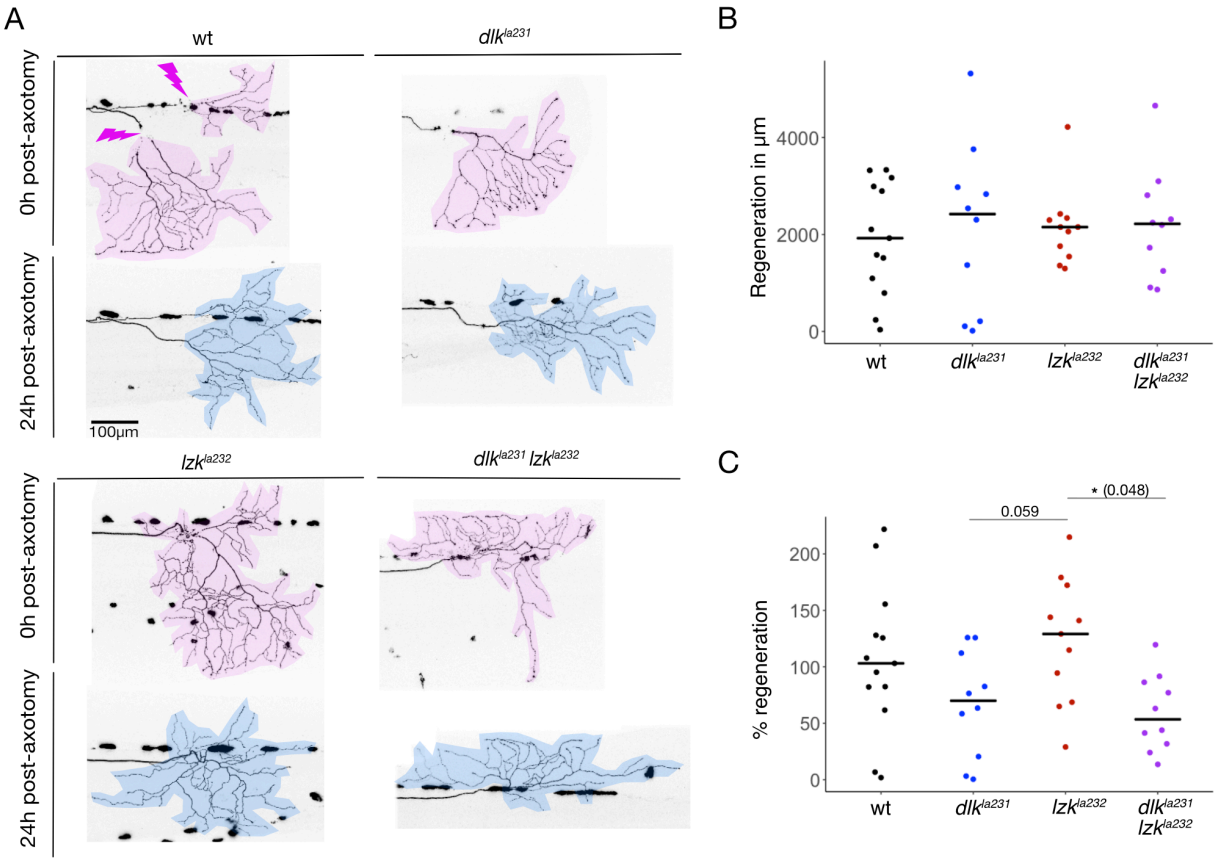
A
wt
dlk la231
0h post-axotomy
24h post-axotomy
100µm
lzk la232
dlk la231 lzk la232
B
Regeneration in µm
4000
2000
0
wt
dlk la231
lzk la232
dlk la231 lzk la232
C
% regeneration
200
150
100
50
0
0.059
* (0.048)
wt
dlk la231
lzk la232
dlk la231 lzk la232

Figure 7

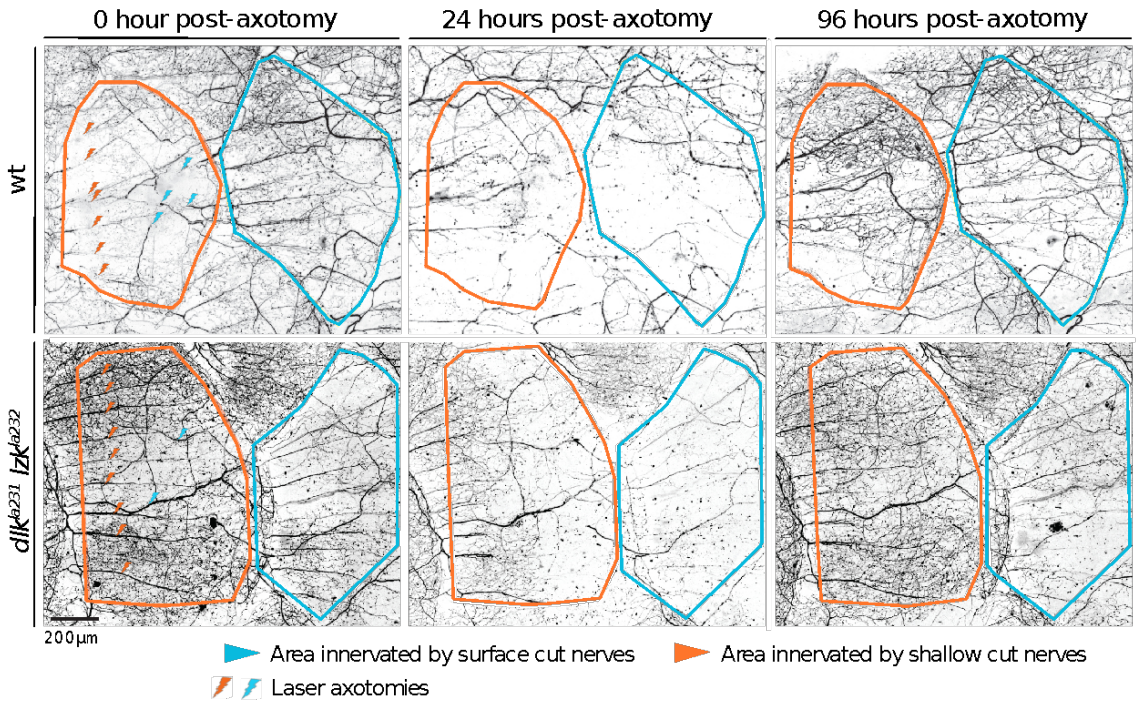
0 hour post-axotomy
24 hours post-axotomy
96 hours post-axotomy
wt
dlk-1ka231 lzk-1ka232
200µm
Area innervated by surface cut nerves
Area innervated by shallow cut nerves
Laser axotomies

Figure 8

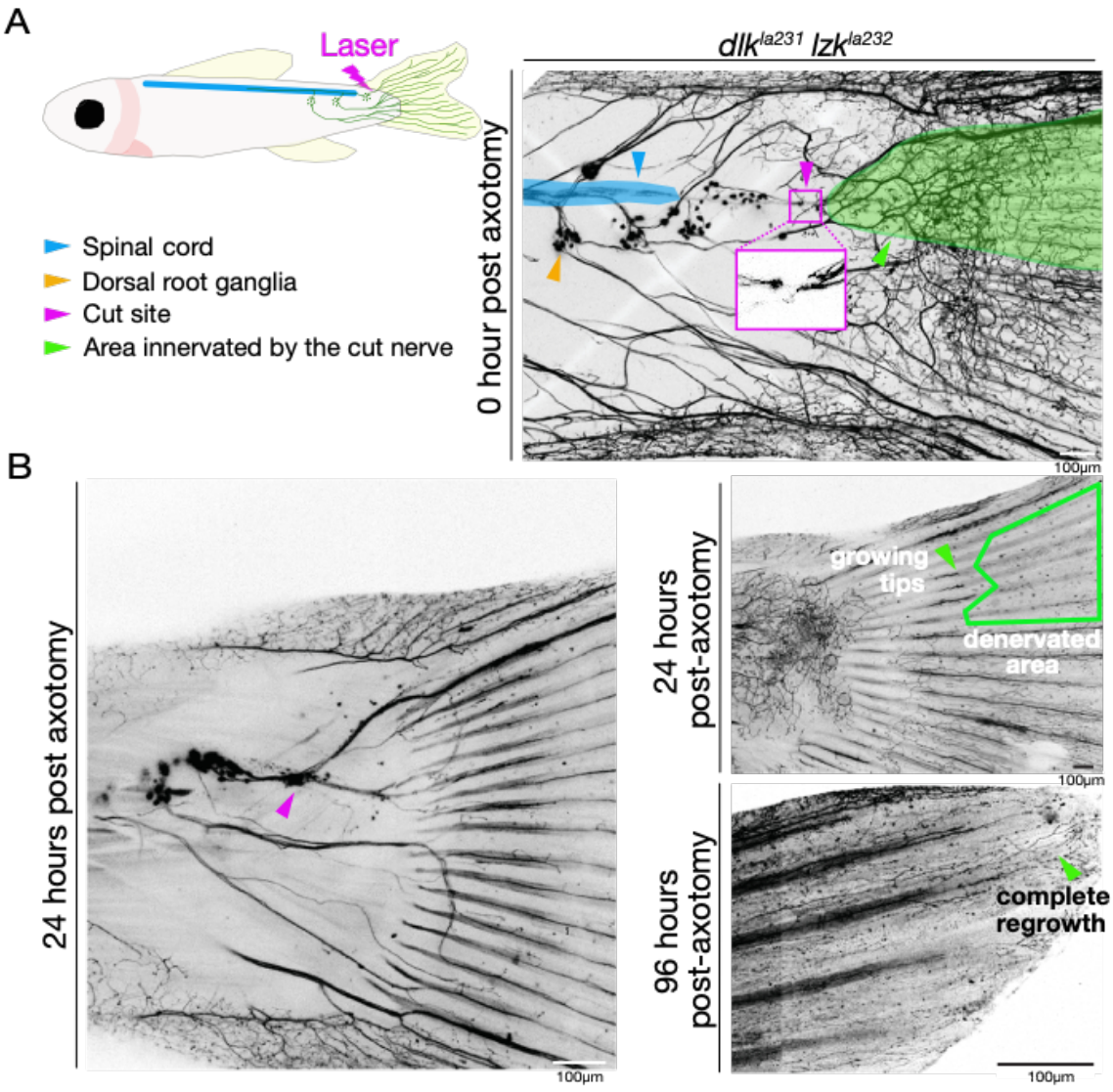
A
Laser
Spinal cord
Dorsal root ganglia
Cut site
Area innervated by the cut nerve
dlk^la231 lzk^la232
0 hour post axotomy
100µm
B
24 hours post axotomy
100µm
24 hours post-axotomy
growing tips
denervated area
100µm
96 hours post-axotomy
complete regrowth
100µm

Figure 9

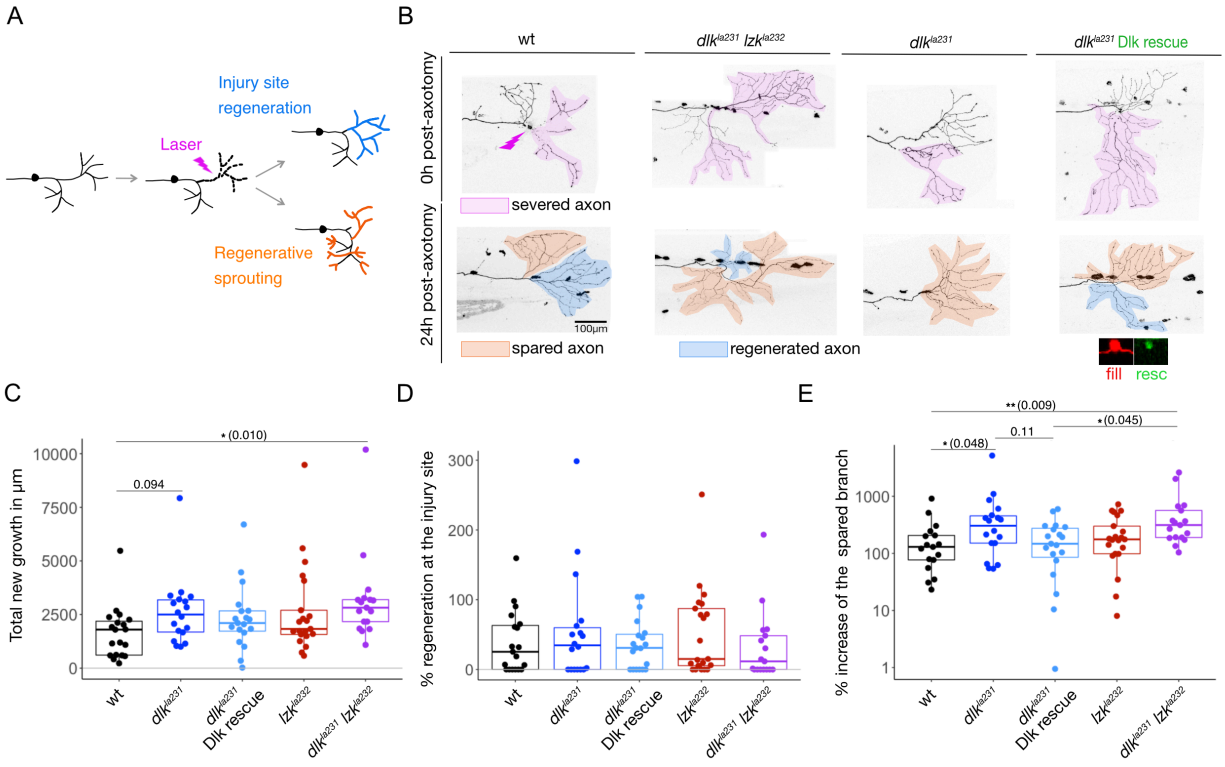
A
Injury site
regeneration
Laser
Regenerative
sprouting
B
wt
dlk^la231 lzk^la232
dlk^la231
dlk^la231 Dlk rescue
0h post-axotomy
24h post-axotomy
severed axon
spared axon
regenerated axon
100µm
fill
resc
C
Total new growth in µm
0.094
* (0.010)
wt
dlk^la231
dlk^la231 Dlk rescue
lzk^la232
dlk^la231 lzk^la232
D
% regeneration at the injury site
E
% increase of the spared branch
* (0.048)
0.11
** (0.009)
* (0.045)

Figure 10

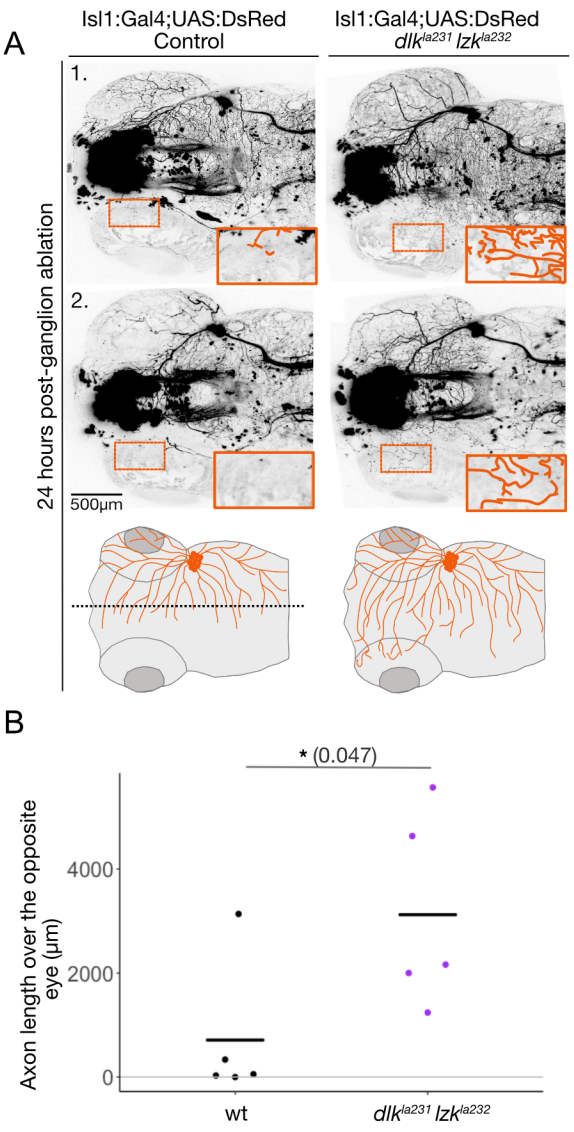
A
Isl1:Gal4;UAS:DsRed
Control
Isl1:Gal4;UAS:DsRed
dlk^la231 lzk^la232
1.
2.
24 hours post-ganglion ablation
500µm
B
* (0.047)
Axon length over the opposite eye (µm)
4000
2000
0
wt
dlk^la231 lzk^la232

References:

Chen L, Nye DM, Stone MC, Weiner AT, Gheres KW, Xiong X, Collins CA, Rolls MM (2016a) Mitochondria and Caspases Tune Nmnat-Mediated Stabilization to Promote Axon Regeneration. PLoS Genet 12:e1006503.

Chen M, Geoffroy CG, Meves JM, Narang A, Li Y, Nguyen MT, Khai VS, Kong X, Steinke CL, Carolino KI, Elzière L, Goldberg MP, Jin Y, Zheng B (2018) Leucine Zipper-Bearing Kinase Is a Critical Regulator of Astrocyte Reactivity in the Adult Mammalian CNS. Cell Rep 22:3587–3597.

Chen M, Geoffroy CG, Wong HN, Tress O, Nguyen MT, Holzman LB, Jin Y, Zheng B (2016b) Leucine Zipper-bearing Kinase promotes axon growth in mammalian central nervous system neurons. Sci Rep 6:31482.

Craig EA, Stevens MV, Vaillancourt RR, Camenisch TD (2008) MAP3Ks as central regulators of cell fate during development. Dev Dyn 237:3102–3114.

Curcio M, Bradke F (2018) Axon Regeneration in the Central Nervous System: Facing the Challenges from the Inside. Annu Rev Cell Dev Biol 34:495–521.

Dickson HM, Zurawski J, Zhang H, Turner DL, Vojtek AB (2010) POSH is an intracellular signal transducer for the axon outgrowth inhibitor Nogo66. J Neurosci 30:13319–13325.

El-Brolosy MA, Kontarakis Z, Rossi A, Kuenne C, Günther S, Fukuda N, Kikhi K, Boezio GLM, Takacs CM, Lai S-L, Fukuda R, Gerri C, Giraldez AJ, Stainier DYR (2019) Genetic compensation triggered by mutant mRNA degradation. Nature Available at: http://dx.doi.org/10.1038/s41586-019-1064-z.

Gallo KA, Johnson GL (2002) Mixed-lineage kinase control of JNK and p38 MAPK pathways. Nat Rev Mol Cell Biol 3:663–672.

Gau P, Poon J, Ufret-Vincenty C, Snelson CD, Gordon SE, Raible DW, Dhaka A (2013) The zebrafish ortholog of TRPV1 is required for heat-induced locomotion. J Neurosci 33:5249–5260.

Ghosh AS, Wang B, Pozniak CD, Chen M, Watts RJ, Lewcock JW (2011) DLK induces developmental neuronal degeneration via selective regulation of proapoptotic JNK activity. J Cell Biol 194:751–764.

Goodwani S, Fernandez C, Acton PJ, Buggia-Prevot V, McReynolds ML, Ma J, Hu CH, Hamby ME, Jiang Y, Le K, Soth MJ, Jones P, Ray WJ (2020) Dual Leucine Zipper Kinase Is Constitutively Active in the Adult Mouse Brain and Has Both Stress-Induced and Homeostatic Functions. Int J Mol Sci 21 Available at: http://dx.doi.org/10.3390/ijms21144849.

Grueber WB, Sagasti A (2010) Self-avoidance and tiling: Mechanisms of dendrite and axon spacing. Cold Spring Harb Perspect Biol 2:a001750.

Hammarlund M, Nix P, Hauth L, Jorgensen EM, Bastiani M (2009) Axon regeneration requires a conserved MAP kinase pathway. Science 323:802–806.

Han L, Dong X (2014) Itch mechanisms and circuits. Annu Rev Biophys 43:331–355.

Higashijima S, Hotta Y, Okamoto H (2000) Visualization of cranial motor neurons in live transgenic zebrafish expressing green fluorescent protein under the control of the islet-1 promoter/enhancer. J Neurosci 20:206–218.

Hirai S-I, Banba Y, Satake T, Ohno S (2011) Axon Formation in Neocortical Neurons Depends on Stage-Specific Regulation of Microtubule Stability by the Dual Leucine Zipper Kinase–c-Jun N-Terminal Kinase Pathway. J Neurosci 31:6468–6480.

Hirai S-I, Cui DF, Miyata T, Ogawa M, Kiyonari H, Suda Y, Aizawa S, Banba Y, Ohno S (2006) The c-Jun N-terminal kinase activator dual leucine zipper kinase regulates axon growth and neuronal migration in the developing cerebral cortex. J Neurosci 26:11992–12002.

Issa FA, Mazzochi C, Mock AF, Papazian DM (2011) Spinocerebellar ataxia type 13 mutant potassium channel alters neuronal excitability and causes locomotor deficits in zebrafish. J Neurosci 31:6831–6841.

Itoh A, Horiuchi M, Bannerman P, Pleasure D, Itoh T (2009) Impaired regenerative response of primary sensory neurons in ZPK/DLK gene-trap mice. Biochem Biophys Res Commun 383:258–262.

Jin Y, Zheng B (2019) Multitasking: Dual Leucine Zipper-Bearing Kinases in Neuronal Development and Stress Management. Annu Rev Cell Dev Biol 35:501–521.

Katz HR, Menelaou E, Hale ME (2021) Morphological and physiological properties of Rohon-Beard neurons along the zebrafish spinal cord. J Comp Neurol 529:1499–1515.

Kwan KM, Fujimoto E, Grabher C, Mangum BD, Hardy ME, Campbell DS, Parant JM, Yost HJ, Kanki JP, Chien C-B (2007) The Tol2kit: a multisite gateway-based construction kit for Tol2 transposon transgenesis constructs. Dev Dyn 236:3088–3099.

Letunic I, Bork P (2007) Interactive Tree Of Life (iTOL): an online tool for phylogenetic tree display and annotation. Bioinformatics 23:127–128.

Li Y, Ritchie EM, Steinke CL, Qi C, Chen L, Zheng B, Jin Y (2021) Activation of MAP3K DLK and LZK in Purkinje cells causes rapid and slow degeneration depending on signaling strength. Elife 10 Available at: http://dx.doi.org/10.7554/eLife.63509.

Ma Z, Zhu P, Shi H, Guo L, Zhang Q, Chen Y, Chen S, Zhang Z, Peng J, Chen J (2019) PTC-bearing mRNA elicits a genetic compensation response via Upf3a and COMPASS components. Nature 568:259–263.

Miller BR, Press C, Daniels RW, Sasaki Y, Milbrandt J, DiAntonio A (2009) A dual leucine kinase-dependent axon self-destruction program promotes Wallerian degeneration. Nat Neurosci 12:387–389.

Miller MA, Pfeiffer W, Schwartz T (2010) Creating the CIPRES Science Gateway for inference of large phylogenetic trees. Gateway Computing Environments Workshop, 2010, 1--8.

Morita T, McClain SP, Batia LM, Pellegrino M, Wilson SR, Kienzler MA, Lyman K, Olsen

ASB, Wong JF, Stucky CL, Brem RB, Bautista DM (2015) HTR7 Mediates Serotonergic Acute and Chronic Itch. Neuron 87:124–138.

Nakata K, Abrams B, Grill B, Goncharov A, Huang X, Chisholm AD, Jin Y (2005) Regulation of a DLK-1 and p38 MAP kinase pathway by the ubiquitin ligase RPM-1 is required for presynaptic development. Cell 120:407–420.

Nye DMR, Albertson RM, Weiner AT, Hertzler JI, Shorey M, Goberdhan DCI, Wilson C, Janes KA, Rolls MM (2020) The receptor tyrosine kinase Ror is required for dendrite regeneration in Drosophila neurons. PLoS Biol 18:e3000657.

O'Brien GS, Martin SM, Söllner C, Wright GJ, Becker CG, Portera-Cailliau C, Sagasti A (2009a) Developmentally regulated impediments to skin reinnervation by injured peripheral sensory axon terminals. Curr Biol 19:2086–2090.

O'Brien GS, Rieger S, Martin SM, Cavanaugh AM, Portera-Cailliau C, Sagasti A (2009b) Two-photon axotomy and time-lapse confocal imaging in live zebrafish embryos. J Vis Exp:1129.

Palanca AMS, Lee S-L, Yee LE, Joe-Wong C, Trinh LA, Hiroyasu E, Husain M, Fraser SE, Pellegrini M, Sagasti A (2013) New transgenic reporters identify somatosensory neuron subtypes in larval zebrafish. Dev Neurobiol 73:152–167.

Rasmussen JP, Sagasti A (2016) Learning to swim, again: Axon regeneration in fish. Exp Neurol 287:318–330.

Rasmussen JP, Vo N-T, Sagasti A (2018) Fish Scales Dictate the Pattern of Adult Skin Innervation and Vascularization. Dev Cell 46:344–359.e4.

Reyes R, Haendel M, Grant D, Melancon E, Eisen JS (2004) Slow degeneration of zebrafish Rohon-Beard neurons during programmed cell death. Dev Dyn 229:30–41.

Robitaille H, Proulx R, Robitaille K, Blouin R, Germain L (2005) The mitogen-activated protein kinase kinase kinase dual leucine zipper-bearing kinase (DLK) acts as a key regulator of keratinocyte terminal differentiation. J Biol Chem 280:12732–12741.

Rosenberg AF, Wolman MA, Franzini-Armstrong C, Granato M (2012) In vivo nerve-macrophage interactions following peripheral nerve injury. J Neurosci 32:3898–3909.

Rossi A, Kontarakis Z, Gerri C, Nolte H, Hölper S, Krüger M, Stainier DYR (2015) Genetic compensation induced by deleterious mutations but not gene knockdowns. Nature 524:230–233.

Sagasti A, Guido MR, Raible DW, Schier AF (2005) Repulsive interactions shape the morphologies and functional arrangement of zebrafish peripheral sensory arbors. Curr Biol 15:804–814.

Schindelin J, Arganda-Carreras I, Frise E, Kaynig V, Longair M, Pietzsch T, Preibisch S, Rueden C, Saalfeld S, Schmid B, Tinevez J-Y, White DJ, Hartenstein V, Eliceiri K, Tomancak P, Cardona A (2012) Fiji: an open-source platform for biological-image analysis. Nat Methods 9:676–682.

Shin JE, Cho Y, Beirowski B, Milbrandt J, Cavalli V, DiAntonio A (2012) Dual leucine zipper

kinase is required for retrograde injury signaling and axonal regeneration. Neuron 74:1015–1022.

Shorey M, Rao K, Stone MC, Mattie FJ, Sagasti A, Rolls MM (2021) Microtubule organization of vertebrate sensory neurons in vivo. Dev Biol Available at: http://dx.doi.org/10.1016/j.ydbio.2021.06.007.

Simard-Bisson C, Bidoggia J, Larouche D, Guérin SL, Blouin R, Hirai S-I, Germain L (2017) A Role for DLK in Microtubule Reorganization to the Cell Periphery and in the Maintenance of Desmosomal and Tight Junction Integrity. J Invest Dermatol 137:132–141.

Stamatakis A (2014) RAxML version 8: a tool for phylogenetic analysis and post-analysis of large phylogenies. Bioinformatics 30:1312–1313.

Steward O, Zheng B, Tessier-Lavigne M (2003) False resurrections: distinguishing regenerated from spared axons in the injured central nervous system. J Comp Neurol 459:1–8.

Stone MC, Albertson RM, Chen L, Rolls MM (2014) Dendrite injury triggers DLK-independent regeneration. Cell Rep 6:247–253.

Summers DW, Milbrandt J, DiAntonio A (2018) Palmitoylation enables MAPK-dependent proteostasis of axon survival factors. Proc Natl Acad Sci U S A 115:E8746–E8754.

Talbot JC, Amacher SL (2014) A streamlined CRISPR pipeline to reliably generate zebrafish frameshifting alleles. Zebrafish 11:583–585.

Tedeschi A, Bradke F (2013) The DLK signalling pathway--a double-edged sword in neural development and regeneration. EMBO Rep 14:605–614.

Thisse B, Heyer V, Lux A, Alunni V, Degrave A, Seiliez I, Kirchner J, Parkhill J-P, Thisse C (2004) Spatial and temporal expression of the zebrafish genome by large-scale in situ hybridization screening. Methods Cell Biol 77:505–519.

Tominaga M, Takamori K (2014) Itch and nerve fibers with special reference to atopic dermatitis: therapeutic implications. J Dermatol 41:205–212.

Tuszynski MH, Steward O (2012) Concepts and methods for the study of axonal regeneration in the CNS. Neuron 74:777–791.

Wang X, Kim JH, Bazzi M, Robinson S, Collins CA, Ye B (2013) Bimodal control of dendritic and axonal growth by the dual leucine zipper kinase pathway. PLoS Biol 11:e1001572.

Watkins TA, Wang B, Huntwork-Rodriguez S, Yang J, Jiang Z, Eastham-Anderson J, Modrusan Z, Kaminker JS, Tessier-Lavigne M, Lewcock JW (2013) DLK initiates a transcriptional program that couples apoptotic and regenerative responses to axonal injury. Proc Natl Acad Sci U S A 110:4039–4044.

Welsbie DS et al. (2017) Enhanced Functional Genomic Screening Identifies Novel Mediators of Dual Leucine Zipper Kinase-Dependent Injury Signaling in Neurons. Neuron 94:1142–1154.e6.

Welsbie DS, Ziogas NK, Xu L, Kim B-J, Ge Y, Patel AK, Ryu J, Lehar M, Alexandris AS, Stewart N, Zack DJ, Koliatsos VE (2019) Targeted disruption of dual leucine zipper kinase and leucine zipper kinase promotes neuronal survival in a model of diffuse traumatic brain injury. Mol Neurodegener 14:44.

Westerfield M, McMurray JV, Eisen JS (1986) Identified motoneurons and their innervation of axial muscles in the zebrafish. J Neurosci 6:2267–2277.

White RM, Sessa A, Burke C, Bowman T, LeBlanc J, Ceol C, Bourque C, Dovey M, Goessling W, Burns CE, Zon LI (2008) Transparent adult zebrafish as a tool for in vivo transplantation analysis. Cell Stem Cell 2:183–189.

Wlaschin JJ, Gluski JM, Nguyen E, Silberberg H, Thompson JH, Chesler AT, Le Pichon CE (2018) Dual leucine zipper kinase is required for mechanical allodynia and microgliosis after nerve injury. Elife 7:e33910.

Xiong X, Wang X, Ewanek R, Bhat P, Diantonio A, Collins CA (2010) Protein turnover of the Wallenda/DLK kinase regulates a retrograde response to axonal injury. J Cell Biol 191:211–223.

Yan D, Jin Y (2012) Regulation of DLK-1 kinase activity by calcium-mediated dissociation from an inhibitory isoform. Neuron 76:534–548.

Yan D, Wu Z, Chisholm AD, Jin Y (2009) The DLK-1 kinase promotes mRNA stability and local translation in C. elegans synapses and axon regeneration. Cell 138:1005–1018.

Yin C, Huang G-F, Sun X-C, Guo Z, Zhang JH (2017) DLK silencing attenuated neuron apoptosis through JIP3/MA2K7/JNK pathway in early brain injury after SAH in rats. Neurobiol Dis 103:133–143.

Zheng C, Atlas E, Lee HMT, Jao SLJ, Nguyen KCQ, Hall DH, Chalfie M (2020) Opposing effects of an F-box protein and the HSP90 chaperone network on microtubule stability and neurite growth in Caenorhabditis elegans. Development 147 Available at: http://dx.doi.org/10.1242/dev.189886.

Chapter 3: DLK and LZK enhancer trap screen

Kadidia Pemba Adula, Hannah Markovic, Alvaro Sagasti

Introduction:

Invertebrate dual leucine zipper-bearing kinase (DLK) and its vertebrate orthologs DLK and leucine zipper kinase (LZK) play important roles in development, homeostasis, and pathological conditions. While organism-wide studies of DLK and LZK localization have focused on tissue level mRNA expression, their cell type specificity within tissues is not well understood. Invertebrate studies reported DLK action to be in specific neuronal cell types *in vivo*, whereas in most mammalian studies, the cells in which DLK and LZK act remain unclear. Invertebrate DLK is expressed in touch-sensing neurons and motor neurons (Xiong and Collins 2012; Hammarlund et al. 2009; Yan et al. 2009; Stone et al. 2014). In mammals, including rodents and humans, DLK and LZK expression is mainly neuronal along with a few other organs. In humans, DLK transcripts were present in the brain, kidney, and skin tissues (Reddy and Pleasure 1994; Blouin et al. 1996; Holzman, Merritt, and Fan 1994). A mouse study looking at DLK protein levels in embryos confirmed these findings (Hirai et al. 2005). Human LZK mRNA transcripts were detected in the pancreas, kidney, and the brain (Sakuma et al. 1997). LZK is also present in rodents' brains (Pozniak et al. 2013). Prior to this thesis, *in situ* hybridization showed DLK distribution in zebrafish to be neuronal (“ZFIN Publication: Thisse et Al., 2004” n.d.). I show that DLK and LZK act cell-autonomously to promote motor neuron regeneration. However, the excessive growth phenotype seen in spared Rohon-Beard touch-sensing axons was partially rescued by cell-autonomous expression of DLK. Therefore, the creation of transgenic lines labeling DLK and LZK expressions would facilitate the identification of cell types expressing these kinases and complement my rescue experiments.

Research over the last two decades posit DLK and LZK as drivers of diverse responses to neuronal insult. DLK and LZK activation resulted in axon regeneration, lack of axon regeneration, axon degeneration, and even cell death (Jin and Zheng 2019; Tedeschi and

Bradke 2013; Asghari Adib, Smithson, and Collins 2018). DLK and LZK responses to injury within the same context are similar and sometimes additive. I show that DLK and LZK are genetically redundant in promoting motor axon regeneration in zebrafish. Elucidating the cell-type-specific patterns of DLK and LZK expression in the nervous system is an important step towards understanding this diversity of responses. Are DLK and LZK always expressed in the same cells? Do some cells only express these kinases under pathological conditions?

Key developmental and evolutionary questions can also be addressed using DLK and LZK expression lines. Unlike LZK, mammalian DLK evolved a function in the organogenesis of several tissues including the nervous system (Nadeau, Grondin, and Blouin 1997). As a result, DLK deletion early in development is fatal in rodents but not in zebrafish or invertebrates (Hirai et al. 2005). LZK mutant mice develop normally (Welsbie et al. 2017). Surprisingly, DLK deletion is not fatal in adults. Tracking the spatio-temporal expression patterns and levels of DLK would provide clues to this evolutionary divergence among vertebrates for early developmental survival.

Thanks to its optical clarity and genetic tractability, zebrafish is an excellent model in which to observe DLK and LZK expression patterns. Using the CRISPR/cas9 system, we attempted to insert the GAL4 gene upstream of DLK and LZK start sites (Kimura et al. 2015; Julien et al. 2018). The constructs were injected into a UAS reporter line. Adults with germline insertions were visually screened and the expression patterns were characterized in larvae. Unfortunately, multiple PCR validation attempts were unsuccessful. Assays to determine genetic compensation and genetic linkage using DLK and LZK individual mutant lines also failed.

Materials and Methods

Zebrafish husbandry

Zebrafish (Danio rerio) were raised at 28.5ºC following a 14h/10h light/dark cycle. Embryos were grown in embryo water (0.3 g/L Instant Ocean Salt, 0.1% methylene blue).

CRISPR gRNA synthesis:

A Cas9 construct adapted for use in zebrafish was chosen for the CRISPR experiments. Two optimal Cas9 target sites upstream of DLK and LZK start sites were generated on the CRISPRscan website. The “short oligo method to generate gRNA” protocol was used to amplify the guide RNAs via PCR (Montague et al. 2014). The target sequences were selected to cut and insert a donor plasmid containing the GAL4 gene into the genome. A heat shock promoter drives the GAL4 gene and is followed by a polyA tail. This donor construct was extracted from an original pBluescript- SK-Gbait-Hsp-Gal4FF-BGHpA plasmid procured from Shin-Ichi Higashijima (Kimura et al. 2015). At the one-cell-stage, 2-3nL of CRISPR injection mix (150ng/uL of Cas9 mRNA, 7ng/uL of donor plasmid (GAL4), 7ng/uL of gRNA targeting the donor plasmid, and 7ng/uL of gRNA targeting DLK or LZK) was injected into the cell of the embryo. Injected embryos were of a Tg(UAS:nfsb-mCherry) background.

Confocal imaging

To block pigmentation and facilitate imaging, embryos were treated with phenylthiourea (PTU) at 22-23 hpf. Larva were anesthetized with 0.2 mg/mL MS-222 in embryo media (0.08%) before mounting. A plastic ring was mounted onto a coverslip using vacuum grease. Individual larvae were embedded in 1% agarose and mounted directly on the cover slip inside the chamber. Upon solidification of the agarose (~15 minutes). The ring was then filled with tricaine-containing embryo media and sealed with a glass slide (O’Brien et al. 2009). Live confocal images were collected on an LSM 800 using a 10X air objective (Plan-NEOFLUAR, NA= 0.3) or 20X air objective (Plan-APOCHROMAT, NA= 0.8). Images were acquired with Zen Blue software from Zeiss.

Table: Plasmids, reagents, zebrafish lines

Plasmids	Source

SK-Gbait-Hsp-Gal4FF-BGHpA	(Kimura et al. 2015)
Reagents	
pCS2-nCas9n	Addgene, #47929
HiScribe T7 High Yield RNA Synthesis kit	New England Biolabs, #E2050S
Qiagen RNeasy Mini Kit	Qiagen, #74104
Phenylthiourea	Sigma, CAS#103855
Zebrafish lines	
Tg(NeuroD:GFP)	(Obholzer et al. 2008)
Tg(isl2b:GFP)	(Pittman, Law, and Chien 2008)
Tg(UAS:nfsb-mCherry)	(Davison et al. 2007)
dlk^{la231}	This thesis
lzk^{la232}	This thesis

Results

Creation of enhancer traps

Enhancer trap lines were created using CRISPR/Cas9 to insert the Gal4-VP16 gene into the promoter region of either DLK or LZK in Tg(UAS:nfsb-mCherry) zebrafish embryos. In these enhancer traps, the DLK or LZK regulatory elements should drive expression of Gal4-VP16, which will then drive expression of nfsb-mCherry, allowing analysis of gene expression by documenting red fluorescence. I first used the CRISPRscan website to identify optimal gRNA

sites in the 5' upstream regions of the DLK and LZK genes (Figure 1A, Table 1). Two guides, targeting two different regions, were selected for each gene. I synthesized these guide RNAs and injected each along with Cas9 mRNA, a plasmid with the Gal4-VP16 gene, and a guide RNA to cut the Gal4-containing plasmid, into a Tg(UAS:nfsb-mCherry) fish line (Figure 1B). Cas9 should be translated in the embryo and specifically cut both the Gal4 plasmid and the zebrafish genome using the two gRNAs. When DNA is repaired, the Gal4 plasmid should insert into the genome at a low frequency, and drive nfsb-mCherry expression (Figure 1C-D).

Because the Tg(UAS:nfsb-mCherry) line is capable of being promiscuously activated in all cells, especially early in development, I screened injected embryos for mCherry expression at 24 hpf. Although much of the expression may come from the unincorporated Gal4 plasmid, the fluorescence level was a good measure of the amount of Gal4 plasmid successfully injected. Screening embryos for fluorescence can increase the yield of founders to 25% or more (Kimura et al, 2014). These embryos were grown to adulthood. After pre-screening 15-20 fish per injected guide RNA by PCR for Gal4 incorporation in tail tissue, I crossed these fish to WT and screened resulting embryos for mCherry fluorescence. I identified one presumed founder each for the DLK (*et*^{la233}) and LZK (*et*^{la234}) enhancer traps.

Characterization of *et*^{la233} and *et*^{la234}

et^{la233} and et^{la234} enhancer trap founders were crossed to WT fish, yielding progeny heterozygous for both *et*^{la233}:Gal4-VP16 (or *et*^{la234}:Gal4-VP16) and Tg(UAS:nfsb-mCherry). mCherry expression was imaged in these progenies with confocal microscopy. These images showed that *et*^{la233} was expressed in some spinal cord neurons, muscles, the brain, the eye, and the nose at 24 hpf (Figure 2A-E). The proportion of spinal cord neurons expressing *et*^{la233} was greater than those expressing *et*^{la234} (Figure 2C, 2G, 3C, 3G). At 48 hpf, *et*^{la233} was also expressed in photoreceptors and no longer expressed in the nose (Figure 2F-I). At 72 hpf, it also was expressed in the kidney (Figure 2J-N). By 96 hpf, *et*^{la233} was only expressed in

muscles, photoreceptors, and the kidney (Figure 2O-S). *et*^{la234} was expressed in some spinal cord neurons, motor neurons, and muscle cells at 24 hpf (Figure 3A-D). By 48 hpf, it was also expressed in the vasculature, enteric neurons, part of the brain, some heart cells, and either actinotrichia or pigment cells (Figure 3E-G). By 72 hpf, expression was turned on in photoreceptors and the kidney, in addition to all locations it was expressed at 48 hpf (Figure 3H-L). By 96 hpf, it was only expressed in muscles, the brain, photoreceptors, the kidney, and smooth muscles surrounding the intestine (Figure 3M-R).

et^{la233} and *et*^{la234} appeared to share expression in muscle cells, spinal cord neurons, the brain, eye, and kidney during different time points in development (Table 2). Although there were similarities in overall expression patterns, the two enhancer traps were expressed in distinct cell types perhaps only overlapping in the spinal cord, photoreceptors, and the kidney. Interestingly, motor neurons frequently synapsed with a muscle cell that also expressed the enhancer traps (Figure 2C, 2G). Although both *et*^{la233} and *et*^{la234} were expressed in the brain, their expression patterns were clearly different. *et*^{la233} is widely expressed, whereas *et*^{la234} is expressed in a specific area behind the ear (Figure 2D, 2H, 3K, 3P). *et*^{la234} is also expressed in the vasculature, smooth muscles, and in cells on the ventral and posterior edge of the yolk which resemble actinotrichia or pigment cells, while *et*^{la233} was not (Figure 3G, J, O, N, I). The *et*^{la233} expression patterns are similar to DLK *in situ* data suggesting proper insertion of GAL4 (Thisse and Thisse, 2004).

I crossed the enhancer trap lines to the Tg(isl2b:GFP) and Tg(NeuroD:GFP) reporter lines (expressed in sensory neurons and motor neurons, respectively) to narrow down the cell types expressing the *et*^{la233} and *et*^{la234} (Figure 4). *et*^{la233} and *et*^{la234} seem to be expressed in sparse sensory neurons across the spinal cord (Figure 4A, D, E, G). The expression of *et*^{la233} and *et*^{la234} in a subset of sensory neurons indicates that either this expression is specific to a subtype of sensory neurons, or that UAS was downregulated in some cells. Crossing *et*^{la234} to the

Tg(NeuroD:GFP) line did not provide much insight. Although this line should express GFP in all neurons other than sensory neurons, there were some neurons at the ventral side of the spinal cord which appeared to express *et*^{la234} but not NeuroD (Figure 4I). However, the Tg(isl2b:GFP) line showed that sensory neurons were on the dorsal side of the spinal cord (Figure 4G). This implies that there were additional neurons, which were not sensory neurons, where NeuroD was not expressed.

PCR validation of the enhancer traps failed

GAL4 insertion into the correct locus could not be validated by PCR. The gene trap technique used in this assay enables the insertion in either direction. Therefore, primers were designed to verify insertion site as well as orientation. Moreover, multiple copies of the donor plasmid can be incorporated at one location which can also be detected by PCR. Multiple primer pairs and annealing temperatures were tested; however, PCR bands did not match the expected sizes. While the GAL4 sequence itself was incorporated, we could not pinpoint its insertion in either *et*^{la233} or *et*^{la234}. Although inverse PCR could reveal the exact location of GAL4 insertion in the genome, the process can be lengthy. Instead, genetic compensation and genetic linkage determination were next used to assess the potential DLK and LZK enhancer traps.

The *et*^{la233} and *et*^{la234} do not reflect DLK and LZK genetic compensation

Transcriptional compensation of mutant mRNA by gene with redundant functions occurs even in heterozygous mutants (El-Brolosy et al, 2019). I showed that DLK and LZK genetically compensate for each other in motor neuron regeneration in zebrafish. While *dlk*^{la231} mutants regenerate a little less well than *lzk*^{la232}, *dlk*^{la231} *lzk*^{la232} double mutants show severe deficits. Were GAL4 to be correctly inserted upstream of DLK and LZK start sites in *et*^{la233} and *et*^{la234} respectively, DLK and LZK transcriptional compensation for each other would be apparent in the enhancer traps. To test for transcriptional compensation, the *et*^{la234} enhancer trap was crossed to *dlk*^{la231} mutants whereas the *et*^{la233} enhancer trap was crossed to *lzk*^{la232} mutants (Figure 5).

Embryos were imaged at 72 hpf. While *et*^{la234} is only expressed in a subset of neurons (as is most evident in the brain), it is expected to show expression in an increased number of neurons in the *dlk*^{la231} +/- and *dlk*^{la231} -/- backgrounds. Since the expression pattern of the *et*^{la234} was identical in *dlk*^{la231} +/-, *dlk*^{la231} -/- and in embryos WT for DLK, *et*^{la234} does not show the transcriptional compensation by LZK (Figure 5A-C). While *et*^{la233} is not expressed in the vasculature, it is expected to label blood vessels in the *lzk*^{la232} +/- and *lzk*^{la232} -/- backgrounds. However, the expression pattern of the et^{la233} was identical in *lzk*^{la232} +/-, *lzk*^{la232} -/- and in embryos WT for LZK (Figure 5D-F). Therefore, *et*^{la233} does not show the transcriptional compensation by DLK. *et*^{la233} is not an enhancer trap of DLK. Similarly, *et*^{la234} is not an enhancer trap of LZK.

The enhancer traps are not genetically linked to DLK and LZK mutations

Were *et*^{la233} and *et*^{la234} to be properly inserted upstream of DLK and LZK start sites respectively, genetic linkage would be in effect. As a result, crossing *et*^{la233} homozygous line to *dlk*^{la231} homozygous line could never result in a homozygous DLK mutant positive for *et*^{la233}. Similarly, a homozygous LZK mutant could not be positive for *et*^{la234}. However, seven *dlk*^{la231} homozygous mutants were positive for *et*^{la233}. One *lzk*^{la232} homozygous mutant was positive for *et*^{la233}. As a result, GAL4 in *et*^{la233} and *et*^{la234} are not correctly inserted in DLK's and LZK's 5'UTR regions.

Figure legends

Figure 1: Assay to incorporate Gal4 into DLK and LZK 5' UTR using CRISPR-Cas9

A. Representation of the locations of each guide RNA. **B.** A Gal4-VP16 plasmid, a guide RNA to cut the plasmid, a guide RNA for the genome, and Cas9 mRNA were injected into Tg(UAS:nfsb-mCherry) embryos. **C.** After injection into zebrafish embryos, the Cas9 mRNA will be translated into Cas9 protein (purple). The guide RNAs (green) for the DLK 5' UTR and for the Gal4 plasmid should bind to their homologous regions and induce Cas9 to produce double-stranded breaks. At low frequency, the Gal4-VP16 sequence should be incorporated into the genome

while repairs are made to the DNA. **D.** Upon DLK or LZK promoter elements activation, Gal4-VP16 would bind to the UAS sequence, in turn promoting nfsb-mCherry expression. **E-F.** PCR primers were designed to amplify a region spanning from within the Gal4 plasmid, across the expected insertion site, and into the DLK gene.

Figure 2: *et*^{la233} expression in developing zebrafish. *et*^{la233}:Gal4/+;UAS:mCherry/+ embryos were imaged for mCherry expression using confocal microscopy every 24 hours**. A-E.** *et*^{la233} expression at 24 hpf. **B.** Developing Rohon-Beard neurons. **D.** The brain from a dorsal view. **F-I.** *et*^{la233} expression at 48 hpf. **H.** The brain is viewed across the anterior-posterior axis. **J-N.** *et*^{la233} expression at 72 hpf. **O-S.** *et*^{la233} expression at 96 hpf. **S.** Neurons behind the eye, viewed from the anterior-posterior axis.

A, F, J, O. Muscles. **C, G, L, Q.** Motor and other spinal cord neurons. **E, I, N.** Photoreceptors. **K, P.** Sensory neurons in the tail. **M, R.** Kidney.

Figure 3: *et*^{la234} expression in developing zebrafish. *et*^{la234}:Gal4/+;UAS:mCherry/+ fish were imaged for mCherry expression using confocal microscopy every 24 hours. **A-D.** *et*^{la233} expression at 24 hpf. **C.** Spinal cord neurons from the anterior-posterior axis. **D.** Spinal cord neurons from a dorsal view. **E-G.** *et*^{la233} expression at 48 hpf. **H-L.** *et*^{la233} expression at 72 hpf. **I.** Actinotrichia or pigment cells (arrowhead). **M-R.** *et*^{la233} expression at 96 hpf. **N.** Smooth muscles lining the intestine.

A, E, H, M. Muscles. **B, F.** Rohon-Beard neurons in the tail. **G, J, O.** Spinal cord neurons and vasculature. **K, P.** Brain. **L, R.** Photoreceptors.

Figure 4: et^{la233} and et^{la234} are expressed in a subset of sensory neurons. An Tg(isl2b:GFP) transgenic line, which expresses GFP in somatosensory neurons, was crossed to *et*^{la233}(**A-D**) and *et*^{la234} (**E-G**) enhancer traps and imaged at 48 hpf using confocal microscopy. A

Tg(NeuroD:GFP) transgenic line, which expresses GFP in all neurons except touch-sensing neurons, was also crossed to the *et*^{la234} enhancer trap and imaged similarly (**H-I**).

Figure 5: LZK and DLK genetic compensation is not reflected in *et*^{la233} or *et*^{la234}

Embryos were imaged for mCherry fluorescence at 72 hpf using confocal microscopy (**A-F**). **A.** *et*^{la234}:Gal4/+; UAS:mCherry/+ **B.** *dlk*^{la231}+/-; et^{la234}:Gal4/+; UAS:mCherry/+ **C.** *dlk*^{la231}-/-; *et*^{la234}:Gal4/+; UAS:mCherry/+. Since the expression pattern of the *et*^{la234} is identical in *dlk*^{la231}+/-, *dlk*^{la231}-/- and in embryos WT for DLK, *et*^{la234} is not an enhancer trap of LZK (**A-C**). **D.** *et*^{la233}:Gal4/+; UAS:mCherry/+ **E.** *lzk*^{la232}+/-; *et*^{la233}:Gal4/+; UAS:mCherry/+ **F.** *lzk*^{la232}-/-; *et*^{la233}:Gal4/+; UAS:mCherry/+. Since the expression pattern of the *et*^{la233} is identical in *lzk*^{la232}+/- embryos, *lzk*^{la232}-/- in embryos WT for DLK (**D-F**), *et*^{la233} is not an enhancer trap of DLK.

Table 1: CRISPR guide RNA Sequences. The NGG sequence is underlined within the genome sequence. This sequence is not homologous to the guide RNA sequence but is important for Cas9 functionality. The gRNA sequence is in red font under “Short oligo ordered”.

Table 2: *et*^{la233} and *et*^{la234} expression during zebrafish development. DLK and LZK are both expressed in neurons and muscles early in development, but this expression is turned off by 4 days post-fertilization. By 4 days, DLK is only expressed in the kidney and photoreceptors, whereas LZK is expressed in the vasculature, kidney, and photoreceptors.

Figures

Figure 1:

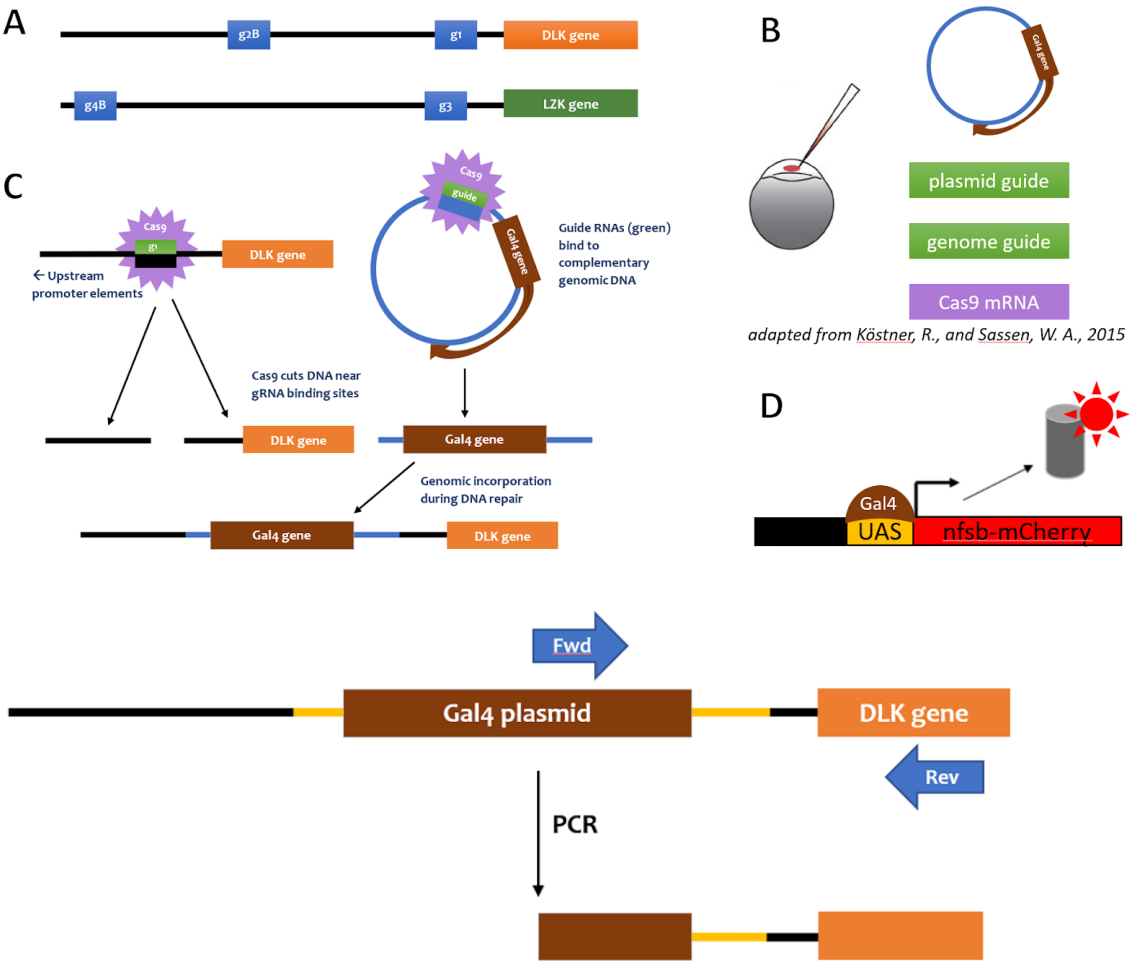
A
g2B
g1
DLK gene
g4B
g3
LZK gene
B
Gal4 gene
plasmid guide
genome guide
Cas9 mRNA
adapted from Köstner, R., and Sassen, W. A., 2015
C
Cas9
g1
DLK gene
← Upstream promoter elements
Cas9
guide
Gal4 gene
Guide RNAs (green) bind to complementary genomic DNA
Cas9 cuts DNA near gRNA binding sites
DLK gene
Gal4 gene
Genomic incorporation during DNA repair
Gal4 gene
DLK gene
D
Gal4
UAS
nfsb-mCherry
Fwd
Gal4 plasmid
DLK gene
Rev
PCR

Figure 2:

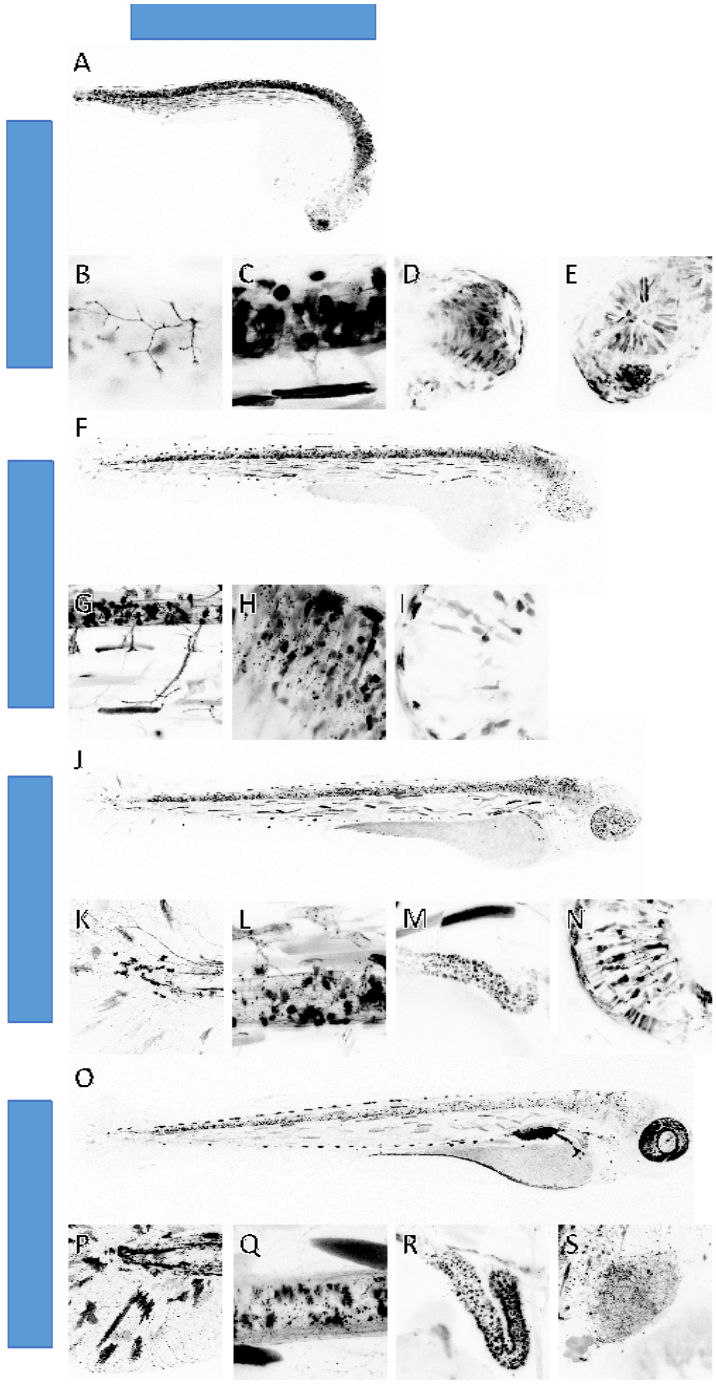

Figure 3:

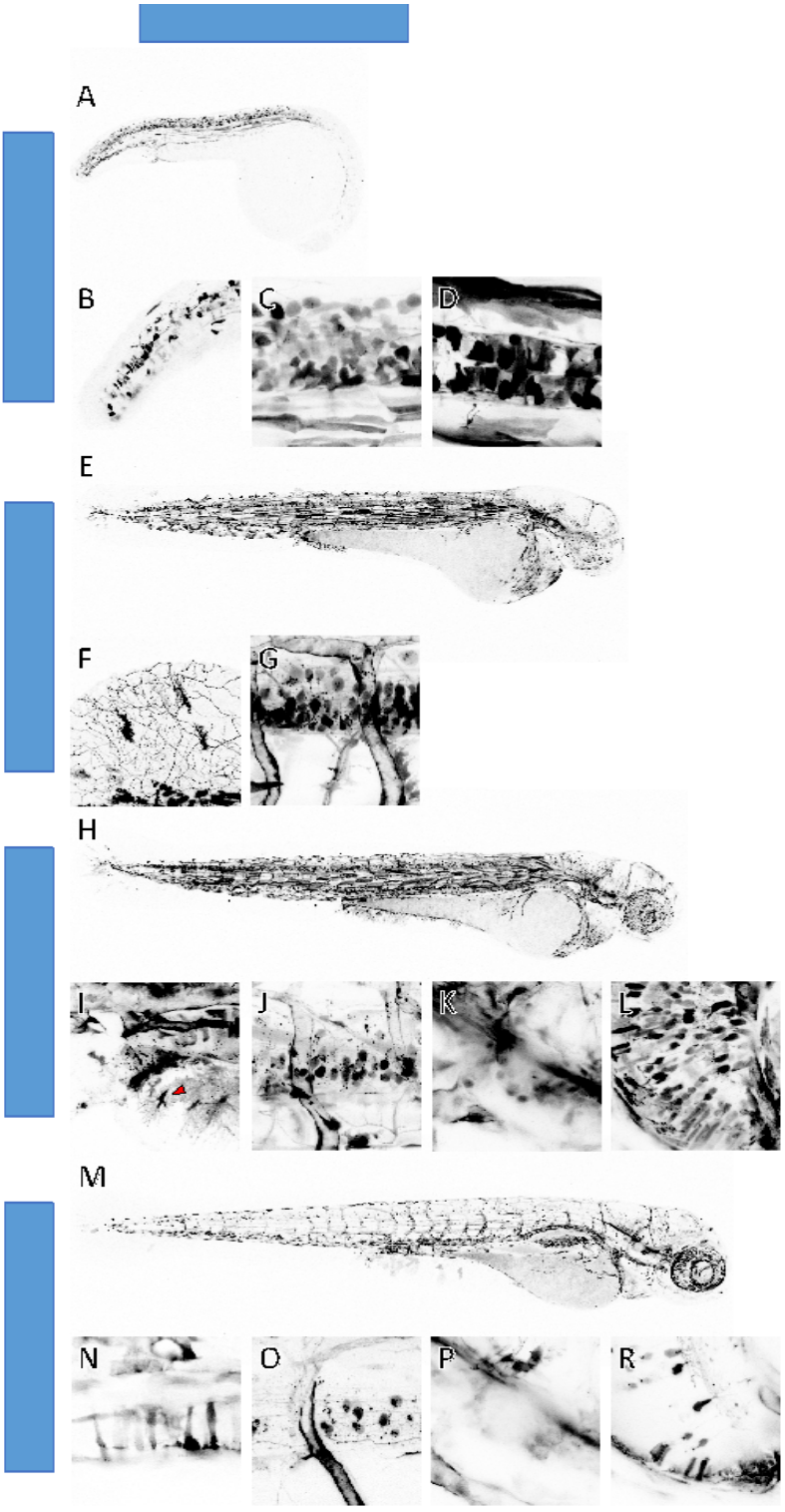

Figure 4:

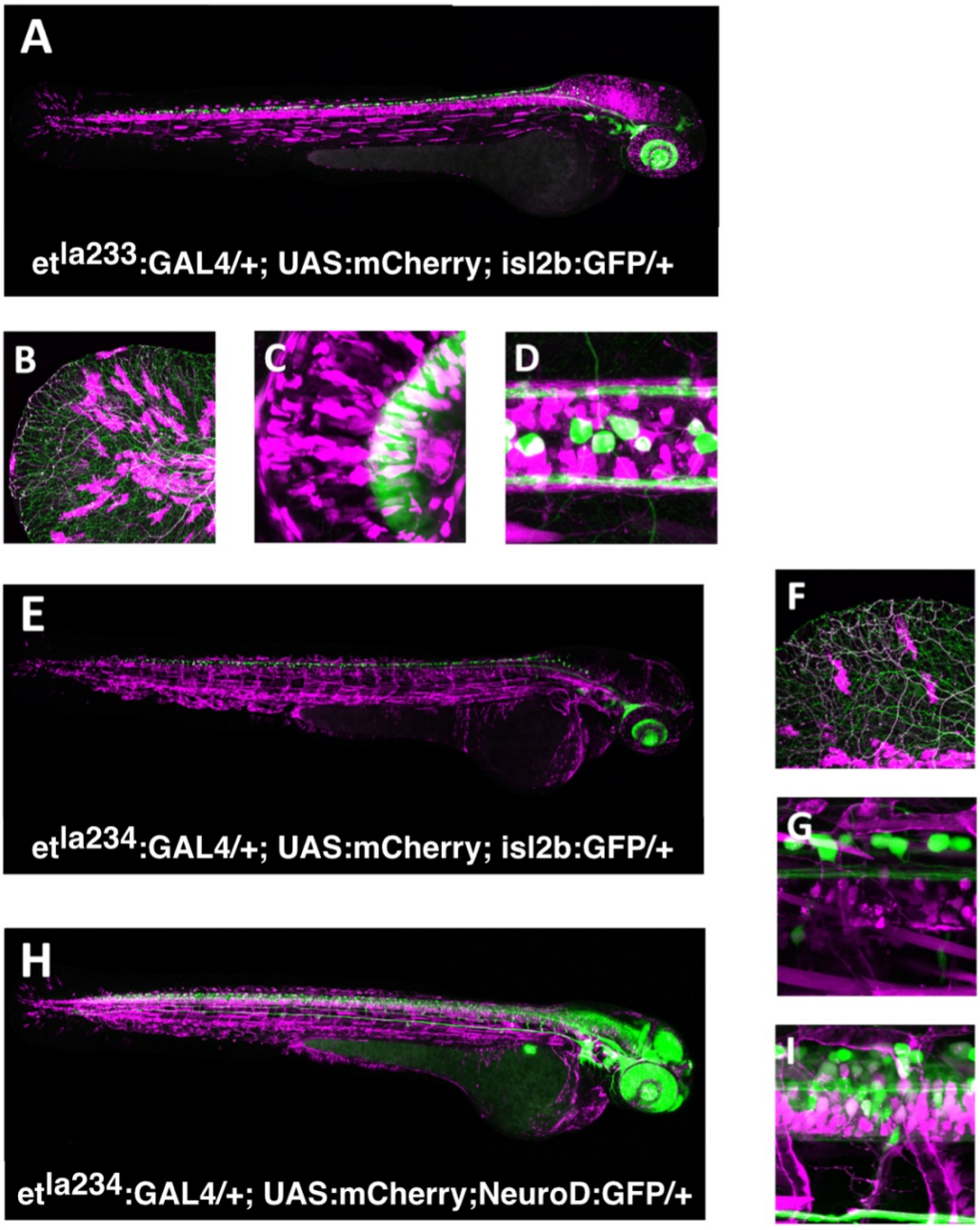
A
et^la233:GAL4/+; UAS:mCherry; isl2b:GFP/+
B
C
D
E
et^la234:GAL4/+; UAS:mCherry; isl2b:GFP/+
F
G
H
et^la234:GAL4/+; UAS:mCherry;NeuroD:GFP/+
I

Figure 5:

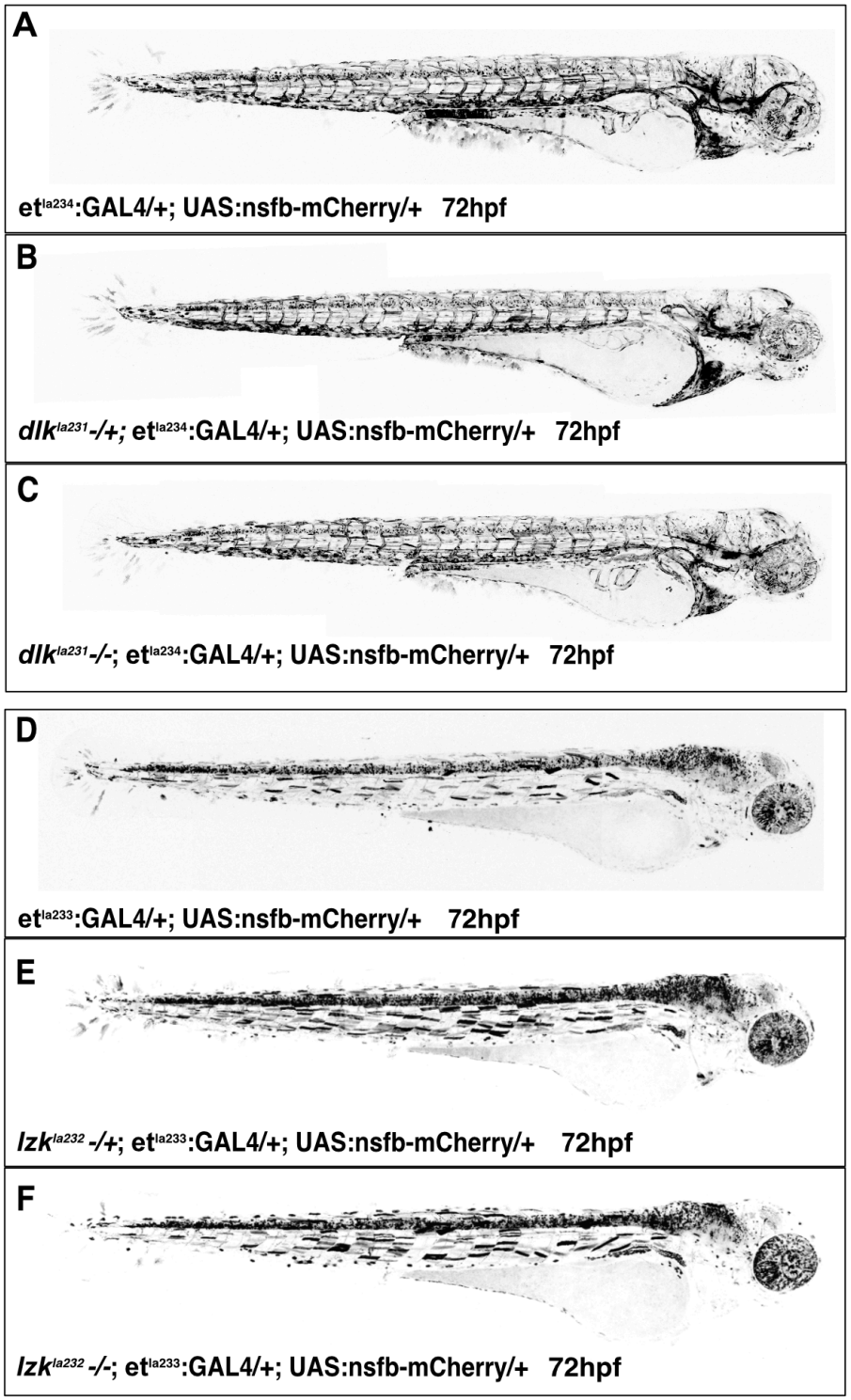
A
et la234 :GAL4/+; UAS:nsfb-mCherry/+ 72hpf
B
dlk la231 -/+; et la234 :GAL4/+; UAS:nsfb-mCherry/+ 72hpf
C
dlk la231 -/-; et la234 :GAL4/+; UAS:nsfb-mCherry/+ 72hpf
D
et la233 :GAL4/+; UAS:nsfb-mCherry/+ 72hpf
E
lzk la232 -/+; et la233 :GAL4/+; UAS:nsfb-mCherry/+ 72hpf
F
lzk la232 -/-; et la233 :GAL4/+; UAS:nsfb-mCherry/+ 72hpf

Table 1

Guide RNA	**Homologous DNA sequence in genome PAM**	**Short oligo ordered**
DLK 1	CGGTGCCCGTTCTGAAGGG TGGG	cgctaatacgactcactata**GGGTGCCCGT TCTGAAGGGT**gttttagagctagaaatagc
DLK 2B	TGCATTGCCCGAGTCCCTC ATGG	cgctaatacgactcactata**GGCATTGCCC GAGTCCCTCA**gttttagagctagaaatagc
LZK 3	AGGCGTGTCATAAACCCCA TCGG	cgctaatacgactcactata**GGGCGTGTCA TAAACCCCAT**gttttagagctagaaatagc
LZK 4B	GCACACAGCAGGAGACGGA TTGG	cgctaatacgactcactata**GGACACAGCA GGAGACGGAT**gttttagagctagaaatagc

Table 2

Time point	et[233]	et[234]
24 hpf	spinal cord (including sensory and motor neurons), muscles, brain, eye, nose	spinal cord (including sensory and motor neurons), muscles
48 hpf	spinal cord (including sensory and motor neurons), muscles, brain, photoreceptors	spinal cord (including sensory and motor neurons), muscles, vasculature, enteric neurons, brain, heart, actinotrichia or pigment cells

72 hpf	spinal cord (including sensory and motor neurons), muscles, photoreceptors, kidney	spinal cord (including sensory and motor neurons), muscles, vasculature, enteric neurons, brain, heart, actinotrichia or pigment cells, photoreceptors, kidney
96 hpf	muscles, photoreceptors, kidney	muscles, brain, photoreceptors, kidney, smooth muscles

Conclusion and future directions:

As a significant cause of disability in humans, neuronal dysfunction is expected to remain a top health priority. Thanks to basic research using model organisms, we have acquired some mechanistic understanding of axon damage and repair processes. Axon regeneration is influenced by positive and negative cues coming from the damaged neuron itself, as well as from its environment. While most mammalian studies focus on extrinsic factors, assessing the contribution of intrinsic factors is necessary for a complete view of the regenerative process. Though it appears we are still far from cures, despite advances in the field, the outlook is optimistic. We have a wealth of data accumulated over decades of axon damage research. The difficulty lies in the seemingly variable outcomes to neuronal insult, which include axon regeneration, lack of axon regeneration, collateral sprouting, and cell death. I discerned four experimental factors that affect these outcomes: the environment of the cell, neuronal cell-type specificity, the scale of the injury, and subcellular localization. The key to understanding the conditions that result in different injury outcomes is to compare studies based on these four experimental factors. With careful comparison, patterns in studies conducted under similar parameters start to emerge. The same approach can be used to understand the context-specificity of activating invertebrate DLK's, and both DLK and LZK in vertebrates, to outcomes following axon injury.

Using an experimental protocol I designed, which accounts for the four parameters previously described, I investigated DLK and LZK function following axon injury. I cut axons with single cell resolution in zebrafish, a level of precision not yet possible with mammals in vivo. This vertebrate model has the strengths associated with invertebrate models, such as optical clarity, genetic tractability, and the capacity for single cell resolution. As a vertebrate, zebrafish share more in common with mammals but enable mosaic labeling of specific neuronal cell-types to assess their intrinsic regenerative capacities.

I found that DLK promotes axon regeneration in zebrafish MNs, which is consistent with studies in other species. DLK is required for axon regeneration in roundworms, flies and rodents (Asghari Adib, Smithson, and Collins 2018; Tedeschi and Bradke 2013; Jin and Zheng 2019). Here, I am comparing apples to apples as the cell type studied is the same. The environment around MN in the mammalian PNS, in flies and roundworms, and in zebrafish PNS is permissive. MNs were completely severed and the damage occurred in the same cellular compartment: the axon. Additionally, my work is the first to show genetic redundancy of DLK and LZK function in promoting axon regeneration in motor neurons.

While these kinases are required for axon regeneration in MNs, they are not required in RB touch-sensing neurons following complete axotomy. Surprisingly, DLK and LZK are essential to prevent excessive sprouting in non-injured branches following partial axotomy. Additionally, DLK and LZK regulate post-injury collateral sprouting at the population level in touch-sensing neurons. The sprouting phenotype I found was not seen following sciatic nerve crush in mice with a conditional deletion of DLK in DRGs and a few other cell types. Instead, they saw reduced regrowth compared to wildtype animals (Shin et al. 2012). Several conditions are different between the zebrafish and mouse models. This discrepancy could be due to the limited ability of neurons to regrow in the mammalian PNS, despite its permissiveness. Another possibility is that the excessive sprouting phenotype I saw in double mutants after partial axotomy is due to both cell autonomous and non-cell-autonomous contributions. While every cell had DLK and LZK mutations in the zebrafish model, the mouse study only deleted DLK in a few cell types, including DRGs. This could be the reason why they failed to see excessive growth. This idea would also explain why my cell-type-specific DLK and LZK rescues were partial. Immune cells are potential candidates for DLK and LZK non-neuronal action. A mouse study indicated that LZK is upregulated in astrocytes following nerve injury, and DLK expression also activates and recruits microglia to the site of injury (Wlaschin et al. 2018; M. Chen et al.

2018). The best comparison for my data would be to a sciatic crush following ubiquitous deletion of DLK and LZK in adult rodents.

As for an invertebrate comparison, DLK was required for axon regeneration in Drosophila touch-sensing neurons following complete axotomy (Stone et al. 2014). Despite the similarities in experimental factors between the zebrafish model and this *Drosophila* study, it may not be appropriate to compare DLK function in invertebrate touch-sensing neurons with that of vertebrates' because the homologous cell types are structurally different. Vertebrate touch-sensing neurons are pseudounipolar with two axons and no dendrites, whereas fly touch-sensing neurons have canonical dendrites and an axon.

Interpreting the excessive sprouting phenotype could benefit from a more detailed understanding of the cell types in which DLK and LZK are expressed. To inform my axotomy studies, I set out to create DLK and LZK reporter lines in zebrafish. Since the transcriptional expression levels of these kinases are normally kept low, I designed GAL4 gene traps to amplify the signals. When crossed to UAS reporter lines, these enhancer lines would visualize the spatio-temporal expression of the kinases, as well as identify the populations of cells in which they are expressed. Validation experiments revealed incorrect insertions of GAL4, but creating such an *in vivo* tool remains an important future goal. Alternatively, a fluorescent gene could be directly inserted upstream of the kinases in the genome. Fluorescent screening could then be coupled with a nervous system-wide injury assay, such as the application of a neurotoxic drug, to upregulate DLK and LZK expression levels.

Vertebrate DLK and LZK evolved an additional side to their multifaceted functions wherein, at high expression levels, they signal cell death in neurons. It is clear that DLK and LZK are expressed in the mammalian nervous system, as evidenced by DLK and LZK RNA detection in human and rodent tissues (Reddy and Pleasure 1994; Sakuma et al. 1997; Holzman, Merritt, and Fan 1994; Blouin et al. 1996). Studies also reported DLK protein expression in mice (Hirai et al. 2002, 2005). Therefore, it is surprising that overexpressing these kinases in live rodents

leads to cell death (Yunbo Li et al. 2021). I also found DLK and LZK overexpression to be toxic to neurons in the zebrafish model. However, careful titration of the plasmids enabled the normal development of MN and RB neurons, as well as the rescue of mutant injury phenotypes. I suspect that DLK and LZK activity is tightly regulated by neurons. Overwhelming the cell's ability to maintain DLK and LZK to specific levels in particular compartments may lead to inappropriate signaling resulting in cell death.

While DLK and LZK over-expression leads to cell death in vertebrates, DLK over-expression in *Drosophila* and *C.elegans* does not. DLK-induced apoptosis in vertebrates involves BAX's permeabilization of mitochondrial outer membrane (MOMP) and release of cytochrome C, which then activates caspases (Dhanasekaran and Reddy 2008; de Los Reyes Corrales, Losada-Pérez, and Casas-Tintó 2021; Tsuruta et al. 2004). The MOMP phenomenon does not occur in *Drosophila* nor in *C.elegans (Oberst, Bender, and Green 2008)*. However, studies in the *Crassostrea gigas* oyster and in various planaria flatworms reported that these invertebrates undergo MOMP-mediated apoptosis (Yingxiang Li et al. 2017; Bender et al. 2012). It would be interesting to determine if DLK overexpression results in the cell death of oyster and planaria neurons.

In the future, further physiological experiments would offer insights into the mechanism underlying DLK and LZK regulation of collateral sprouting in touch-sensing neurons. Why do double mutant peripheral axons grow more and occupy more space than controls following partial axotomy? DLK and LZK signaling may enable RB neurons to differentiate between injured and non-injured axon branches. I hypothesize that in double mutants, vesicles are equally trafficked between the damaged axon branch and the non-injured ones following partial axotomy. This could be tested by making twelve-hour live-recordings of vesicle trafficking in wildtypes and double mutants. If my hypothesis is correct, then DLK and LZK signaling direct cargos, such as vesicles and mitochondria, toward the injured axon branch and away from uninjured ones.

In double mutants, the spared branches of RB axons sprout excessively following partial axotomy. RB axon branches do not extend excessively during development, likely because tiling is still occurring. Based on these findings, I hypothesize that spared axon branches in double mutants grow faster than in wildtype to cover the denervated area. Photo-conversion could be used to differentiate a partially cut RB from non-photo-converted neighbors to assess post-injury tiling. Live-imaging of wildtype and double mutant RBs could be used to compare their regenerative growth rates. Cytoskeletal dynamics in the proximal axon and at growth cones could also be analyzed with actin and microtubule reporters.

Further molecular studies can also be undertaken to address the genetic redundancy of DLK and LZK action in MN. While individual mutants can regenerate, double mutants exhibit severe deficits. I hypothesize that both DLK and LZK activate JNK in response to axon damage to promote axon regeneration. If my hypothesis is correct, repeating axotomies of wildtype MNs in the presence of a JNK inhibitory drug should result in severe regeneration impairments. The double mutant post-injury phenotype should not worsen with exposure to a JNK inhibitor. These experiments and others will provide insights into how to approach the treatment of axon damage, a serious biomedical issue. Axon injuries have diverse origins and, unsurprisingly, result in diverse outcomes. The tailoring of treatment to the contextual insult is an exciting line of inquiry that may offer patients some relief sooner rather than later. In this thesis, I showed that DLK and LZK direct cell-type-specific and injury type-specific responses to axon injury. Investments in precise drug delivery technologies would facilitate the transition to cell-type-specific targeting of DLK and LZK. Diseases such as Alzheimer's, and frontotemporal lobar degeneration (FTLD), which only affect a particular population of neurons, would also benefit from such strategies(Fu, Hardy, and Duff 2018). The emergence of cell-type-specific treatments for axon damage will signal our entry into a new age of precision medicine.

References:

Asghari Adib, Elham, Laura J. Smithson, and Catherine A. Collins. 2018. “An Axonal Stress Response Pathway: Degenerative and Regenerative Signaling by DLK.” *Current Opinion in Neurobiology* 53 (December): 110–19.

Bastmeyer, M., M. Bähr, and C. A. Stuermer. 1993. “Fish Optic Nerve Oligodendrocytes Support Axonal Regeneration of Fish and Mammalian Retinal Ganglion Cells.” *Glia* 8 (1): 1–11.

Bastmeyer, M., M. Beckmann, M. E. Schwab, and C. A. Stuermer. 1991. “Growth of Regenerating Goldfish Axons Is Inhibited by Rat Oligodendrocytes and CNS Myelin but Not but Not by Goldfish Optic Nerve Tract Oligodendrocytelike Cells and Fish CNS Myelin.” *The Journal of Neuroscience: The Official Journal of the Society for Neuroscience* 11 (3): 626–40.

Beirowski, Bogdan, Elisabetta Babetto, Michael P. Coleman, and Keith R. Martin. 2008. “The WldS Gene Delays Axonal but Not Somatic Degeneration in a Rat Glaucoma Model.” *The European Journal of Neuroscience* 28 (6): 1166–79.

Bender, Cheryl E., Patrick Fitzgerald, Stephen W. G. Tait, Fabien Llambi, Gavin P. McStay, Douglas O. Tupper, Jason Pellettieri, Alejandro Sánchez Alvarado, Guy S. Salvesen, and Douglas R. Green. 2012. “Mitochondrial Pathway of Apoptosis Is Ancestral in Metazoans.” *Proceedings of the National Academy of Sciences of the United States of America* 109 (13): 4904–9.

Blouin, R., J. Beaudoin, P. Bergeron, A. Nadeau, and G. Grondin. 1996. “Cell-Specific Expression of the ZPK Gene in Adult Mouse Tissues.” *DNA and Cell Biology* 15 (8): 631–42.

Bounoutas, Alexander, Qun Zheng, Michael L. Nonet, and Martin Chalfie. 2009. “Mec-15 Encodes an F-Box Protein Required for Touch Receptor Neuron Mechanosensation,

Synapse Formation and Development.” *Genetics* 183 (2): 607–17, 1SI – 4SI.

Burton, P. R., and J. L. Paige. 1981. “Polarity of Axoplasmic Microtubules in the Olfactory Nerve of the Frog.” *Proceedings of the National Academy of Sciences of the United States of America* 78 (5): 3269–73.

Chen, Meifan, Cédric G. Geoffroy, Jessica M. Meves, Aarti Narang, Yunbo Li, Mallorie T. Nguyen, Vung S. Khai, et al. 2018. “Leucine Zipper-Bearing Kinase Is a Critical Regulator of Astrocyte Reactivity in the Adult Mammalian CNS.” *Cell Reports* 22 (13): 3587–97.

Chen, Meifan, Cédric G. Geoffroy, Hetty N. Wong, Oliver Tress, Mallorie T. Nguyen, Lawrence B. Holzman, Yishi Jin, and Binhai Zheng. 2016. “Leucine Zipper-Bearing Kinase Promotes Axon Growth in Mammalian Central Nervous System Neurons.” *Scientific Reports* 6 (August): 31482.

Chen, Xiqun, Margarita Rzhetskaya, Tatyana Kareva, Ross Bland, Matthew J. During, A. William Tank, Nikolai Kholodilov, and Robert E. Burke. 2008. “Antiapoptotic and Trophic Effects of Dominant-Negative Forms of Dual Leucine Zipper Kinase in Dopamine Neurons of the Substantia Nigra in Vivo.” *The Journal of Neuroscience: The Official Journal of the Society for Neuroscience* 28 (3): 672–80.

Chisholm, Andrew D. 2013. “Cytoskeletal Dynamics in Caenorhabditis Elegans Axon Regeneration.” *Annual Review of Cell and Developmental Biology* 29 (July): 271–97.

Coleman, Michael P., and Marc R. Freeman. 2010. “Wallerian Degeneration, Wld(s), and Nmnat.” *Annual Review of Neuroscience* 33: 245–67.

Collins, Catherine A., Yogesh P. Wairkar, Sylvia L. Johnson, and Aaron DiAntonio. 2006. “Highwire Restrains Synaptic Growth by Attenuating a MAP Kinase Signal.” *Neuron* 51 (1): 57–69.

David, S., and A. J. Aguayo. 1981. “AXONAL ELONGATION INTO PERIPHERAL NERVOUS-SYSTEM BRIDGES AFTER CENTRAL NERVOUS-SYSTEM INJURY IN ADULT-RATS.” *Science* 214 (4523): 931–33.

Davison, Jon M., Courtney M. Akitake, Mary G. Goll, Jerry M. Rhee, Nathan Gosse, Herwig Baier, Marnie E. Halpern, Steven D. Leach, and Michael J. Parsons. 2007. “Transactivation from Gal4-VP16 Transgenic Insertions for Tissue-Specific Cell Labeling and Ablation in Zebrafish.” *Developmental Biology* 304 (2): 811–24.

Dhanasekaran, D. N., K. Kashef, C. M. Lee, H. Xu, and E. P. Reddy. 2007. “Scaffold Proteins of MAP-Kinase Modules.” *Oncogene* 26 (22): 3185–3202.

Dhanasekaran, D. N., and E. P. Reddy. 2008. “JNK Signaling in Apoptosis.” *Oncogene* 27 (48): 6245–51.

Dickson, Heather M., Jonathan Zurawski, Huanqing Zhang, David L. Turner, and Anne B. Vojtek. 2010. “POSH Is an Intracellular Signal Transducer for the Axon Outgrowth Inhibitor Nogo66.” *The Journal of Neuroscience: The Official Journal of the Society for Neuroscience* 30 (40): 13319–25.

Elion, E. A. 2001. “The Ste5p Scaffold.” *Journal of Cell Science* 114 (Pt 22): 3967–78.

Eto, Kaoru, Takeshi Kawauchi, Makiko Osawa, Hidenori Tabata, and Kazunori Nakajima. 2010. “Role of Dual Leucine Zipper-Bearing Kinase (DLK/MUK/ZPK) in Axonal Growth.” *Neuroscience Research* 66 (1): 37–45.

Faux, M. C., and J. D. Scott. 1996. “Molecular Glue: Kinase Anchoring and Scaffold Proteins.” *Cell* 85 (1): 9–12.

Fernandes, Kimberly A., Jeffrey M. Harder, Simon W. John, Peter Shrager, and Richard T. Libby. 2014. “DLK-Dependent Signaling Is Important for Somal but Not Axonal Degeneration of Retinal Ganglion Cells Following Axonal Injury.” *Neurobiology of Disease* 69 (September): 108–16.

Fu, Hongjun, John Hardy, and Karen E. Duff. 2018. “Selective Vulnerability in Neurodegenerative Diseases.” *Nature Neuroscience* 21 (10): 1350–58.

Fukuyama, K., M. Yoshida, A. Yamashita, T. Deyama, M. Baba, A. Suzuki, H. Mohri, et al. 2000. “MAPK Upstream Kinase (MUK)-Binding Inhibitory Protein, a Negative Regulator of

MUK/dual Leucine Zipper-Bearing Kinase/leucine Zipper Protein Kinase." *The Journal of Biological Chemistry* 275 (28): 21247–54.

Gallo, Kathleen A., and Gary L. Johnson. 2002. "Mixed-Lineage Kinase Control of JNK and p38 MAPK Pathways." *Nature Reviews. Molecular Cell Biology* 3 (9): 663–72.

Ghosh-Roy, Anindya, Zilu Wu, Alexandr Goncharov, Yishi Jin, and Andrew D. Chisholm. 2010. "Calcium and Cyclic AMP Promote Axonal Regeneration in Caenorhabditis Elegans and Require DLK-1 Kinase." *The Journal of Neuroscience: The Official Journal of the Society for Neuroscience* 30 (9): 3175–83.

Goodwani, Sunil, Celia Fernandez, Paul J. Acton, Virginie Buggia-Prevot, Morgan L. McReynolds, Jiacheng Ma, Cheng Hui Hu, et al. 2020. "Dual Leucine Zipper Kinase Is Constitutively Active in the Adult Mouse Brain and Has Both Stress-Induced and Homeostatic Functions." *International Journal of Molecular Sciences* 21 (14). https://doi.org/10.3390/ijms21144849.

Haeusgen, Wiebke, Thomas Herdegen, and Vicki Waetzig. 2011. "The Bottleneck of JNK Signaling: Molecular and Functional Characteristics of MKK4 and MKK7." *European Journal of Cell Biology* 90 (6-7): 536–44.

Hammarlund, Marc, Paola Nix, Linda Hauth, Erik M. Jorgensen, and Michael Bastiani. 2009. "Axon Regeneration Requires a Conserved MAP Kinase Pathway." *Science* 323 (5915): 802–6.

Heidemann, S. R., J. M. Landers, and M. A. Hamborg. 1981. "Polarity Orientation of Axonal Microtubules." *The Journal of Cell Biology* 91 (3 Pt 1): 661–65.

Hirai, Syu-Ichi, De Feng Cui, Takaki Miyata, Masaharu Ogawa, Hiroshi Kiyonari, Yoko Suda, Shinichi Aizawa, Yumi Banba, and Shigeo Ohno. 2006. "The c-Jun N-Terminal Kinase Activator Dual Leucine Zipper Kinase Regulates Axon Growth and Neuronal Migration in the Developing Cerebral Cortex." *The Journal of Neuroscience: The Official Journal of the Society for Neuroscience* 26 (46): 11992–2.

Hirai, Syu-Ichi, Atsumi Kawaguchi, Ryutaro Hirasawa, Masaya Baba, Tetsuo Ohnishi, and Shigeo Ohno. 2002. “MAPK-Upstream Protein Kinase (MUK) Regulates the Radial Migration of Immature Neurons in Telencephalon of Mouse Embryo.” *Development* 129 (19): 4483–95.

Hirai, Syu-Ichi, Atumi Kawaguchi, Jun Suenaga, Makiko Ono, De Feng Cui, and Shigeo Ohno. 2005. “Expression of MUK/DLK/ZPK, an Activator of the JNK Pathway, in the Nervous Systems of the Developing Mouse Embryo.” *Gene Expression Patterns: GEP* 5 (4): 517–23.

Holland, Sabrina M., Kaitlin M. Collura, Andrea Ketschek, Kentaro Noma, Toby A. Ferguson, Yishi Jin, Gianluca Gallo, and Gareth M. Thomas. 2016. “Palmitoylation Controls DLK Localization, Interactions and Activity to Ensure Effective Axonal Injury Signaling.” *Proceedings of the National Academy of Sciences of the United States of America* 113 (3): 763–68.

Holzman, L. B., S. E. Merritt, and G. Fan. 1994. “Identification, Molecular Cloning, and Characterization of Dual Leucine Zipper Bearing Kinase. A Novel Serine/threonine Protein Kinase That Defines a Second Subfamily of Mixed Lineage Kinases.” *The Journal of Biological Chemistry* 269 (49): 30808–17.

Issa, Fadi A., Christopher Mazzochi, Allan F. Mock, and Diane M. Papazian. 2011. “Spinocerebellar Ataxia Type 13 Mutant Potassium Channel Alters Neuronal Excitability and Causes Locomotor Deficits in Zebrafish.” *The Journal of Neuroscience: The Official Journal of the Society for Neuroscience* 31 (18): 6831–41.

Itoh, Aki, Makoto Horiuchi, Peter Bannerman, David Pleasure, and Takayuki Itoh. 2009. “Impaired Regenerative Response of Primary Sensory Neurons in ZPK/DLK Gene-Trap Mice.” *Biochemical and Biophysical Research Communications* 383 (2): 258–62.

Itoh, Takayuki, Makoto Horiuchi, Raymond H. Ikeda Jr, Jie Xu, Peter Bannerman, David Pleasure, Josef M. Penninger, Cathy Tournier, and Aki Itoh. 2014. “ZPK/DLK and MKK4

Form the Critical Gateway to Axotomy-Induced Motoneuron Death in Neonates." *The Journal of Neuroscience: The Official Journal of the Society for Neuroscience* 34 (32): 10729–42.

Jin, Yishi, and Binhai Zheng. 2019. "Multitasking: Dual Leucine Zipper-Bearing Kinases in Neuronal Development and Stress Management." *Annual Review of Cell and Developmental Biology* 35 (October): 501–21.

Julien, Donald P., Alex W. Chan, Joshua Barrios, Jaffna Mathiaparanam, Adam Douglass, Marc A. Wolman, and Alvaro Sagasti. 2018. "Zebrafish Expression Reporters and Mutants Reveal That the IgSF Cell Adhesion Molecule Dscamb Is Required for Feeding and Survival." *Journal of Neurogenetics* 32 (4): 336–52.

Karney-Grobe, Scott, Alexandra Russo, Erin Frey, Jeffrey Milbrandt, and Aaron DiAntonio. 2018. "HSP90 Is a Chaperone for DLK and Is Required for Axon Injury Signaling." *Proceedings of the National Academy of Sciences of the United States of America* 115 (42): E9899–9908.

Katz, Hilary R., Evdokia Menelaou, and Melina E. Hale. 2021. "Morphological and Physiological Properties of Rohon-Beard Neurons along the Zebrafish Spinal Cord." *The Journal of Comparative Neurology* 529 (7): 1499–1515.

Kimura, Yukiko, Yu Hisano, Atsuo Kawahara, and Shin-Ichi Higashijima. 2015. "Efficient Generation of Knock-in Transgenic Zebrafish Carrying Reporter/driver Genes by CRISPR/Cas9-Mediated Genome Engineering." *Scientific Reports*. https://doi.org/10.1038/srep06545.

Liao, Edward H., Wesley Hung, Benjamin Abrams, and Mei Zhen. 2004. "An SCF-like Ubiquitin Ligase Complex That Controls Presynaptic Differentiation." *Nature* 430 (6997): 345–50.

Li, Yingxiang, Linlin Zhang, Tao Qu, Xueying Tang, Li Li, and Guofan Zhang. 2017. "Conservation and Divergence of Mitochondrial Apoptosis Pathway in the Pacific Oyster, Crassostrea Gigas." *Cell Death & Disease*. https://doi.org/10.1038/cddis.2017.307.

Li, Y., C. L. Schlamp, K. P. Poulsen, and R. W. Nickells. 2000. “Bax-Dependent and Independent Pathways of Retinal Ganglion Cell Death Induced by Different Damaging Stimuli.” *Experimental Eye Research* 71 (2): 209–13.

Li, Yunbo, Erin M. Ritchie, Christopher L. Steinke, Cai Qi, Lizhen Chen, Binhai Zheng, and Yishi Jin. 2021. “Activation of MAP3K DLK and LZK in Purkinje Cells Causes Rapid and Slow Degeneration Depending on Signaling Strength.” *eLife* 10 (January). https://doi.org/10.7554/eLife.63509.

Los Reyes Corrales, Teresa de, María Losada-Pérez, and Sergio Casas-Tintó. 2021. “JNK Pathway in CNS Pathologies.” *International Journal of Molecular Sciences* 22 (8). https://doi.org/10.3390/ijms22083883.

Mata, Marina, Steven E. Merritt, Guang Fan, Geng Geng Yu, and Lawrence B. Holzman. 1996. “Characterization of Dual Leucine Zipper-Bearing Kinase, a Mixed Lineage Kinase Present in Synaptic Terminals Whose Phosphorylation State Is Regulated by Membrane Depolarization via Calcineurin.” *The Journal of Biological Chemistry* 271 (28): 16888–96.

Meriin, A. B., and M. Y. Sherman. 2005. “Role of Molecular Chaperones in Neurodegenerative Disorders.” *International Journal of Hyperthermia: The Official Journal of European Society for Hyperthermic Oncology, North American Hyperthermia Group* 21 (5): 403–19.

Miller, Bradley R., Craig Press, Richard W. Daniels, Yo Sasaki, Jeffrey Milbrandt, and Aaron DiAntonio. 2009. “A Dual Leucine Kinase-Dependent Axon Self-Destruction Program Promotes Wallerian Degeneration.” *Nature Neuroscience* 12 (4): 387–89.

Montague, Tessa G., José M. Cruz, James A. Gagnon, George M. Church, and Eivind Valen. 2014. “CHOPCHOP: A CRISPR/Cas9 and TALEN Web Tool for Genome Editing.” *Nucleic Acids Research* 42 (Web Server issue): W401–7.

Nadeau, André, Gilles Grondin, and Richard Blouin. 1997. “In Situ Hybridization Analysis of ZPK Gene Expression During Murine Embryogenesis.” *Journal of Histochemistry & Cytochemistry*. https://doi.org/10.1177/002215549704500114.

Nakata, Katsunori, Benjamin Abrams, Brock Grill, Alexandr Goncharov, Xun Huang, Andrew D. Chisholm, and Yishi Jin. 2005. “Regulation of a DLK-1 and p38 MAP Kinase Pathway by the Ubiquitin Ligase RPM-1 Is Required for Presynaptic Development.” *Cell* 120 (3): 407–20.

Nihalani, D. 2001. “Mixed Lineage Kinase-Dependent JNK Activation Is Governed by Interactions of Scaffold Protein JIP with MAPK Module Components.” *The EMBO Journal*. https://doi.org/10.1093/emboj/20.13.3447.

Nihalani, Deepak, Steven Merritt, and Lawrence B. Holzman. 2000. “Identification of Structural and Functional Domains in Mixed Lineage Kinase Dual Leucine Zipper-Bearing Kinase Required for Complex Formation and Stress-Activated Protein Kinase Activation *.” *The Journal of Biological Chemistry* 275 (10): 7273–79.

Oberst, A., C. Bender, and D. R. Green. 2008. “Living with Death: The Evolution of the Mitochondrial Pathway of Apoptosis in Animals.” *Cell Death and Differentiation* 15 (7): 1139–46.

Obholzer, Nikolaus, Sean Wolfson, Josef G. Trapani, Weike Mo, Alex Nechiporuk, Elisabeth Busch-Nentwich, Christoph Seiler, et al. 2008. “Vesicular Glutamate Transporter 3 Is Required for Synaptic Transmission in Zebrafish Hair Cells.” *The Journal of Neuroscience: The Official Journal of the Society for Neuroscience* 28 (9): 2110–18.

O’Brien, Georgeann S., Sandra Rieger, Seanna M. Martin, Ann M. Cavanaugh, Carlos Portera-Cailliau, and Alvaro Sagasti. 2009. “Two-Photon Axotomy and Time-Lapse Confocal Imaging in Live Zebrafish Embryos.” *Journal of Visualized Experiments: JoVE*, no. 24 (February): 1129.

Ousman, Shalina S., Ariana Frederick, and Erin-Mai F. Lim. 2017. “Chaperone Proteins in the Central Nervous System and Peripheral Nervous System after Nerve Injury.” *Frontiers in Neuroscience* 11 (February): 79.

Palanca, Ana Marie S., Sung-Ling Lee, Laura E. Yee, Carlee Joe-Wong, Le A. Trinh, Elizabeth

Hiroyasu, Majid Husain, Scott E. Fraser, Matteo Pellegrini, and Alvaro Sagasti. 2013. “New Transgenic Reporters Identify Somatosensory Neuron Subtypes in Larval Zebrafish.” *Developmental Neurobiology* 73 (2): 152–67.

Pinto, Maria J., Diogo Tomé, and Ramiro D. Almeida. 2021. “The Ubiquitinated Axon: Local Control of Axon Development and Function by Ubiquitin.” *The Journal of Neuroscience: The Official Journal of the Society for Neuroscience* 41 (13): 2796–2813.

Pittman, Andrew J., Mei-Yee Law, and Chi-Bin Chien. 2008. “Pathfinding in a Large Vertebrate Axon Tract: Isotypic Interactions Guide Retinotectal Axons at Multiple Choice Points.” *Development* 135 (17): 2865–71.

Pozniak, Christine D., Arundhati Sengupta Ghosh, Alvin Gogineni, Jesse E. Hanson, Seung-Hye Lee, Jessica L. Larson, Hilda Solanoy, et al. 2013. “Dual Leucine Zipper Kinase Is Required for Excitotoxicity-Induced Neuronal Degeneration.” *The Journal of Experimental Medicine* 210 (12): 2553–67.

Qi, Maosong, and Elaine A. Elion. 2005. “MAP Kinase Pathways.” *Journal of Cell Science* 118 (Pt 16): 3569–72.

Rallis, Andrew, Bingwei Lu, and Julian Ng. 2013. “Molecular Chaperones Protect against JNK- and Nmnat-Regulated Axon Degeneration in Drosophila.” *Journal of Cell Science* 126 (Pt 3): 838–49.

Reddy, U. R., and D. Pleasure. 1994. “Cloning of a Novel Putative Protein Kinase Having a Leucine Zipper Domain from Human Brain.” *Biochemical and Biophysical Research Communications* 205 (2): 1494–95.

Sakuma, H., A. Ikeda, S. Oka, Y. Kozutsumi, J. P. Zanetta, and T. Kawasaki. 1997. “Molecular Cloning and Functional Expression of a cDNA Encoding a New Member of Mixed Lineage Protein Kinase from Human Brain.” *The Journal of Biological Chemistry* 272 (45): 28622–29.

Sengupta Ghosh, Arundhati, Bei Wang, Christine D. Pozniak, Mark Chen, Ryan J. Watts, and

Joseph W. Lewcock. 2011. “DLK Induces Developmental Neuronal Degeneration via Selective Regulation of Proapoptotic JNK Activity.” *The Journal of Cell Biology* 194 (5): 751–64.

Shin, Jung Eun, Yongcheol Cho, Bogdan Beirowski, Jeffrey Milbrandt, Valeria Cavalli, and Aaron DiAntonio. 2012. “Dual Leucine Zipper Kinase Is Required for Retrograde Injury Signaling and Axonal Regeneration.” *Neuron* 74 (6): 1015–22.

Steward, Oswald, Binhai Zheng, and Marc Tessier-Lavigne. 2003. “False Resurrections: Distinguishing Regenerated from Spared Axons in the Injured Central Nervous System.” *The Journal of Comparative Neurology* 459 (1): 1–8.

Stone, Michelle C., Richard M. Albertson, Li Chen, and Melissa M. Rolls. 2014. “Dendrite Injury Triggers DLK-Independent Regeneration.” *Cell Reports* 6 (2): 247–53.

Suenaga, Jun, De Feng Cui, Isao Yamamoto, Shigeo Ohno, and Syu-Ichi Hirai. 2006. “Developmental Changes in the Expression Pattern of the JNK Activator Kinase MUK/DLK/ZPK and Active JNK in the Mouse Cerebellum.” *Cell and Tissue Research* 325 (1): 189–95.

Summers, Daniel W., Erin Frey, Lauren J. Walker, Jeffrey Milbrandt, and Aaron DiAntonio. 2020. “DLK Activation Synergizes with Mitochondrial Dysfunction to Downregulate Axon Survival Factors and Promote SARM1-Dependent Axon Degeneration.” *Molecular Neurobiology* 57 (2): 1146–58.

Summers, Daniel W., Jeffrey Milbrandt, and Aaron DiAntonio. 2018. “Palmitoylation Enables MAPK-Dependent Proteostasis of Axon Survival Factors.” *Proceedings of the National Academy of Sciences of the United States of America* 115 (37): E8746–54.

Taipale, Mikko, Daniel F. Jarosz, and Susan Lindquist. 2010. “HSP90 at the Hub of Protein Homeostasis: Emerging Mechanistic Insights.” *Nature Reviews. Molecular Cell Biology* 11 (7): 515–28.

Tedeschi, Andrea, and Frank Bradke. 2013. “The DLK Signalling Pathway--a Double-Edged

Sword in Neural Development and Regeneration." *EMBO Reports* 14 (7): 605–14.

Tsuruta, Fuminori, Jun Sunayama, Yasunori Mori, Seisuke Hattori, Shigeomi Shimizu, Yoshihide Tsujimoto, Katsuji Yoshioka, Norihisa Masuyama, and Yukiko Gotoh. 2004. "JNK Promotes Bax Translocation to Mitochondria through Phosphorylation of 14-3-3 Proteins." *The EMBO Journal* 23 (8): 1889–99.

Tuszynski, Mark H., and Oswald Steward. 2012. "Concepts and Methods for the Study of Axonal Regeneration in the CNS." *Neuron* 74 (5): 777–91.

Wang, Fang, Donald P. Julien, and Alvaro Sagasti. 2013. "Journey to the Skin: Somatosensory Peripheral Axon Guidance and Morphogenesis." *Cell Adhesion & Migration* 7 (4): 388–94.

Watkins, Trent A., Bei Wang, Sarah Huntwork-Rodriguez, Jing Yang, Zhiyu Jiang, Jeffrey Eastham-Anderson, Zora Modrusan, Joshua S. Kaminker, Marc Tessier-Lavigne, and Joseph W. Lewcock. 2013. "DLK Initiates a Transcriptional Program That Couples Apoptotic and Regenerative Responses to Axonal Injury." *Proceedings of the National Academy of Sciences of the United States of America* 110 (10): 4039–44.

Welsbie, Derek S., Katherine L. Mitchell, Vinod Jaskula-Ranga, Valentin M. Sluch, Zhiyong Yang, Jessica Kim, Eugen Buehler, et al. 2017. "Enhanced Functional Genomic Screening Identifies Novel Mediators of Dual Leucine Zipper Kinase-Dependent Injury Signaling in Neurons." *Neuron* 94 (6): 1142–54.e6.

Whitmarsh, A. J. 2006. "The JIP Family of MAPK Scaffold Proteins." *Biochemical Society Transactions* 34 (Pt 5): 828–32.

Wlaschin, Josette J., Jacob M. Gluski, Eileen Nguyen, Hanna Silberberg, James H. Thompson, Alexander T. Chesler, and Claire E. Le Pichon. 2018. "Dual Leucine Zipper Kinase Is Required for Mechanical Allodynia and Microgliosis after Nerve Injury." *eLife* 7 (July): e33910.

Xiong, Xin, and Catherine A. Collins. 2012. "A Conditioning Lesion Protects Axons from Degeneration via the Wallenda/DLK MAP Kinase Signaling Cascade." *The Journal of*

Neuroscience: The Official Journal of the Society for Neuroscience 32 (2): 610–15.

Xu, Z., A. C. Maroney, P. Dobrzanski, N. V. Kukekov, and L. A. Greene. 2001. “The MLK Family Mediates c-Jun N-Terminal Kinase Activation in Neuronal Apoptosis.” *Molecular and Cellular Biology* 21 (14): 4713–24.

Yan, Dong, and Yishi Jin. 2012. “Regulation of DLK-1 Kinase Activity by Calcium-Mediated Dissociation from an Inhibitory Isoform.” *Neuron* 76 (3): 534–48.

Yan, Dong, Zilu Wu, Andrew D. Chisholm, and Yishi Jin. 2009. “The DLK-1 Kinase Promotes mRNA Stability and Local Translation in C. Elegans Synapses and Axon Regeneration.” *Cell* 138 (5): 1005–18.

Yang, Jing, Zhuhao Wu, Nicolas Renier, David J. Simon, Kunihiro Uryu, David S. Park, Peter A. Greer, Cathy Tournier, Roger J. Davis, and Marc Tessier-Lavigne. 2015. “Pathological Axonal Death through a MAPK Cascade That Triggers a Local Energy Deficit.” *Cell* 160 (1-2): 161–76.

“ZFIN Publication: Thisse et Al., 2004.” n.d. Accessed May 18, 2021. https://zfin.org/ZDB-PUB-040907-1.

Zheng, Chaogu, Emily Atlas, Ho Ming Terence Lee, Susan Laura Javier Jao, Ken C. Q. Nguyen, David H. Hall, and Martin Chalfie. 2020. “Opposing Effects of an F-Box Protein and the HSP90 Chaperone Network on Microtubule Stability and Neurite Growth in Caenorhabditis Elegans.” *Development* 147 (12). https://doi.org/10.1242/dev.189886.